SAND2014-18911R

Combustion Instability in Spray-Guided Stratified-Charge Engines – A Review

Todd D. Fansler[1,4], David L. Reuss[2,3], Volker Sick[2], and Rainer N. Dahms[3]
[1]Engine Research Center, University of Wisconsin – Madison
[2]Dept. of Mechanical Engineering, The University of Michigan
[3]Combustion Research Facility, Sandia National Laboratories, Livermore, CA
[4]Corresponding author

ABSTRACT

This paper presents a comprehensive and detailed review of research to understand combustion instabilities (principally rare, random misfires and partial burns) in spray-guided stratified-charge (SGSC) engines operated at part load with highly stratified fuel-air-residual mixtures. The primary emphasis is on experiments using advanced high-speed optical imaging diagnostics to characterize and quantity the sensitivity of ignition and flame propagation to strong, cyclically varying temporal and spatial gradients in the flow field and in the fuel-air-residual mixture distribution. Modeling work is integrated in order to show the resulting advances in simulations, to extract additional insight, and to provide a conceptual framework for the discussion.

For SGSC engines using multi-hole injectors, significant findings include the beneficial effects of spark stretching and locally rich ignition. Combustion instability is dominated by convective flow fluctuations that impede motion of the flame kernel toward the bulk of the fuel, coupled with low flame speeds due to locally lean mixtures adjacent to the kernel. Significant differences are apparent in SGSC engines using outwardly opening piezo-electric injectors, in which ignition and early flame-kernel growth are influenced by the spray's characteristic recirculation vortex. For both injections systems, several factors are identified that underlie the benefits of multi-pulse injection. The spray and the intake/compression-generated flow field influence each other, and flow-field fluctuations affect the spray and combustion stability with both injection systems.

Questions not resolved (by our own research or by that of others reviewed here) include (1) the extent to which rare random misfires in piezo SGSC engines are exclusively or predominantly caused by complete failure to form a flame kernel as opposed to failure of a flame kernel to survive and grow, which is the situation in multi-hole-injection SGSC engines; (2) the extent to which combustion proceeds via partially premixed flame propagation as opposed to

mixing-controlled combustion under the exceptionally late-injection conditions that permit SGSC operation on E85-like fuels with very low NOx and soot emissions; and (3) the effects of flow-field variability on later stages of combustion, where the mixing of the heterogeneous fuel-air distribution within the piston bowl becomes important.

Keywords: Direct injection, stratified charge, spark ignition, optical diagnostics, numerical simulation, cyclic dispersion, cyclic variation, piezo-electric injectors, multi-hole injectors, SIDI, DISI, GDI, ethanol-gasoline blends

Introduction

In general, engine combustion is most efficient when the fuel-air mixture is diluted (with air or exhaust gas or both) as much as possible. Dilution (1) reduces part-load pumping losses compared to throttled operation, (2) reduces heat losses and NOx production by reducing the gas temperature in the cylinder, and (3) increases the ratio of specific heats $\gamma = C_P/C_V$ and thereby increases the work extracted per unit volume expansion. The downside is that dilution also reduces flame speed and can lead to problems with ignition and complete combustion. For spark-ignited (SI) gasoline engines, a propagating flame can be ignited and sustained over a relatively limited fuel-air-diluent range. Therefore, taking full benefit of charge dilution requires that the fuel-air mixture be concentrated in the ignitable range around the spark plug; in other words, the engine must operate with a stratified charge (SC).

The benefits of stratified SI engine operation, as well as its sensitivity to design and operating conditions, have long been recognized. A century ago (!), Ricardo[1] experimented with a divided-chamber stratified-charge engine and concluded that

> working with a stratified charge . . . is possible and the high efficiency theoretically obtainable from it can be approached. The worst feature about it is that, *if not just right, it may be very wrong;* a small change in form or dimension may upset the whole system. (italics added)

Types of stratified-charge SI engines

The attraction of increased fuel efficiency has led to many efforts to bring stratified-charge SI engines into production. Some of these achieved a mild degree of stratification through timed port fuel injection and the interaction of the incoming fuel with the in-cylinder flow field, exploiting swirl[2] or tumble[3, 4]. These approaches will not be discussed further here.

More germane to the topic of this paper were early efforts with direct injection (DI)[5, 6]. These designs, which injected fuel more-or-less directly at the spark plug, fall into the category now referred to as *spray-guided* stratified-charge (SGSC) engines[6] (Figure 1). Some of these programs were extensive in terms of time and resources (e.g., Texaco TCCS[7-9], Ford FCP and PROCO[10-12], General Motors DISC[13-17], and several DI two-stroke designs[18]). United Parcel Service converted GM six-cylinder truck engines to the TCCS design; field tests in some 500 of their delivery trucks over a two-year period in the early 1980's[19] showed fuel-economy improvement of 30–35% relative to the unmodified engine. A fleet of 100 vehicles equipped with air-assist-injection two-stroke SGSC engines was tested in Australia over a three-year period in the late 1990's.[20] Ultimately, however, all of these early spray-guided engine programs foundered due, at least in part, to one or more of the following problems: combustion instability, excessive unburned hydrocarbon (HC) and/or NOx emissions, and soot at heavier loads.[6]

In the mid-1990's, DI stratified-charge engines with a wider spacing between the injector and the spark plug reached production in Japan and Europe.[6, 21] Mitsubishi, Toyota and Nissan employed *wall-guided* side-injection configurations in which the fuel spray was directed at a contoured bowl or cavity in the piston crown that redirected the fuel cloud toward the spark plug (Figure 1, center), while VW employed an *air-guided* arrangement that relied more on the interaction of the in-cylinder air flow with the spray to form the desired stratified mixture (Figure 1, right). Unfortunately, these engines did not reach their full fuel-economy potential in real-world driving and also experienced problems with elevated HC and soot emissions. The HC emissions, which were a generic issue with these and earlier SC designs, were dominated by overmixing and lean flame quenching at the edges of the fuel cloud[6, 18]. Engine-out soot emissions originated predominantly in pool fires fed by liquid fuel films on the piston surface[22]. NOx emissions reduction was – and continues to be – an issue for all SC engines because the engine operates with an overall lean fuel-air ratio, precluding the use of the traditional three-way catalyst that reduces NO in the absence of oxygen in the exhaust stream[6].

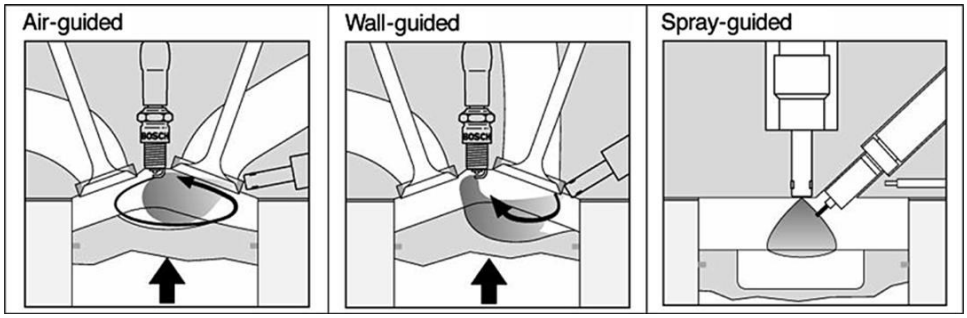

Figure 1. Categories of stratified-charge SI engines: spray-guided (left), wall-guided (center), and air-guided (right).[6]

Spray-guided stratified-charge (SGSC) engines with improved fuel economy and lower emissions reached production in Europe initially in 2006 and continue in naturally aspirated and turbocharged designs.[23-27] The close coupling (in both space and time) between injection and ignition in SG engines improves fuel economy by enabling expanded speed-load and dilution ranges for stratified operation. Viable SG engines also employ a carefully optimized piston bowl. Through its interaction with the spray downstream of the injector and spark plug, the bowl is important in stratified mixture preparation and therefore in flame development and combustion stability. The bowl is also crucial to confining the fuel in a relatively compact cloud and therefore to reducing unburned HCs from overly lean/dilute zones.

During ignition and flame-kernel growth, the close injection-ignition coupling in SGSC engines produces high velocities and intense turbulence (up to an order of magnitude higher than in homogeneous-charge SI engines). The spark plasma, the ignition kernel(s), and the growing flame all are subjected to steep and cyclically varying gradients in the liquid and vapor fuel concentrations and the velocity fields. These factors, which can produce unfavorable conditions for robust ignition and flame growth, are a central focus of this review.

The perennial problem of SGSC combustion instability

The issue of combustion stability – in particular, rare (often << 1:1000 cycles), apparently random misfires and partial burns that are not due to gross injection or ignition system failure – has plagued SC engines from the earliest attempts and continues to limit the maximum dilution and the range of injection and ignition timings that can be achieved in practice. Figure 2 illustrates the situation with a graph of indicated mean effective pressure

(IMEP) for two sets of 375 consecutive fired cycles at light-load (near-idle) operation of a SGSC engine (to be described later). In one case, engine operation is highly stable. In the other data set, almost every cycle burns as well as in the first case except for a misfire and a partial burn.[28] The two cases differ by only one degree in the spark timing, clearly illustrating Ricardo's statement quoted above how sensitive stratified-charge operation can be. Reducing that sensitivity and increasing the robustness of SGSC operation is a major development goal.

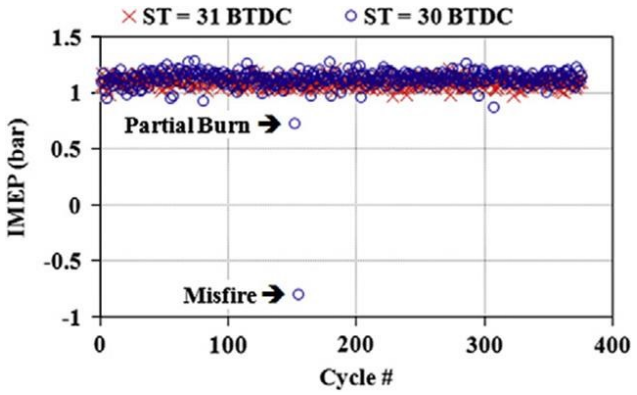

Figure 2. Combustion stability for two spark timings (ST) in the University of Michigan optical engine. The physical end of injection is at 32°BTDC.[28]

In practice, acceptable combustion stability in SGSC engines is evaluated by sweeping the injection (usually quoted as the commanded end-of-injection (EOI)) and ignition timings, seeking maximum IMEP (and minimum fuel consumption) subject to constraints on cyclic variation, misfire rate, and emissions (HCs, CO, NOx and soot). Cyclic variation is usually gauged by the coefficient of variation (COV) of IMEP; a maximum COV(IMEP) of 3–5% is typical. In this paper, misfires will be defined by IMEP < 0, while partial burns will usually be defined by a final fuel mass fraction burned FMFB < 0.6, although sometimes an IMEP criterion will be used for convenience. To probe key phenomena in combustion instability using optical (and other) diagnostics, we perturb dilution, spark timing and injection timing about the optimum while being careful that misfires and partial burns remain rare and random events, as we shall discuss in more detail later in the paper when we consider prior-cycle effects and fluctuations in spark characteristics, equivalence ratio and velocity.

Given the importance of ignition and early kernel growth to successful combustion (illustrated for SGSC in Figure 3), earlier studies using optical diagnostics in two-stroke SG and in four-stroke WG and AG engines naturally have focused on the fuel concentration near the

spark gap[6, 18, 29-31]. Although fuel-air equivalence-ratio fluctuations over a sufficiently wide range to inhibit or prevent ignition were detected, there typically was not a simple correlation with combustion stability. For example, Ghandhi & Bracco[31] observed that a significant fraction of cycles in a two-stroke SGSC engine had a measured equivalence ratio far leaner than the lean ignitability limit, but nevertheless ignited and burned well. They attributed this behavior to significant movement of the stratified fuel-air mixture during the finite spark duration (~1 ms), which could allow ignitable mixture to reach the spark even if it were not present there during the brief (~10 ns) interval of their equivalence-ratio measurement.

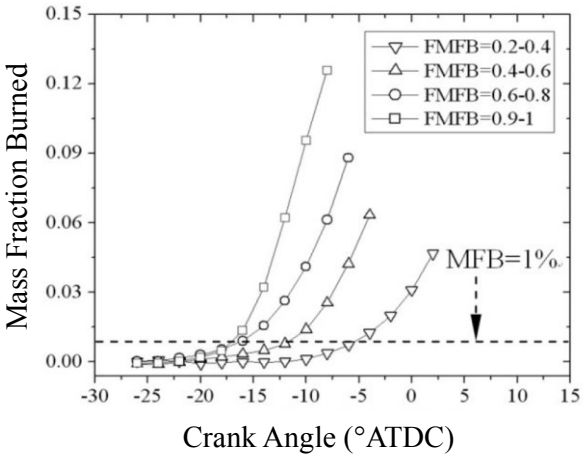

Figure 3. Conditional heat-release analysis illustrates the importance of the earliest stage of combustion in a spray-guided stratified-charge engine that was intentionally operated off optimum conditions to obtain a wide range of final mass fraction burned (FMFB).[32] High-speed imaging of flame growth showed that the dashed line indicating 1 % MFB corresponds to an equivalent flame diameter of about 10 mm.

Scope of the paper

This review concentrates on sources of combustion instability in SGSC engines operated at part load with highly stratified fuel-air-residual mixtures, focusing specifically on ignition and flame-kernel growth. Mid-burn and late-burn phenomena affect efficiency, IMEP and emissions through the phasing and completeness of the combustion event;[30] by definition, however, they have no effect on misfires. Moreover, Figure 3 implies that slow or delayed combustion at the earliest stage can significantly affect the overall success of SGSC combustion.[32] Mid- and late-burn phenomena will not be discussed further except in passing.

SGSC Fuel-injection systems

Two very different types of high-pressure (~10–20 MPa) gasoline injectors have dominated SGSC activity over the 10–15 years: solenoid-actuated inwardly-opening (pintle) multi-hole injectors and piezo-electrically-actuated outwardly opening injectors (which are sometimes called A-injectors). For brevity, we will refer to these simply as multi-hole (MH) and piezo injectors, respectively. The latter term is admittedly a partial misnomer since their distinctive spray structure (see below) does not depend intrinsically on piezo-electric actuation.[33] Piezo-electric actuation provides variable lift and very fast response, which greatly facilitate precise fuel metering, especially for small injected quantities with closely spaced multiple injections. Under these conditions, in contrast, typical solenoid injectors operate in a ballistic regime (i.e., the injector does not fully open before it is commanded to close), and the precision and repeatability of closely spaced injections can be problematic.[27] Considerable effort has been devoted to developing a rapid-response outwardly opening solenoid injector.[33] Reviews[34, 35] and some comparisons of SGSC engines with multi-hole and piezo injectors using experiments[36, 37] and numerical simulation[38] are available; further references and details will be included in the second half of this paper.

As illustrated in Figure 4, the basic spray structure differs greatly between multi-hole-and outwardly opening injectors (whether piezo- or solenoid-actuated). [23, 24, 35, 39-41] The piezo-injector spray has a hollow-cone structure, albeit with marked striations or filaments.[35, 42, 43] Both multi-hole and piezo sprays maintain their basic structure but with reduced penetration for injection into increasingly dense gas. Increasing gas density also blurs the filamentary structure and accentuates the toroidal recirculation vortex that is just noticeable about halfway down the spray in the central column of Figure 4 and is more prominent at the tip of the spray on the right.

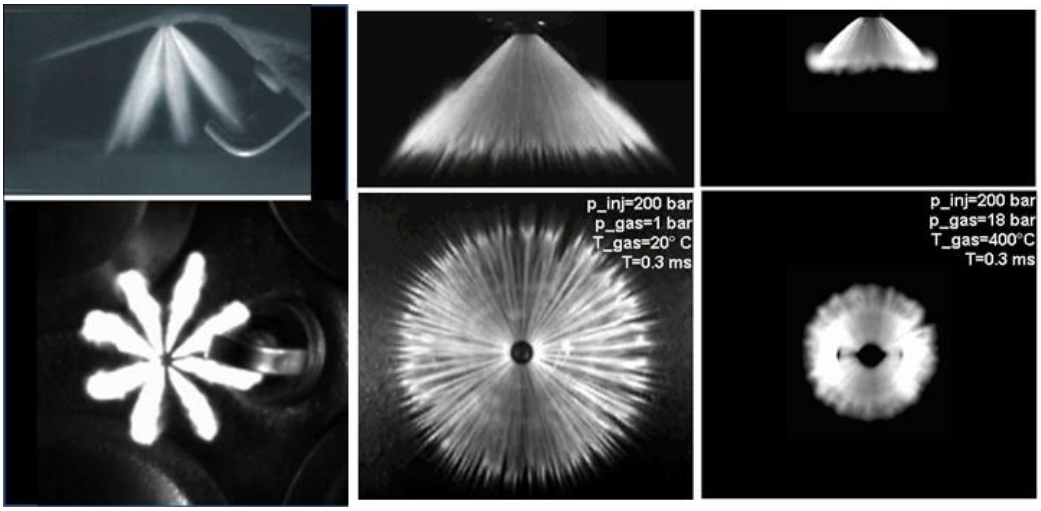

Figure 4. Side and bottom views of a spray from a multi-hole injector (nominal cone angle 60°) in a firing SGSC engine[21] ***(left)***, and sprays into a quiescent chamber from an outwardly opening piezo-electric injector with a nominal cone angle of 90° under room-temperature, atmospheric-pressure conditions ***(center)*** and under high-temperature, high-pressure conditions typical of injection timing for stratified-charge combustion[24] ***(right).***

Organization of the paper

The significant differences between these two injector types create a natural division of this review paper into two major parts. First, we review combustion instability in SGSC engines with multi-hole injectors, drawing primarily on research in which we personally participated over the last fifteen years. Experiments employed systematic conditional sampling of in-cylinder-pressure measurements with more detailed high-speed (6–60 kHz) optical imaging diagnostics [particle-image velocimetry (PIV), planar imaging using Mie-scattering and planar laser-induced fluorescence (PLIF), spectrally resolved spark and flame chemiluminescence imaging] in order to characterize in-cylinder flows, fuel sprays, mixture formation, ignition, and combustion. The experimental results and insights have been supplemented by and interpreted within the understanding of spray-guided ignition and combustion that emerges from recent numerical simulations, which highlight the importance of local conditions along and in the vicinity of the extended spark channel (equivalence ratio, dilution, temperature, convective velocity, and turbulent velocity and equivalence-ratio fluctuations) for successful ignition and early flame-kernel development. In the second major division of the paper, we turn to SGSC engines with piezo injectors, where we must rely on the information in the open literature.

The remainder of the paper is organized as follows. Beginning with multi-hole-injection SGSC engines, we first describe the optical engines used in our own research. We then review

experimental results for the key phenomena involved for stable SGSC operation: fuel injection, mixture preparation, ignition, and flame-kernel growth. Next we summarize a comprehensive conceptual and modeling framework for SGSC combustion that developed from those experiments. With that foundation, we systematically review investigations of combustion instability in multi-hole-injection SGSC engines, considering liquid-fuel effects, spark characteristics, cycle-to-cycle coupling, and early flame-kernel motion. Having identified a dominant source of misfires and a significant source of partial burns, we then summarize numerical simulations of double-pulse injection with multi-hole injectors. We conclude our exposition on multi-hole-injection SGSC combustion by reviewing recent results with ethanol-dominated fuel blends, which shed additional light on SGSC combustion instability. Turning to piezo-injection SGSC engines, we follow the same basic path, beginning with stable engine operation and then seeking to identify factors that contribute to unstable ignition and flame-kernel growth. After touching briefly on current SGSC research and development directions, we complete the review by summarizing key points and offering several conclusions.

Stable spray-guided combustion with multi-hole injectors

Before discussing combustion instability in SG engines and its sources, we first summarize the conceptual/modeling framework and its experimental foundation as they have emerged from multi-hole-injection SGSC research. This approach will also serve to outline the stages of combustion, discuss critical phenomena, and establish nomenclature and descriptors. In this section, we focus primarily on "average" behavior that occurs during stable combustion with low cyclic dispersion. The experimental results shown below are selective rather than exhaustive, but are backed up by thousands of high-speed images that show the illustrated phenomena.

Optical engines

Figure 5 shows optical SGSC engines used in our experiments at General Motors R&D (GM),[34, 44-49] and The University of Michigan (UM)[28, 50-54]All obtain optical access through quartz windows in the bottom of their piston bowls using a Bowditch extended-piston/mirror arrangement as well as side access to the clearance volume and to part of the piston bowl via quartz windows in the cylinder head. The second-generation Gen 2 optical engine design differs from the earlier Gen 1 by aligning the injector and spark plug along an axis parallel rather than

perpendicular to the crankshaft, and by locating the spark plug more centrally and in a more vertical orientation. Another difference is that the Gen 1 engine typically operated with near-zero swirl whereas swirl was enhanced in the Gen 2 engine by deactivating one intake valve. The optical engine at Sandia National Laboratories (SNL)[55-58] used to study SGSC operation with ethanol-gasoline fuel blends (e.g., E85) is similar to the Gen 2 with some differences in the modifications for optical access. The UM engine has a full quartz cylinder, whereas the GM and SNL engines have a cooled metal cylinder. The 4-mm square region downstream of the fuel jet and to the right of the spark plug in the UM engine was used to evaluate the equivalence ratio from high-speed planar PLIF data as well as a representative local velocity from PIV. The engines all employ eight-hole solenoid injectors [nominal spray "umbrella" angles of 60° (GM, SNL) and 90° (UM)], extended-electrode spark plugs, and high-energy coil ignition systems.

All four engines were capable of continuous firing over hundreds or thousands of consecutive cycles at the light and moderate loads of interest for stratified operation in naturally aspirated engines. The UM piston-bowl geometry provided full side- and bottom-view optical access, but was somewhat removed from a truly realistic design by its flat surfaces and square corners. The UM engine's range of stable SGSC operation was therefore narrower than in the more realistic Gen 1, Gen 2 and SNL engines, which had more restricted optical access. Comparison with all-metal (optically impaired) engines with geometries similar to the Gen 1[59] and Gen 2[37, 60, 61] optical engines showed reasonable fidelity of the combustion process (e.g., IMEP, COV(IMEP), and early burn durations). Details of the GM, SNL and UM optical engines, including the cylinder-head and piston-bowl and the intake port designs of the two engines, are different enough that the overall conclusions drawn from the measurements are likely to be generic in character.

Readers are referred to the original papers for details of operating conditions and other experimental apparatus such as lasers and high-speed cameras.

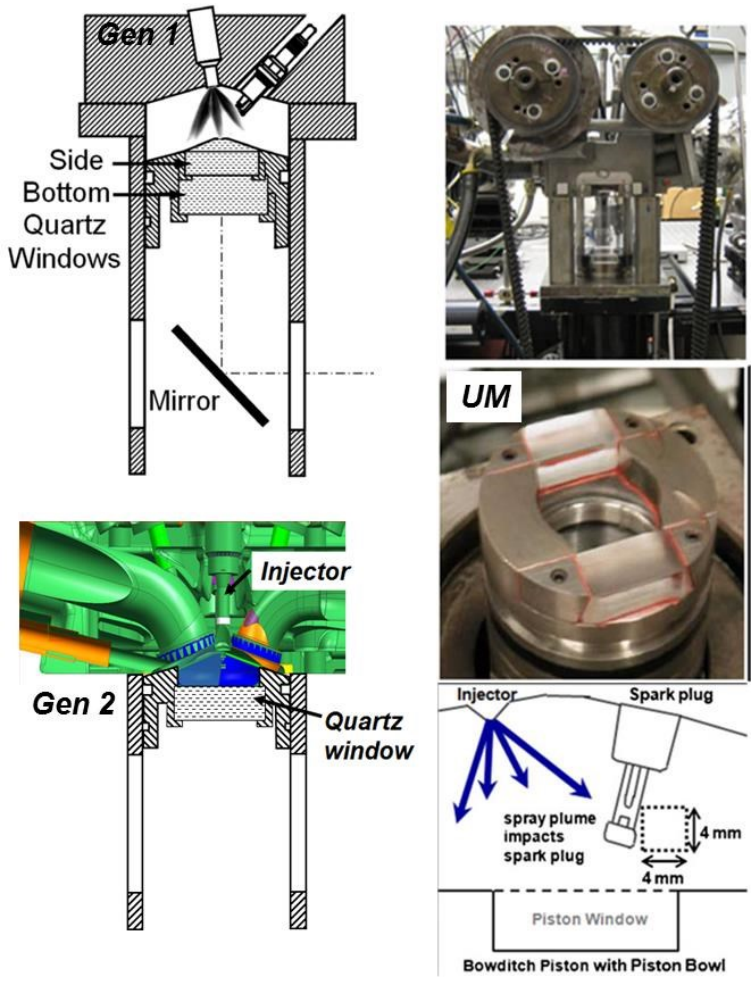

Figure 5. Optical-access engines used at General Motors R&D (***left***) and The University of Michigan (***right***).

Fuel injection and mixture preparation

Figure 6 shows an example from high-speed Mie-scattering imaging of the fuel spray in the Gen 1 optical engine as the spray approaches the spark plug. The bottom view shows that two spray plumes (almost) straddle the center and ground electrodes. The impacting orientation in which one plume directly strikes the center electrode was used in the UM engine and in some of the GM Gen 1 experiments.

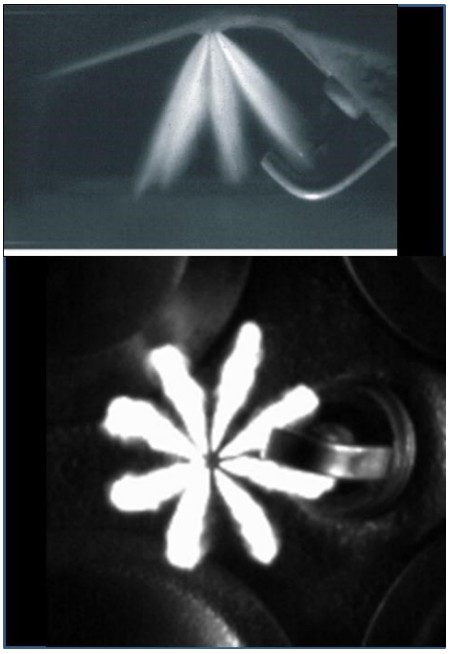

Figure 6. Volume-illuminated side and bottom views of the fuel spray in the Gen 1 optical engine.[48]

Typical injection and spark timings in the GM, UM and other multi-hole-injection SG engines are such that the middle or the tail end of the spray is at or just past the spark gap when the spark is fired. (The less typical "head ignition" as the spray approaches the spark gap will be discussed later, in particular for ethanol-dominated fuel blends.) As illustrated in Figure 7, spark-emission spectroscopy[62] uses CN*-radical emission (385-nm wavelength), normalized by instantaneous spark energy, to provide quantitative measurements of the fuel concentration (expressed here as equivalence ratio) experienced by the spark plasma. The amount of liquid fuel encountered by the spark can also be estimated from C_2* emission (516-nm wavelength)[46]. Figure 7 makes clear that substantial and rapidly varying amounts of liquid fuel are present at typical ignition timings, consistent with high-speed Mie-scattering imaging. Furthermore, even for optimum injection and spark timings (end-of-injection command at 48°BTDC with 40° spark advance), Figure 7 demonstrates that the multi-cycle ensemble-average vapor equivalence ratio is very rich ($<\phi> \approx 2.8$ at 40°BTDC) and the cyclic variations in equivalence ratio are large (rms variation $\sigma(\phi) \approx 1.8$). Computational-fluid-dynamics (CFD) simulation using the GMTEC[63, 64] code yielded results in fairly good agreement with the mean values.[34, 49]

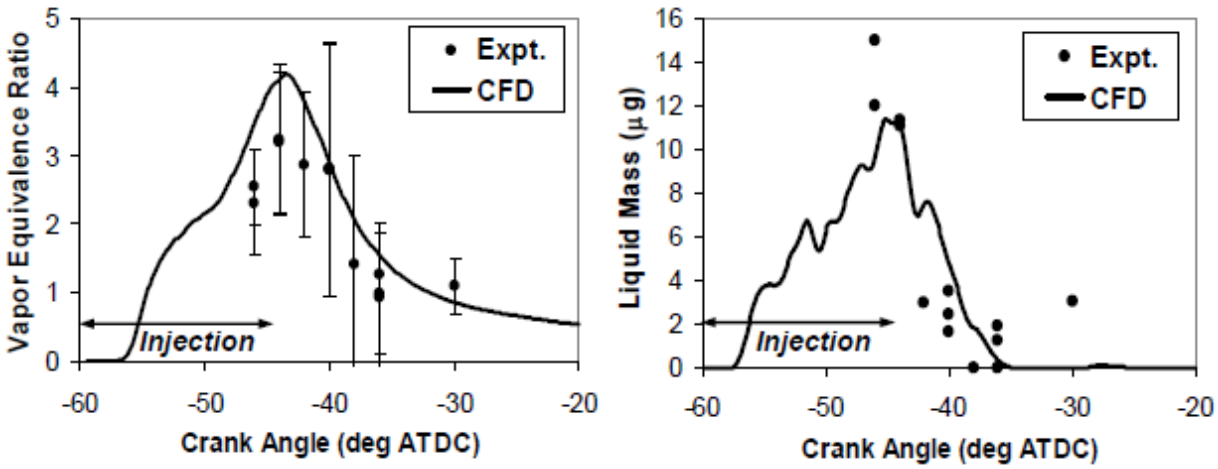

Figure 7. Spark-emission spectroscopy measurements of vapor and liquid fuel at spark gap vs. crank angle in the Gen 1 engine together with CFD simulation. Vertical bars indicate measured rms cycle-to-cycle variation in vapor fuel equivalence ratio. The relative amount of liquid fuel is obtained from C_2* emission and is scaled to match the CFD result at CA = -44°.[34, 46, 49]

Two frames from simultaneous high-speed PIV and PLIF imaging (biacetyl tracer in iso-octane fuel excited with a 355-nm pulsed laser) in the UM optical engine provide a consistent and complementary story. In this example, the physical end of injection is at crank angle 328° and the spark is fired one degree later. The mean equivalence ratios at and downstream of the spark plug (with respect to the spray) are very rich and exhibit steep gradients and rapid variation in time. The mean velocity field displays the effect of the spray momentum, but other complex flow structures are apparent.[50]

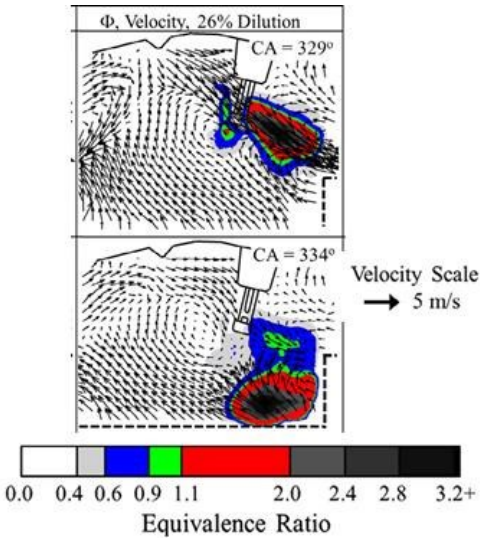

Figure 8. Combined high-speed PLIF imaging of ensemble-mean equivalence ratio superimposed on high-speed PIV measurements of ensemble-mean velocity in a plane through the spark gap in the UM optical engine. The intake air has been diluted with 26% nitrogen to simulate EGR.[50]

Ignition and flame kernel growth

Experimental observations. A feature of the intense spray-spark interaction that is important to ignition and early flame-kernel growth but that is not apparent in either Figure 7 or Figure 8 is the dramatic stretching of the spark plasma channel by the local velocity field, which reflects the combined effects of spray-induced gas motion and the in-cylinder flow field that results from the intake and compression processes. Figure 9 (left) shows a superposition of two successive spark plasma (CN*) images recorded in the Gen 2 engine at 24 000 frames/s. Also shown on the right are the velocity vectors along the plasma channel obtained using a PIV-like cross-correlation analysis. Steep gradients in velocity and in the CN* intensity (relative fuel concentration or equivalence ratio experienced by the spark plasma) are evident on sub-millimeter scales (i.e., smaller than typical CFD mesh cells).[45, 65]

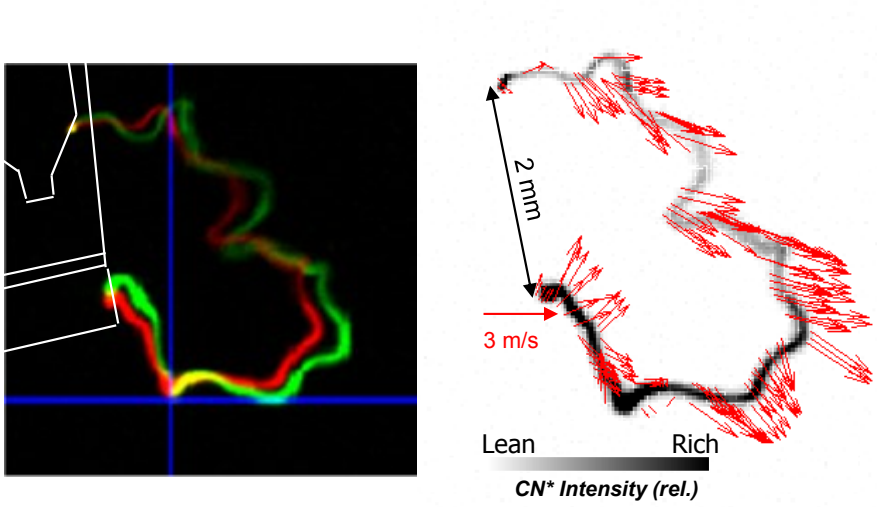

Figure 9. High-speed (24000 frames/s) high-resolution imaging of spark-plasma stretching due to spray-spark interaction in the Gen 2 engine. **Left**: Two successive images of CN* intensity. **Right**: Resulting velocity vectors and relative equivalence ratio along the spark channel.

As shown by the traces of spark (secondary) current and voltage in Figure 10, which were recorded simultaneously with high-speed imaging (not shown), spark stretching during the glow discharge phase is accompanied by an increase in spark voltage until the ignition system can no longer sustain the discharge, at which point a restrike – which may be directly across the spark gap or into the existing stretched plasma channel – will occur if sufficient energy remains in the ignition system coils. The upper example in Figure 10 is for non-injected homogeneous-charge operation with stretching only by the intake-compression-generated flow field[48]; the spark

duration is approximately 2.15 ms. In contrast the lower portion of Figure 10 is for direct injection with "head ignition," i.e., the spark is fired shortly before the arrival of the spray plume at the plug. The high-frequency restrikes reflects very rapid stretching by the intense spray-induced flow[36, 45, 48] and perhaps momentary extinctions due to liquid droplets passing through the plasma[66]. The more intense spray-spark interaction exhausts the energy stored in the ignition system more rapidly, [34, 42, 45] and the overall duration of the spark event is much shorter (about 1.3 ms), even though the total energy delivered to the spark gap (which averages about 120 mJ in the GM experiments) typically increases with higher velocities and greater spark stretching[51, 67].

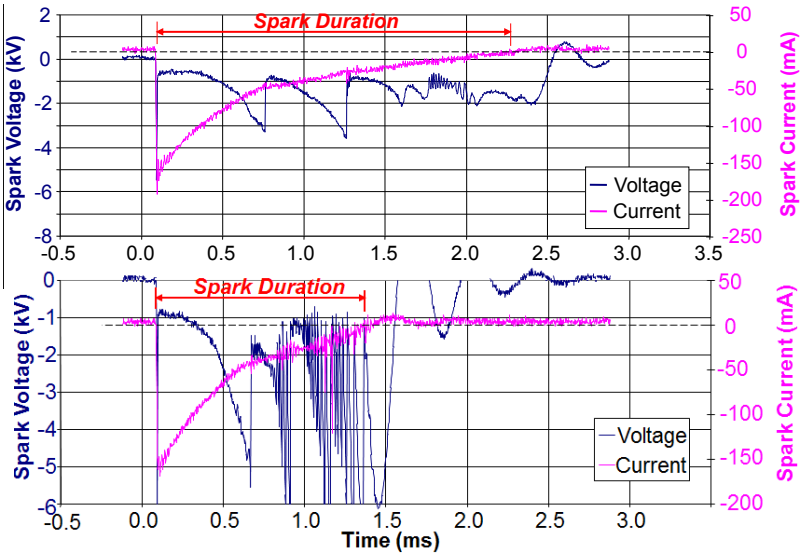

Figure 10. Spark (secondary) voltage and current traces recorded in the Gen 1 optical engine without fuel injection (**upper**)[48] and with the spark fired just before the spray plume reaches the spark plug **(lower)**. The average spark energy for these conditions is 120 mJ.

Figure 11 illustrates two key aspects of ignition and early-kernel development that differ greatly from conventional premixed-charge SI operation. First, as evidenced by broadband (350–800-nm) high-speed imaging, ignition occurs in locally rich regions along the extended spark channel (Figure 11a)[60, 65, 68], with rich glowing "fireballs" detaching from the spark channel (Figure 11b). Second – in marked contrast to the usual picture of an initially spherical flame kernel that gradually becomes more wrinkled by turbulence as it grows – the flame kernel here is non-spherical and highly wrinkled (<~ 1 mm) at even the earliest times (Figure 11c). The images in Figure 11c were obtained using sodium-enhanced combustion luminosity imaging[45, 69], in which thermal emission from a sodium-containing additive in the fuel provides strong, visible-wavelength emission from combustion that otherwise emits predominantly in the ultraviolet and

is therefore invisible to a non-intensified camera. The results in Figure 11 are completely consistent with high-speed planar Mie-scattering imaging of ignition and early flame development[47, 65, 68, 70] as well as with a study in the UM engine using a combination of toluene LIF for fuel distribution imaging and high speed OH* imaging to locate the spark plasma and the developing flame.[54]

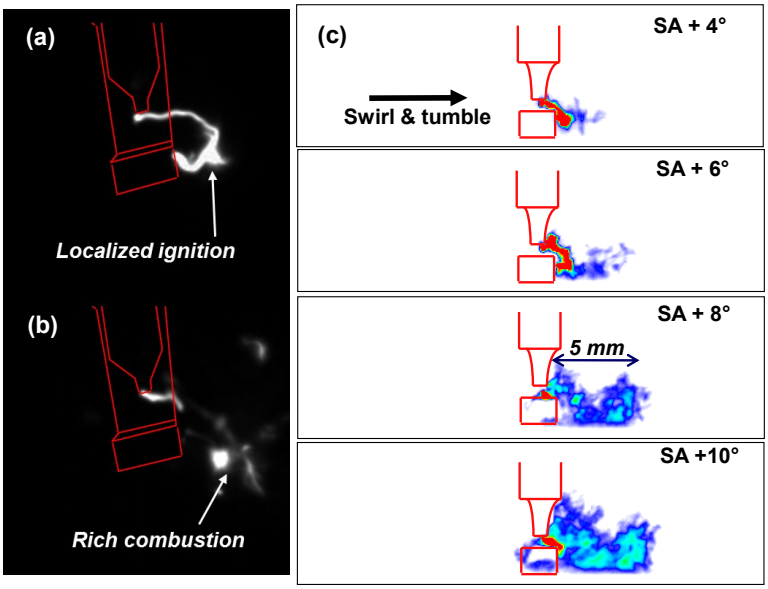

Figure 11. **(a)** and **(b)**: High-speed broadband (350–800 nm) images of localized rich ignition and combustion in the Gen 2 optical engine .[45] **(c)** High-speed sodium-enhanced luminosity imaging of local ignition and wrinkled, non-spherical early flame kernel growth. Note that in this view, the mean swirl and tumble flows reinforce one another near the spark plug, while the spray plumes induce a flow into the page.

Conceptual and modeling framework.

The experimental observations outlined here have provided the foundation for a new comprehensive framework for modeling ignition and combustion in spray-guided engines that has yielded new insight as well as very good agreement with experimental measurements. Here we summarize and illustrate the conceptual and physical aspects of this approach, including a few key comparisons to measurements. The SparkCIMM (spark channel ignition monitoring model) formulation, numerical approach and comparison with experiment have been fully detailed in[60, 65, 68, 70, 71]. The calculations were carried out using the AC-FLuX code[72], an updated version of GMTEC[63, 64].

Key features of the SparkCIMM framework are:

- Realistic sub-grid-scale modeling of the stretched spark plasma by the local flow field is implemented using marker particles that are advected by the local flow field. Restrikes are incorporated when the spark length reaches 10 mm, consistent with experimental observations.
- Local ignition is modeled by launching a nascent flame kernel (50-μm radius, based on the observed plasma-channel width; cf. Figure 9) anywhere along the extended spark channel that both chemical and turbulence criteria for local ignition and kernel-growth are met.
    - The chemical criterion requires that the local temperature of the combustible gas, excited by the simulated plasma channel it surrounds, exceeds the critical crossover or thermal-runaway temperature (T^0) for which chain branching reactions dominate chain termination reaction. This criterion is evaluated by a modified detailed chemical kinetics flamelet model.
    - The turbulence criterion requires that the second Karlovitz number $Ka_\delta = (l_\delta/\eta_K)^2 < 1$, where l_δ is the inner flame reaction zone thickness and η_K is the Kolmogorov length scale, i.e., the scale of the smallest turbulent eddies in the flow field. Physically, this criterion embodies the idea that turbulent eddies on the scale of l_δ or smaller can penetrate and disrupt the inner reaction zone, preventing formation of a flame kernel or extinguishing an existing kernel, whereas eddies that are significantly larger than l_δ wrinkle the flame surface and increase the turbulent flame surface area and burning rate.
    - Energy input from spark to flame kernel is modeled with a simple top-hat function, but a lumped-parameter model of the inductive ignition system could be incorporated as done elsewhere[73-75].
- Multiple flame kernels grow and merge in response to local conditions. Flame growth is tracked by marker particles until the flame is large enough to resolve on the computational grid, after which a level-set approach is applied to track the mean turbulent flame front.
    - A detailed-chemistry flamelet model incorporates local variations in enthalpy (droplet vaporization, heat losses to surfaces, e.g., electrodes), equivalence ratio, velocity, and the substantial turbulent fluctuations in each of these variables. Together with the effects of strong local curvature and molecular fuel properties as embodied by the local (non-unity) Lewis and Markstein numbers, these features lead to non-spherical

early flame growth as shown in Figure 12. These features are consistent with those observed from experiments (Figure 11c). A classical spherical flame kernel model, however, fails to qualitatively reproduce this characteristic flame topology.

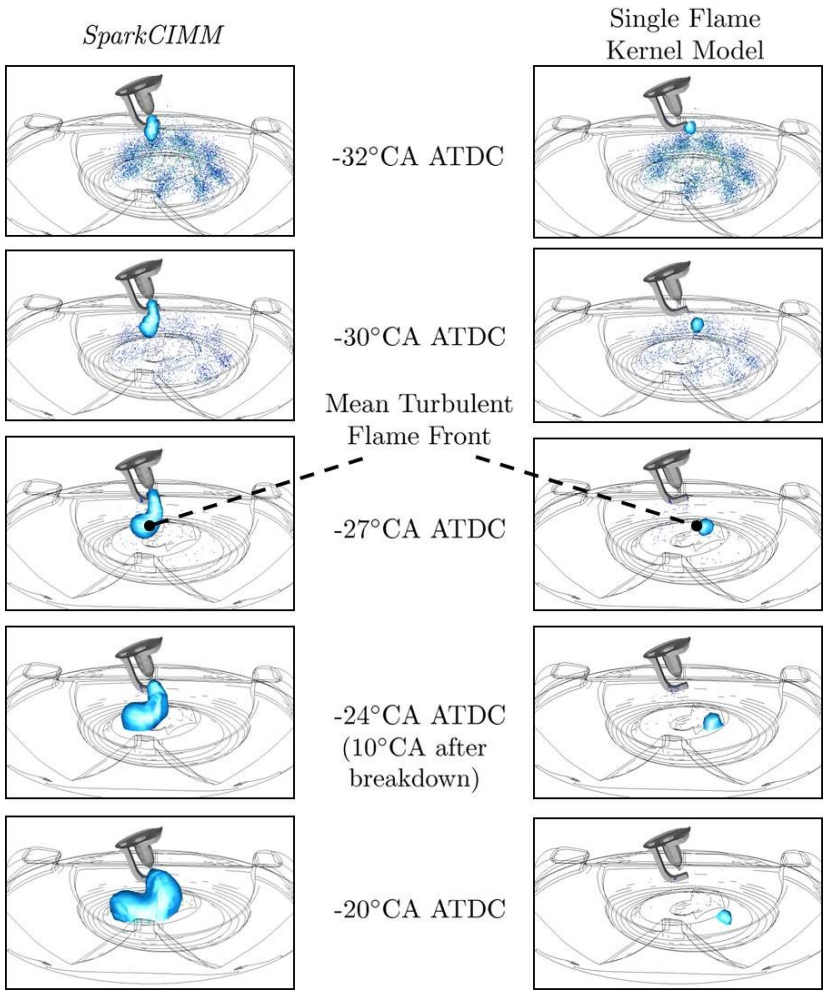

Figure 12. Numerical simulation of early flame front propagation using the SparkCIMM framework and a classical spherical flame kernel ignition model. SparkCIMM shows features of non-spherical flame kernel growth. Adapted from [65].

Figure 13 shows SparkCIMM calculations of equivalence ratios, turbulence kinetic energy, and velocity experienced by the spark plasma channel at three times (0.22, 0.33 and 0.55 ms) after spark breakdown for the Gen 2 engine. The modeled spark stretching and equivalence-ratio gradients are strikingly similar to the experimental results in Figure 9 and Figure 11. The yellow sphere in Figure 13 marks a nascent flame kernel. Ignition is substantially delayed from spark initiation, beginning at 0.49 ms (out of a typical spark duration ~1–3 ms; cf. Figure 10).

Furthermore, ignition occurs at a surprisingly rich equivalence ratio ($\phi \approx 3.5$), which is much richer even than the optimum $\phi \approx 1.5$ found for a wall-guided stratified-charge engine[29]. The near-stoichiometric ($\phi \approx 1$) portion of the spark channel – where ignition would usually be expected to occur first – experiences turbulence that is too intense for good ignition and flame propagation (the Karlovitz-number criterion at work). As illustrated by the detailed-chemistry flamelet calculations in Figure 14, the related effects of Lewis number, stretch and curvature favor ignition in rich zones under conditions of high dilution[65, 70].

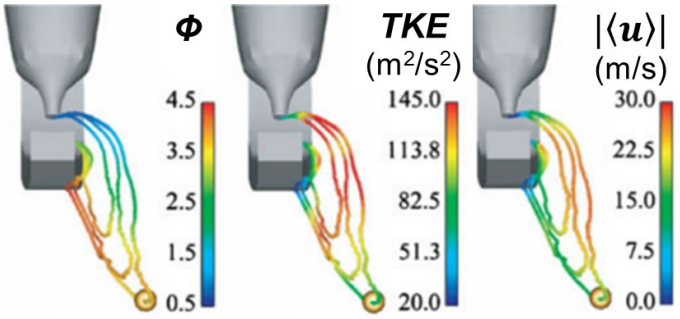

Figure 13. Numerical simulation of spark stretching and local ignition for three times (0.22, 0.33 and 0.55 ms) after spark breakdown. The yellow sphere represents a nascent flame kernel that ignites in a locally rich region[68].

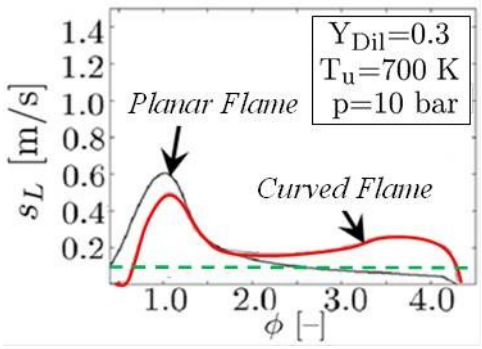

Figure 14. Detailed-chemistry calculations of laminar flame speed vs. equivalence ratio under highly diluted conditions (EGR mass fraction $Y_{Dil} = 0.3$) for a classical planar flame and for a highly curved (1-mm radius) flame using the non-unity Lewis-number SparkCIMM framework. The laminar flame speed for the curved flame is suppressed on the lean side of stoichimetric and greatly enhanced at equivalence ratios richer than the planar case's flammability limit (dashed green line). The calculations are for PRF87 reference fuel at 10 bar pressure and unburned gas temperature of 700 K. Adapted from [70].

The simulations described here were carried out in a RANS (Reynolds-averaged Navier-Stokes) formulation, so that the effects of turbulent fluctuations in enthalpy, equivalence ratio and velocity (kinetic energy) are reflected in the predicted mean behavior, but cyclic dispersion in combustion (e.g., cyclic variation in IMEP) is not predicted directly. An important aspect of the SparkCIMM framework, however, is that its G-equation formulation does provide a metric of

flame intermittency or variability through an explicit equation for the flamefront probability, which is directly comparable to experimental observations. Experimentally, the flamefront probability is evaluated from a series of planar flame images recorded at the same crank angle in many engine cycles. Binarizing the images (1 in enflamed regions and 0 in unburned gas) and averaging the results provides a spatial probability distribution of detected flame[47, 68] or burned gas[50]. Measured flame probability is shown in the center column of Figure 15 for three times after spark breakdown. The left and right columns show the results of calculations with the same chemistry but with a simpler single-kernel ignition model vs. the full SparkCIMM approach[65] respectively. The simpler model[76] neglects spark stretching, lacks local ignition criteria, and ignores effects of fluctuations in equivalence ratio and velocity on early flame-kernel-growth. The elongated shape and growth of the early flame kernel seen in the experiment are predicted reasonably well by the full SparkCIMM approach, whereas at the earliest times the simpler model fails to predict these characteristic features of spray-guided ignition and early combustion. Furthermore, note the high degree of variability (or, in a RANS context, the thick turbulent flame brush) implied by the flame probability values, which are substantially below unity, even for this example with low cyclic dispersion [COV(IMEP) < 5%]. Although SG combustion in the UM engine has not been simulated, experiments show similar variability in inflamed-gas probability distributions (Figure 16).

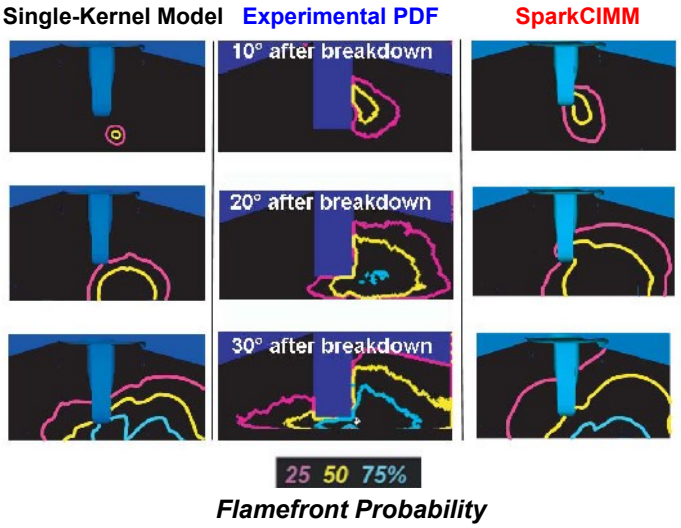

Figure 15. Experimental flamefront probability distributions evaluated from 200 consecutive engine cycles **(center)** compared to simulations using a simple single-kernel igntion model[76] **(left)** and the full SparkCIMM approach **(right)**[65].

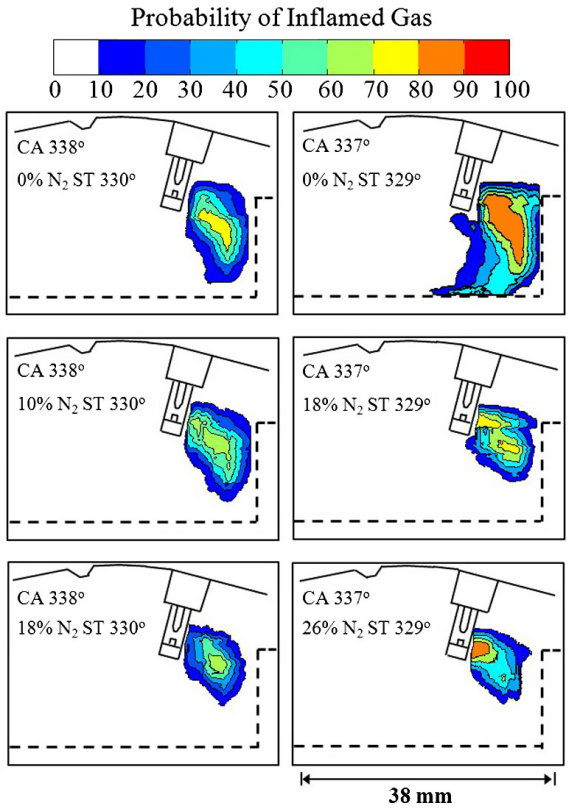

Figure 16. Flamefront probability distributions measured in the UM optical engine for well-burning cycles at different nitrogen dilution levels and two spark timings[50].

Main and late combustion stages. Although the focus of this review is on ignition and early combustion as sources of SG combustion instability, it is worthwhile to summarize a few points regarding later stages of combustion. Figure 17 compares simulated and experimental cylinder-pressure and heat-release results for an all-metal version of the Gen 2 engine at three speed-load conditions[60]. The 2000 RPM speed and load are the same as used in the Gen 2 optical-engine experiments. The overall agreement of simulation and experiment in Figure 17 is excellent. The spray and combustion submodel parameters ("constants") have not been specifically adjusted to achieve agreement in this calculation. However, the various model parameters have been extensively refined over a period of years by colleagues using comparisons to spray measurements (primarily penetration and drop size and velocity) in high-pressure spray chambers, fundamental combustion validation studies, iterative intake simulations to capture discharge coefficients, etc.

Another point is that the SparkCIMM G-equation formulation simulates combustion as flame propagation through all phases, in contrast to earlier concepts and simulations of stratified-charge combustion that invoked a two-stage process in which flame propagation was followed by mixing-controlled burnout[21, 34, 49, 77], i.e., turbulent-diffusive combustion of rich products (unburned fuel, fuel fragments, CO, etc.) as they mix with lean, hot post-flame gases. Experimental observations suggestive of later-stage mixing-controlled combustion included heat-release rates proportional to the amount of unburned fuel remaining in the cylinder[18, 77] and bright, broadband combustion luminosity typically associated with thermal emission from locally rich, diffusive combustion (in contrast to chemiluminescence from early-stage premixed combustion that is much less intense at visible wavelengths)[18, 34, 49, 78, 79]. In the earlier GM simulations[34, 49], the presumed mixing-controlled combustion was simulated using an eddy-dissipation model (effectively single-step kinetics). In the present simulations, the detailed chemistry model predicts that the fuel is consumed in the flame except if the turbulence- and chemistry-based combustion criteria produce local extinction when the flame encounters unburnable mixture conditions (recall, however, that mixtures are predicted to be burnable for substantially richer equivalence ratios than in[49]). The detailed chemistry also deals with oxidation of CO, fuel fragments, etc. Comparison with experiment shows that the simulation only slightly underpredicts the total engine-out unburned hydrocarbons and CO (e.g., simulated combustion efficiency 93.4% vs. 97.4% for the experiment at the 2000 RPM condition in Figure 17.[60]

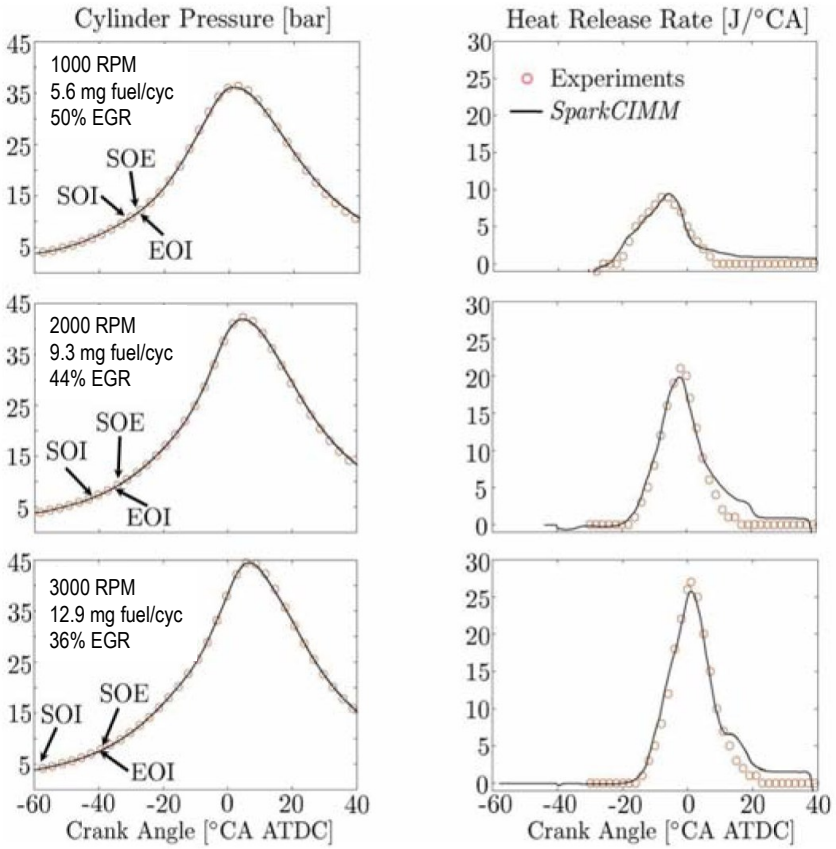

Figure 17. Comparison of SparkCIMM calculations of cylinder pressure and heat-release rate compared to experiments in an all-metal engine of the Gen 2 design for three speeds and loads[60].

Instability of spray-guided combustion with multi-hole injectors

The Introduction mentioned the failure of earlier attempts to relate combustion stability in SG two-stroke and WG four-stroke definitively to the fuel distribution at spark onset. This situation no longer seems very surprising in view of the ignition and flame-kernel-growth phenomena discussed in the preceding section. It is now clear that spark ignition, especially in SG engines, is extended in space and time and must be characterized as such. The ignition event is much more complex than the simple concept of the spark as a nearly instantaneous energy source that is localized across the ~1-mm electrode gap and that initiates a spherical flame kernel within the gap. Furthermore, the flame kernel in the SGSC engines above does not develop quasi-spherically by gradual wrinkling in response to the turbulent in-cylinder flow. To seek sources of instability in SGSC combustion, we therefore turn to further high-speed imaging studies that follow the evolution of the spark and the local flow, spray, mixture and spark conditions within individual cycles and over many consecutive cycles.

Liquid fuel

High-speed imaging in both the GM and UM optical engines shows that some liquid fuel is often present around the time of ignition and early flame-kernel development. Liquid fuel might affect the spark itself[66] or it might cause heat loss from the flame kernel, so it is necessary to assess whether liquid fuel affects combustion instability.

As illustrated earlier (Figure 7), spectrally resolved high-speed imaging of C_2* emission from the spark provides a rough relative measure of the amount of liquid fuel that the spark has encountered.[46] However, extensive characterization of the C_2* intensity during the spark event (in conjunction with time-resolved spark voltage and current measurements) over thousands of cycles and for varying dilution, injection timing and ignition timing failed to correlate this measure of liquid fuel with the incidence of unstable combustion in the Gen 1 optical engine.

High-speed planar Mie-scattering imaging of the fuel spray in the Gen 1 engine using a long-distance microscope, illustrated in Figure 18, showed substantial cyclic variability in the fuel spray as it approaches the spark plug. Variability observed included the spray angle and significant small scale (~1–2 mm) non-uniformities in the liquid distribution, as gauged from the Mie-scattering intensity, which is a measure of total droplet surface area for droplets in the ~15μm range produced by the multi-hole injectors used here. Such fluctuations have been linked to unsteady cavitation within the injector nozzle holes.[35, 80] However, as discussed in detail in [48], neither spray-angle fluctuations (observed within individual cycles as well as from cycle to cycle) nor liquid-distribution non-uniformities correlated with the incidence of misfires or partial burns in the Gen 1 engine. This is in contrast to an earlier study in a SGSC engine using an outwardly opening piezo-electric injector that found spray-angle fluctuations to correlate with combustion instability.[81]

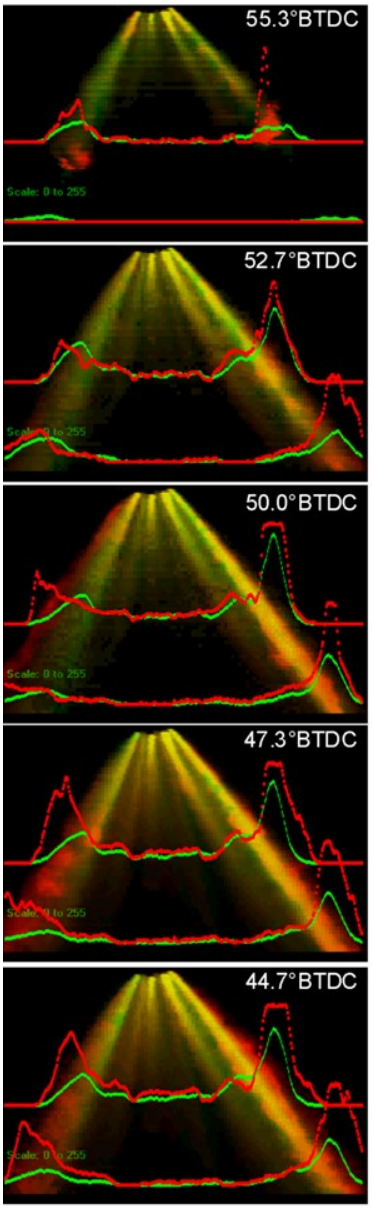

Figure 18. Selected high-resolution planar Mie-scattering images of the fuel spray from one engine cycle (red) overlaid on corresponding images of the ensemble average of 100 continuously fired cycles at the same crank angles (green). With this representation, a spray image would appear yellow throughout if the individual-cycle and ensemble-average images agreed perfectly. Mie-scattering intensities along lines perpendicular to the cylinder axis are plotted at two distances from the injector. The field of view is 9 mm high, and the spark plug is just out of the field of view at the lower right. The individual-cycle images for this cycle show a wider spray angle than seen in the ensemble average. All cycles showed a much less uniform liquid distribution approaching the spark plug than the average[82].

Spark and equivalence-ratio fluctuations

One potential suspect in combustion instability is the incidence of restrikes which, as Figure 10 illustrates, can be frequent in SG engines. A restrike might detach a nascent flame

kernel from the spark channel and thereby deprive it of further energy input, or the spark plasma created by a restrike might be in an unfavorable (e.g., fuel deficient) zone. For more-or-less optimized injection and spark timings, however, extensive attempts to relate the frequency of restrikes to combustion instability have also failed.

In view of the stress placed earlier on the role of the extended spark channel in SG ignition and the fact that spark duration and energy, equivalence ratio and flow velocity all exhibit significant variations from cycle to cycle, one might well suspect combustion instability to correlate to one or more of these properties, either separately or in combination. In all the experiments conducted in our laboratories over several years of intensive investigation, however, no straightforward correlation of this type has emerged. Figure 19 illustrates the situation for SG combustion with strong and dilute mixtures (0 and 26% of air replaced with nitrogen, respectively) in the UM optical engine (Figure 5). Misfires, partial burns and normal-combustion cycles are all scattered randomly and span the same ranges in the plots of spark energy vs. spark duration (Figure 19a,b) and local equivalence ratio vs. local velocity (Figure 19c,d)[50]. For low dilution (Figure 19a,c), there is a slight association of partial burns and misfires with low equivalence ratio and low velocity as measured at spark onset and within the 4×4-mm square region indicated by dashed lines to the right of the spark gap in Figure 5. At the highest dilution (Figure 19b,d), this preference no longer exists, but misfires and partial burns still occur across the population of well burned cycles. An important observation is that *in all misfires and partial burn cycles, flame kernels were observed at and immediately after ignition but did not evolve to robust combustion*. With an exception for an unusual operating condition to be discussed next, flame kernels were also always observed in the Gen 1 and Gen 2 data.

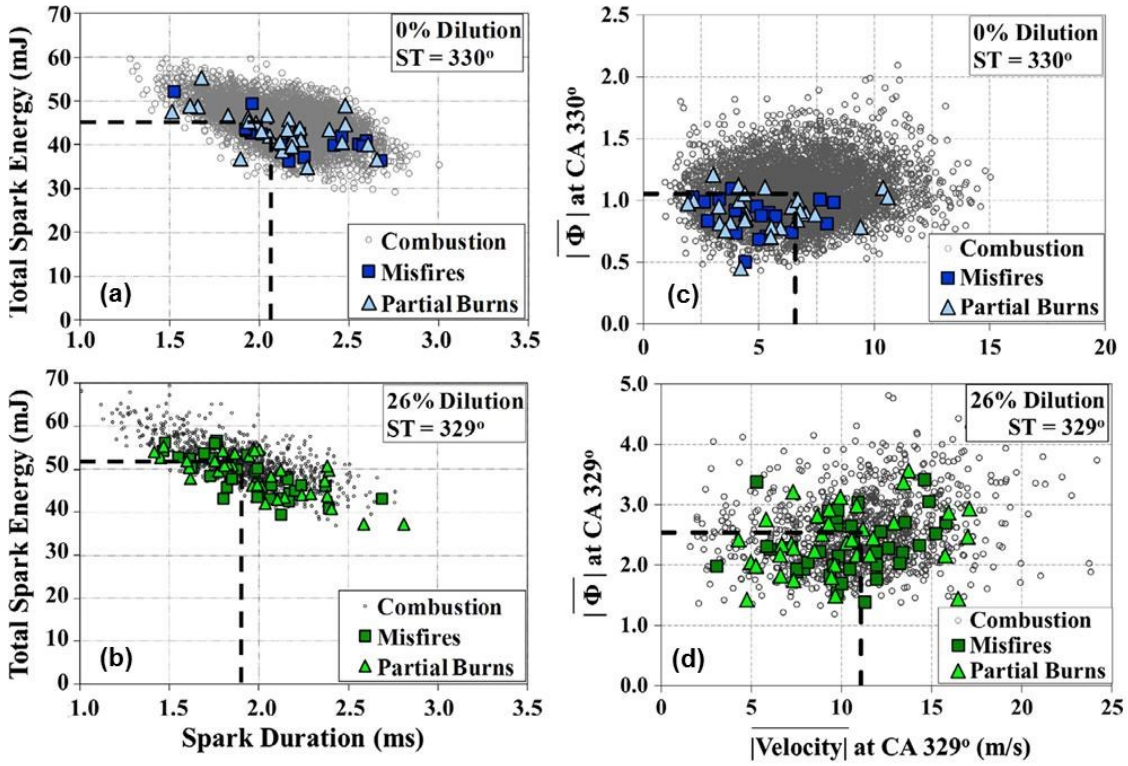

Figure 19. Conditions near the spark gap for dilute SG combustion in the UM optical engine: (a, b) spark energy vs. spark duration; (c, d) equivalence ratio and spatial mean velocity evaluated in the 4×4-mm square region indicated by dashed lines to the right of the spark gap in Figure 5. For all cycles, a flammable mixture exists. No consistent distinguishes misfires and partial burns from normal combustion cycles. Conditions: 45 mJ mean spark energy with (a, c) 0% nitrogen dilution and spark timing 329° = 31°BTDC; (b, d) 26% nitrogen dilution and spark timing 329° = 31°BTDC. Dashed lines indicate the ensemble average values. Adapted from [50].

Overadvanced ignition. A notable and instructive exception to the statements of the preceding two paragraphs can occur if the spark is fired well before the start of injection[45] ("head ignition"). Figure 20 contrasts an extreme example (spark timing 62°BTDC) with the optimum spark timing of 34°BTDC for 15% nitrogen dilution in the Gen 2 optical engine. For both spark timings, the commanded end-of-injection (EOI) was 40°BTDC and the physical start of injection (SOI), when fuel emerged from the injector, was about 47°BTDC. Figure 20a shows very stable combustion for the optimum 34° spark advance [COV(IMEP) = 1.8%]. For the greatly overadvanced 62°BTDC spark timing, all cycles burn well except for a small number of total misfires.

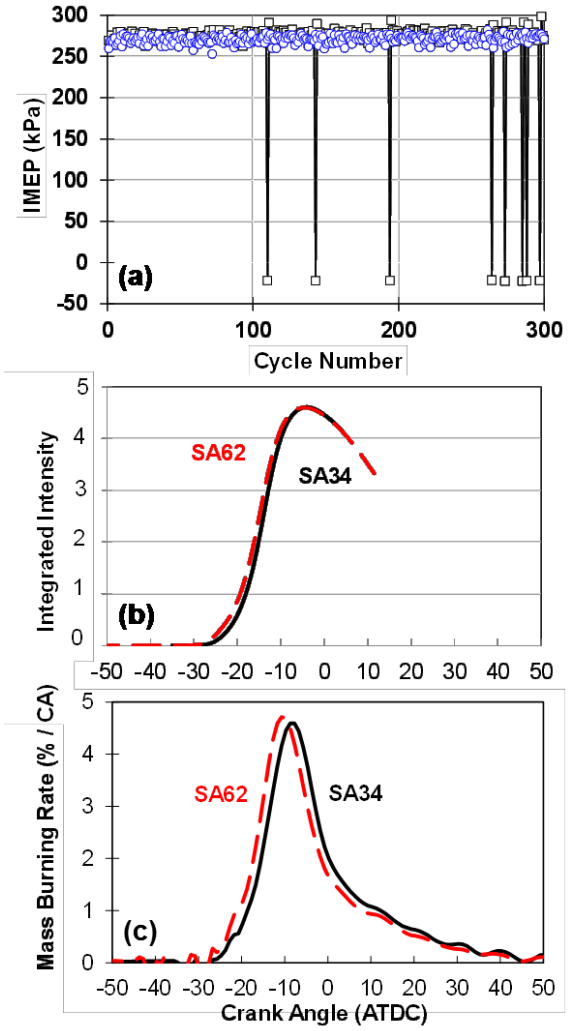

Figure 20. **(a)** Combustion stability, **(b)** spatially integrated combustion luminosity (viewed through the piston-bottom window) and **(c)** mass-burning rate in the Gen 2 optical engine with 15% nitrogen dilution for two spark advances (SA): the optimum timing of 34°BTDC and a greatly overadvanced timing of 62°BTDC such that the spark is fired well before the start of injection. In **(a)**, open blue circles denote the 34° spark advance and open black squares denote 62° spark advance. Note that the misfires are followed by cycles with slightly higher than average IMEP due to unburned fuel retained in the cylinder. Adapted from[45].

Because the 62° spark advance is before the start of fuel injection, the early spark channel is stretched relatively gradually by the turbulent in-cylinder flow (e.g., Figure 10 upper). However, as the spray reaches the spark plasma, the strong spray-induced flow (and perhaps spark interaction with liquid droplets) leads to multiple, very rapid restrikes (similar to but sometimes more violent than in the lower portion of Figure 10) in all cycles. During the most intense spray-spark interaction, spark luminosity is observed, but no flame kernel develops because the proper combination of local equivalence ratio and turbulence intensity is not present;

the discussion associated with Figure 13 suggests that this is because the mean velocity and turbulence intensity are too high. The ensemble- and spatially-averaged sodium-enhanced combustion luminosity and heat-release data in Figure 20b,c show that, on average, sustained ignition does not occur until about 28°BTDC, i.e., the about the same time that successful ignition is observed for the optimal 34°BTDC spark timing.

This behavior originates in the fact that, as illustrated in Figure 10, strong spray-spark interaction and extensive restriking deplete the available spark energy more rapidly and shorten the spark duration compared to less severe conditions. High-speed imaging shows that for the optimal spark timing of 34°BTDC in Figure 20, the spark is fired roughly 0.6 ms after the spray arrives at the electrodes whereas for the overadvanced spark timing of 62°BTDC, the spark is fired roughly 1.5 ms *before* the spray arrives. The spark durations illustrated in Figure 10 are 2.15 and 1.3 ms, however, so it is not surprising that for the misfire cycles in Figure 20a, insufficient spark energy remains to ignite the mixture by the time that favorable equivalence ratio, velocity and turbulence intensity conditions finally prevail near the end of the injection event. In other words, for the very early spark timing, combustion is either near optimum (because the mixture will be rich and the N_2 dilution level here is moderate) if adequate spark energy is still present or a complete misfire *without formation of a flame kernel* if it is not. Note that this is the *only* situation in which we have observed misfires without flame-kernel formation in multi-hole SGSC engines.

The highly overadvanced spark timing in Figure 20 represents an extreme example of "head ignition," i.e., trying to ignite the head of the spray as it approaches the spark gap, in contrast to the more usual situation of "tail ignition" in which much or all of the spray has passed the spark gap before the spark is fired. Head ignition will be discussed later in connection with recent SNL results on SG combustion using ethanol-dominated fuel blends[56-58].

Prior-cycle effects

A question that naturally arises – especially in engines with a high residual fraction – is the extent to which successive cycles are coupled. This is assessed using the return map in Figure 21, in which the IMEPs of successive cycles are cross-plotted[50]. Figure 21 employs a large statistical ensemble including a range of dilutions and spark timings from the UM optical engine. In general, misfire and partial-burn cycles (identified here on an IMEP basis rather than using final

mass fraction burned) are preceded and followed by normal cycles, except for the most dilute case where two poor cycles occur in succession. For these most dilute cases, overall combustion stability is poor enough [COV(IMEP) up to 36%] that two poor cycles in a row could well occur for a completely random process.[50] A slightly stronger-than-normal cycle typically follows a misfire due to unburned fuel retained in the cylinder (this is very apparent with the isolated misfires in Figure 20a). Statistically, misfires and partial burns are rare (~1% or less) random events that are not significantly coupled to the preceding cycle.

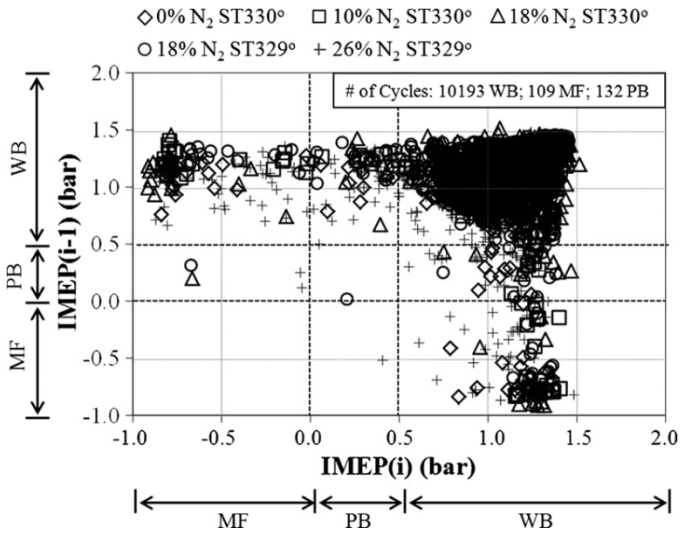

Figure 21. Return map in which IMEP values for all cycles are plotted against IMEP values of the preceding cycle for several dilution levels and spark timings (ST). Misfire (MF), partial burn (PB) and well burning (WB) IMEP ranges are indicated along the axes. All but 6 poor burning cycles are preceded by normal cycles, implying that statistically, misfires and partial burns are rare (~1%) random events that are not significantly coupled to the preceding cycle.[50]

Early flame-kernel motion

Substantial new insight into sources of combustion instability in SGSC engines has come from high-speed imaging over thousands of individual engine cycles to follow the motion of the early flame kernel relative to the measured or simulated fuel-distribution. Here we find it convenient to trace the clues systematically through the GM and UM engine studies.

Gen 1 engine. Broadband imaging of the spark channel and early rich combustion revealed distinctive features of misfire cycles[47]. Figure 22a shows a RANS simulation of the fuel distribution (represented by the green $\phi = 1$ isosurface) and early combustion using the earlier GMTEC code[34, 49]. The simulation predicts that the flame kernel must move (propagate and

advect) downward to reach the bulk of the fuel, which is located well down in the piston bowl. Below, in Figure 22b, are typical broadband images of broadband luminosity from early rich combustion in four normal, well burning cycles with 30% nitrogen dilution selected from a set of 2000 consecutive cycles recorded at 60 kHz frame rate together with cylinder-pressure data and spark voltage and current. (Note that the bottom of the cylinder-head window limits the view into the piston bowl.) Figure 22c shows broadband images for all four total misfire cycles in the 2000-cycle ensemble. A striking difference between the good-combustion and misfire cycles is that for all the misfires, the spark and early rich combustion moved *upward*, away from the expected location of the bulk of the fuel in the piston bowl.

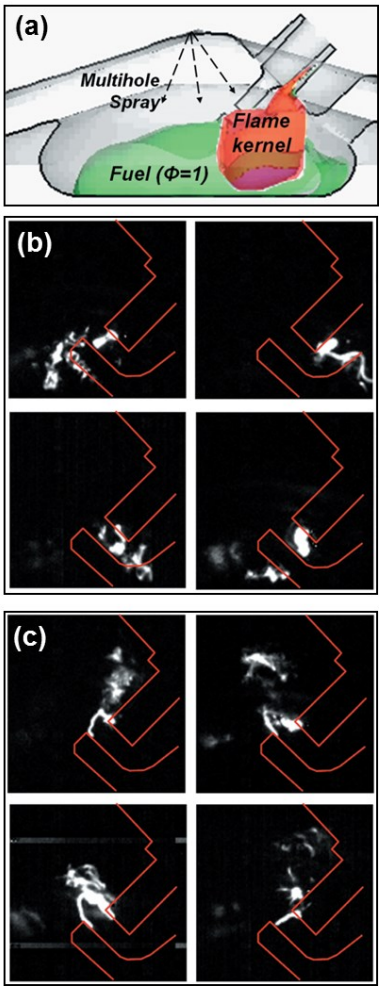

Figure 22. (a) CFD simulation of fuel distribution and early flame kernel in Gen 1 optical engine. **(b)** Broadband visible-wavelength images of the spark and early rich combustion taken from four normal cycles of a high-speed digital video of 2000 cycles (30% nitrogen dilution). (c) Broadband visible-wavelength images for all four misfires out of the same set of 2000 cycles. Adapted from [47].

Increasing the nitrogen dilution from 30 to 34% led to six misfires in a set of 1000 cycles. Figure 23 shows the path of the geometric centroid of the spark and early rich combustion luminosity identified by analysis of 60 kHz image sequences for these six misfires over a 2.5 ms period. Again, these results strongly suggest that for all the misfires, the early flame failed to propagate downward towards the bulk of the fuel.

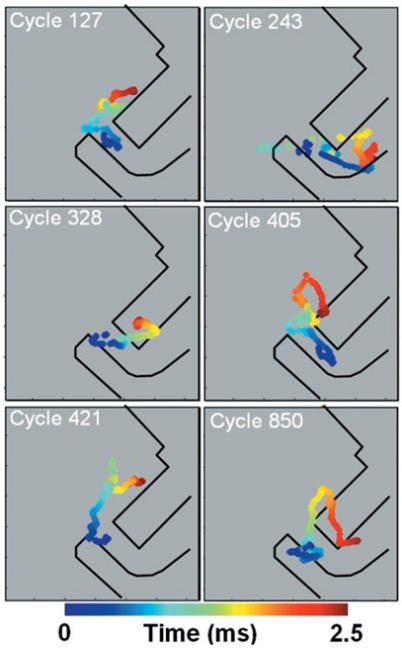

Figure 23. Paths followed by the centroid of the spark and early rich combustion luminosity for six misfire cycles at 34% nitrogen dilution in the Gen 1 engine[47]. Most of the fuel is expected to be located below the field of view as shown in Figure 22a.

Conditioning the same image-tracking analysis on IMEP to separate good burns from poor burns (misfires and partial burns) for the 30% dilution case yielded the statistical representation in Figure 24, in which histograms of the horizontal and vertical displacement of the spark and rich combustion luminosity centroid are plotted along the borders of representative images. The relevant portion of the CFD simulation from Figure 22a is also shown on the same spatial scale and aligned with the combustion images. A large fraction of the poor-burn cycles (IMEP < 1 bar) as well as all of the misfires exhibit spark and early rich combustion luminosity that moved upward rather than downward.[47] (The restricted field of view causes the histogram for downward-moving luminosity centroids to terminate slightly above the bottom of the cylinder-head window.)

These observations imply that, for part-load operation with a highly stratified charge and heavy dilution in the Gen 1 engine, *unfavorable motion of the spark and early flame kernel is a*

significant (probably dominant) source of rare, random misfires and an important factor in poor burns.

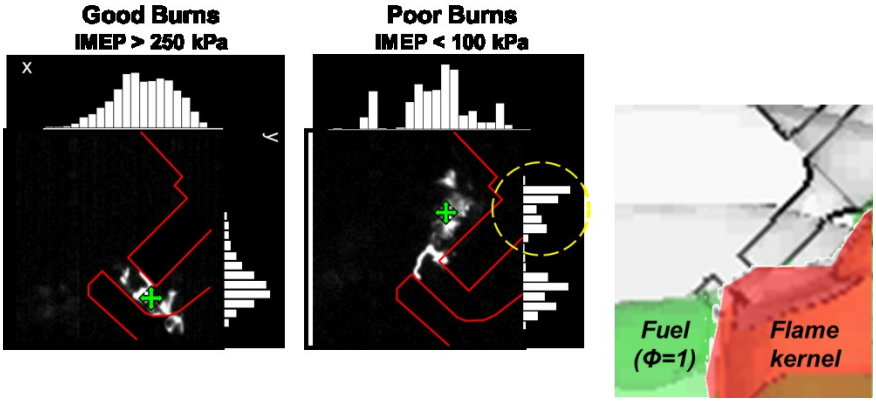

Figure 24. Conditional histograms of the rich-combustion image centroid location from 20–30° (1.67–2.5 ms) after spark initiation for 30% nitrogen dilution together with numerical simulation results for the same spatial region. The small green crosses mark the centroid in the sample images. The dashed yellow circle highlights the poor-burn cycles that exhibit spark and early rich combustion zones that failed to move downward toward the expected location of the fuel in the bottom of the bowl.[47]

Gen 2 engine. Conditional analysis of high-speed (12 kHz) planar Mie-scattering imaging of early combustion in the Gen 2 optical engine complements and reinforces this scenario[47]. With this approach, burning regions are indicated by the disappearance of the silicone-oil seed particles that scatter the high-repetition-rate laser light. This provides a more complete picture than the broadband (350–800 nm) imaging which is insensitive to combustion leaner than $\phi \sim 2$. To provide a statistical representation, the results are depicted as flame PDFs.

Figure 25 shows flame PDFs conditioned on IMEP for four crank angles with 30% N_2 dilution.[47] The PDF representation differs somewhat from Figure 16. In Figure 25, the probability of flame is shown in shades of red (from 0 in black to 100% in fully saturated red) together with superimposed contour lines. The green-shaded regions in the upper left of the images represent relatively bright Mie-scattering that may be due to residual spray droplets, non-uniform distribution of the scattering particles induced by the piston motion or the flame, or scattering from soot. The flame development for good-burning cycles is consistent with the in-cylinder charge motion predicted by numerical simulations[34, 49]: the flame first emerges on the right of the spark gap, then propagates to the right and downward into the piston bowl (beneath the field of view), and finally reappears moving upward to the left of the spark electrodes. The

flame PDFs for the poor-burning cycles (IMEP < 1 bar) show a propensity for propagation up toward the cylinder head (e.g., crank angle –10°ATDC) as well as overall slower flame growth.

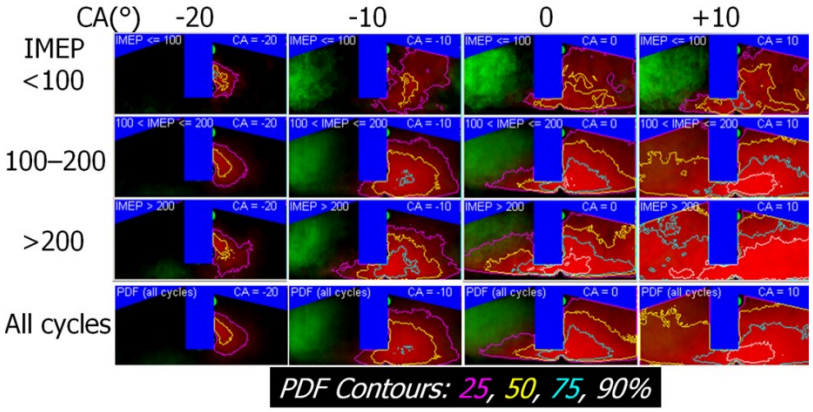

Figure 25. Flame PDFs conditioned on IMEP (in kPa) at four crank angles for operation with 30% nitrogen dilution.[47] The bottom row shows the unconditioned PDF accumulated over all cycles.

A brief word of caution: although planar images such as Figure 25 provide quantitative measurements of flame growth in the plane of the laser sheet, they do not give a complete picture of overall flame growth due to out-of-plane motion. Flame kernel motion is driven by a combination of convection velocity and local burning velocity, the latter of which responds strongly to local equivalence ratio and turbulence [recall the Karlovitz-number and crossover-temperature (chemistry) criteria discussed earlier].

The interaction of the spray, gas flow field and flame kernel with the spark electrodes leads to differences in flame development with different spark-plug designs. Figure 26 compares early combustion (here with 25% N_2 dilution) with a three-ground-electrode spark plug to the J-gap plug design used in all the rest of our experiments.[47] Factors that likely differ between the two plug geometries include different equivalence-ratio distributions and different out-of-plane convection velocities. Both of these would reflect the different spray/spark-plug interactions and different blockage of the in-cylinder swirl and tumble flow. Overall, the three-ground plug appears more susceptible to early flame growth up toward the cylinder head, which in this instance has two deleterious effects: reduced likelihood that the flame kernel will reach the fuel in the piston bowl and increased heat loss from the flame kernel to the electrodes. Note, however, that the three-ground-electrode spark plug in Figure 26 was simply substituted in the Gen 2 engine with no attempt to optimize the local flow to allow the early flame kernel to escape.

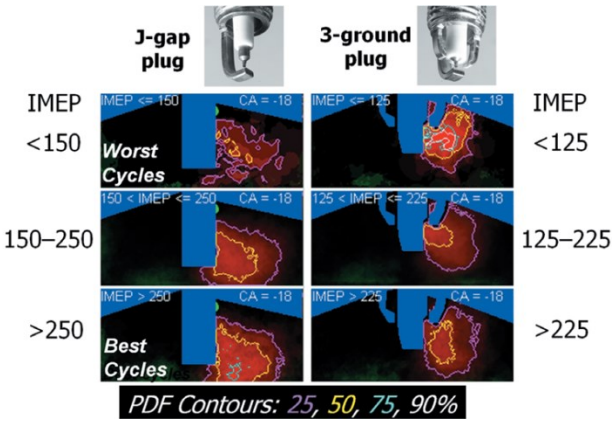

Figure 26. Conditional analysis of early flame development using flame PDFs for two spark-plug geometries (25% nitrogen dilution).[47]

High-speed (4.8 kHz) PIV measurements in the Gen 2 engine reveal local flow structures that vary significantly from cycle to cycle and that have sufficient strength and duration to affect the convection of the spark plasma and early flame kernel, as illustrated by three excerpts from one fired cycle in Figure 27[45]. The end-of-injection command was at 40°BTDC. The spark, initiated at 34°BTDC, is visible between the ground and center electrodes at 30°BTDC and is clearly stretched upward and to the right by a small, relatively strong structure at 20°BTDC. The upward flow continues and strengthens at 10°BTDC, where it is accompanied by bright luminosity due to locally rich combustion.

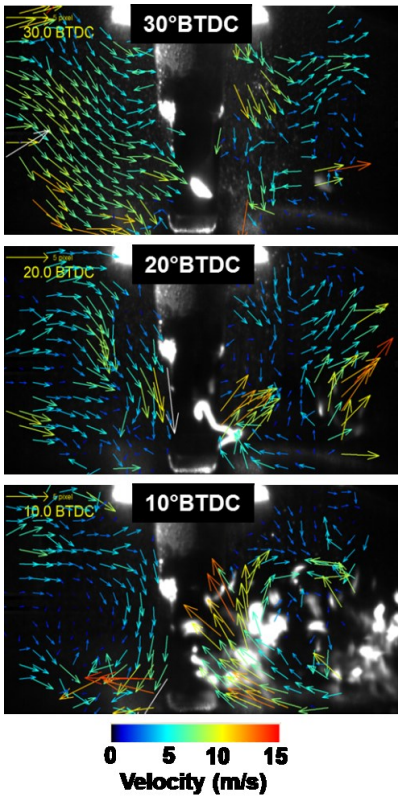

Figure 27. Example of high-speed PIV measurements of the velocity in the plane of the spark gap in one fired cycle of the Gen 2 optical engine. Adapted from[45] . At the 4.8 kHz measurement rate, successive velocity measurements were separated by 2.5° crank angle.

UM optical engine. High-speed planar Mie scattering was also used to track flame-kernel development in the UM optical engine, but the results are more complete and quantitative than in the Gen 1 and Gen 2 engines because they include simultaneous measurements of the flow field and the equivalence-ratio distribution using PIV and PLIF, respectively. The UM optical engine also provides full side-view optical access to the interior of the piston bowl (Figure 5).

Representative individual-cycle image sequences for well burning, partial burn and misfire cycles are shown in Figure 28.[50] The selected test condition (18% nitrogen dilution, spark timing 329°) provides a reasonable value of average IMEP (0.99 bar) and sufficient combustion variability (COV(IMEP) 14%) to provide a statistically useful population of partial burns and misfires without such severe deterioration of combustion that outlier cycles routinely occur in succession.

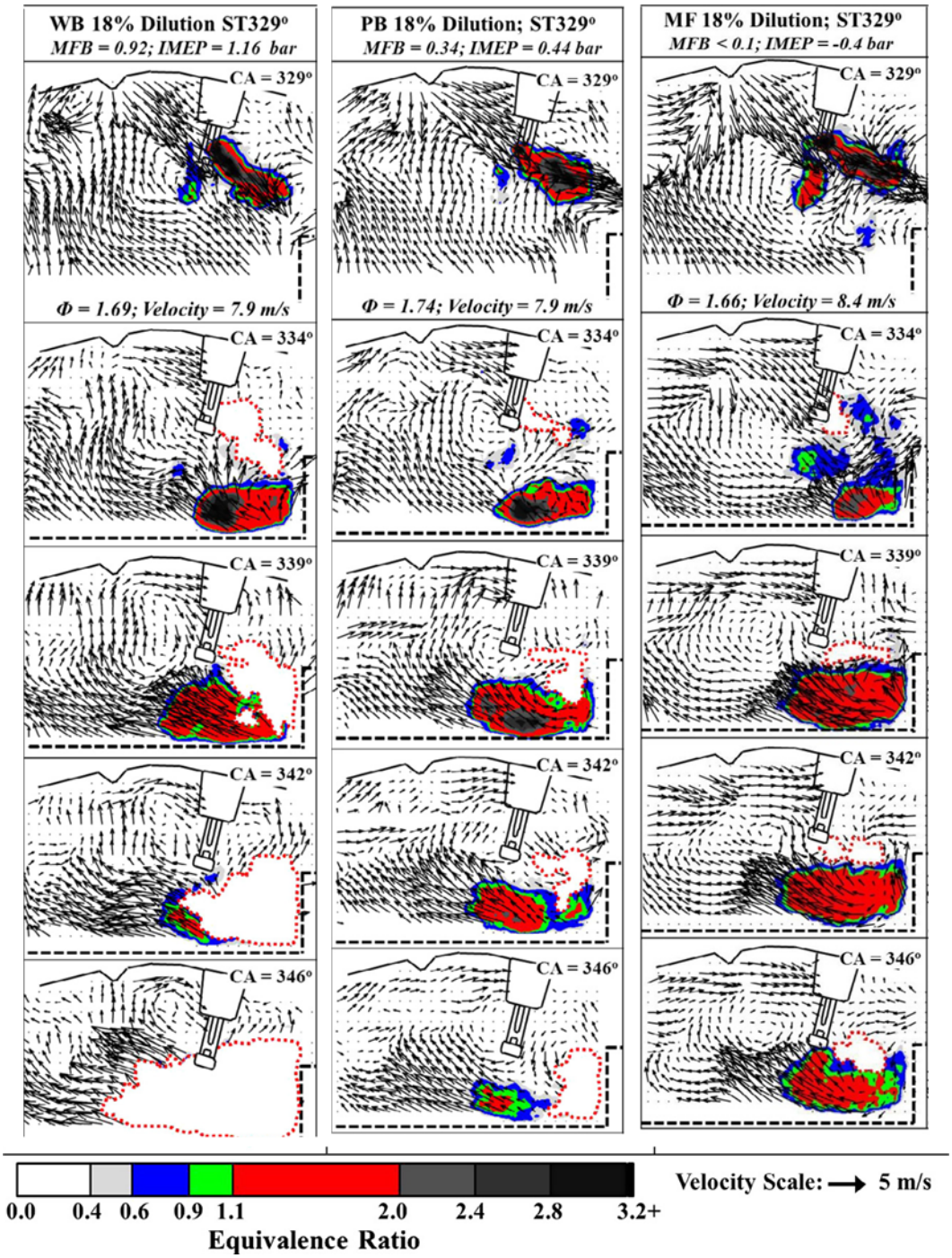

Figure 28. Measurements showing the evolution of the equivalence ratio distribution, flow field, and flame kernel within selected individual well burning (WB), partial burn (PB) and misfire (MF) cycles for the same operating condition (18% N_2 dilution, spark timing 329°) in the UM optical engine. The flame kernel is identified by the absence of Mie scattering from the PIV seed particles and is indicated by the white area surrounded by the dotted red line. Labels at the top of each column give the final mass fraction burned (MFB) and the IMEP for each cycle. Also labeled below the top images are the values of equivalence ratio and velocity magnitude in a 4×4-mm are to the right of the spark gap (see Figure 5). Adapted from [50].

The physical end of injection is at 328°, and when the spark is fired at 329°, all three cases in Figure 28 show strong spray-induced flow along with a fuel plume that has penetrated through the gap. Furthermore, all three cases had nearly the same velocity magnitude and equivalence ratio in the 4×4-mm region used to assess these properties near the spark gap (Figure 5). Five and ten degrees later (CA = 334° and 339°), each case shows a flame kernel and a persistent region of flammable mixture where the fuel plume has impacted the side wall of the piston bowl. However, substantial differences in flame development are apparent. For the well burning cycle, the flame propagates rapidly down the fuel plume into this flammable mixture, whereas for the partial burn and misfire, the kernel remains near the spark gap while transport and mixing lean out the nearby mixture, further retarding the kernel's progress toward the fuel in the lower right corner of the bowl as that fuel continues to mix out.

The velocity fields are quite complex, but some cycles exhibit convective velocities that direct the flame kernel away from the flammable mixture in the lower right of the bowl[50], consistent with the evidence above from the Gen 1 and Gen 2 engines. Figure 29 shows a misfire with *no* dilution, so that one would expect relatively strong flame propagation in the absence of competing effects. In this example, however, strong upward motion appears to push the flame kernel away from the flammable mixture directly beneath the spark plug. Under the influence of this continuing upward flow, the flammable mixture eventually reaches the flame kernel, but the mixture becomes leaner as time progresses and little flame development results (6% final mass fraction burned). An analysis of strain rates and vorticity around the flame kernel showed no correlation with successful or unsuccessful flame growth[83], further strengthening the observation that *low flame speeds in lean regions and convective mismatch of the flame kernel and the stratified fuel cloud are major contributors to failing cycles in SGSC engines*, at least with multi-hole injection.

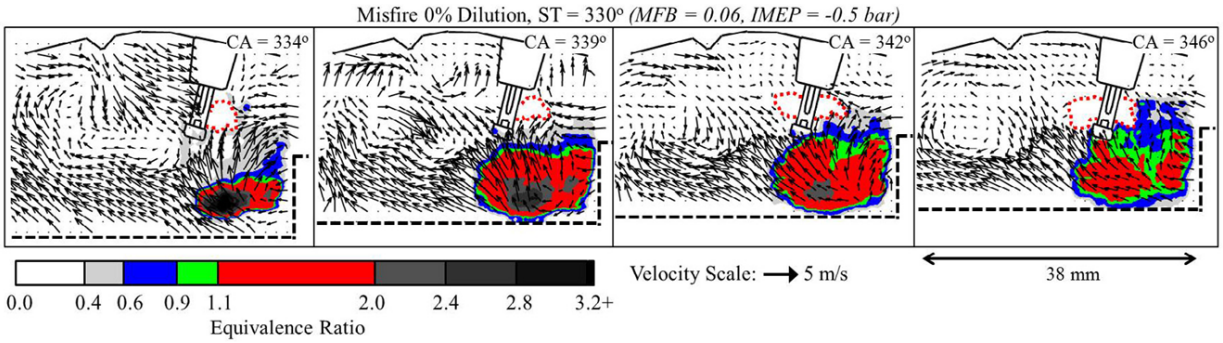

Figure 29. Image sequence for a misfire cycle (spark timing at 330°, 0% dilution) shows that convection velocities can impede flame development by directing the flame in the opposite direction of the flammable mixture.[50]

To characterize flame-kernel growth statistically, Figure 30 shows two-dimensional flame (burned-gas) probability distributions evaluated from the planar Mie scattering from the PIV seed particles.[50] The results here are again for the case of 18% N2 dilution and 329° spark timing, and again the three columns represent well burning, partial burn and misfire cycles. Together with Figure 28, these burned-gas PDFs make clear that successful combustion requires the flame kernel to "chase the tail" of the fuel plume that has passed through the spark gap to reach the bulk of the fuel in the piston bowl. Kernel growth is much faster and more consistent for well burning cycles than for partial burns and misfires.

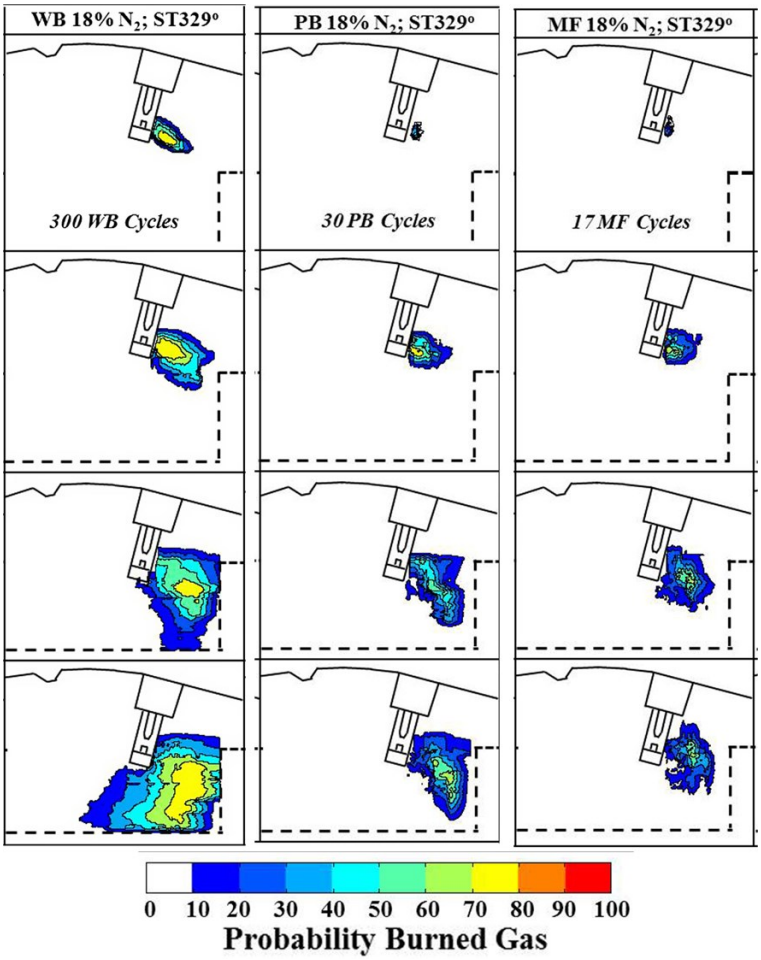

Figure 30. Statistical representation of flame-kernel development for well burning (WB), partial burn (PB) and misfire (MF) cycles at the 18% N_2 dilution level. The number of cycles used to form each two-dimensional PDF of burned gas is labeled on the top image of each column.[50]

The results from the three spray-guided engines studied systematically here indicate that combustion instability is dominated by factors that delay or inhibit the flame kernel from propagating into the main stratified fuel cloud while allowing that stratified fuel cloud to lean out due to transport and mixing. In these multi-hole-injector SGSC engines, *poor cycles are indeed characterized by combustion failure and not ignition failure since an initial flame kernel has been observed in all cases* with reasonable injection and ignition timings. Of course, as Figure 20 illustrates, one can create conditions such that a flame kernel never forms, but that is not the case for the rare, random misfires and partial burns observed with the injectors and spark-plug geometries used here to reach the conclusion just stated.

Specific factors for combustion instabilities identified here are (1) convective flow fluctuations that impede motion of the flame kernel toward the bulk of the fuel, (2) low flame speeds due to locally lean mixtures adjacent to the kernel, and (3) retarded ignition kernel development allowing further lean mixing. The earlier discussion of ignition and flame propagation under spray-guided conditions – in particular the strong favorability of rich conditions and the suppression of laminar flame speed for lean conditions that are predicted for small, highly diluted flame kernels (Figure 14) – suggest that locally lean mixtures may affect early flame kernels even more strongly than one might expect from intuition based on classical planar premixed flames. Overall dilution (with EGR in "real" engines and simulated here with nitrogen) reduces flame speed and exacerbates the effect of the factors identified here.

Double-pulse injection

Multi-pulse injection has been used with both multi-hole injectors and (as we shall review later) with outwardly opening piezo-electric hollow-cone injectors to improve SGSC combustion stability, although the information available in the open literature is less complete and systematic than that discussed above for single-injection SGSC with multi-hole injectors. The overview here is based primarily on the paper of Yang, Solomon and Kuo,[61] which compares numerical simulations with experimental cylinder-pressure and heat-release results for an 800-RPM idle-like condition similar to that in the UM experiments above. The engine design is quite close to the Gen 2 optical engine. The simulations differ from the SparkCIMM G-equation approach outlined above in several respects: the underlying code (Converge), the ignition model (a

moving-sphere energy source), the chemical kinetics (the University of Wisconsin PRF reduced kinetics scheme with n-heptane removed), and the flame model (detailed kinetics on a locally fine-mesh grid). However, the agreement of the simulated and experimental heat-release results is reasonable, and the overall picture agrees with earlier high-speed Mie-scattering imaging of single and double injection under similar conditions. For details, we refer to the original paper.[61]

Figure 31 compares results of the simulation for single and double injection; here the crank angle of firing TDC is taken as 720°. Injection and ignition timings differed slightly for the two cases to reflect the optimized experimental settings. In the double-injection case, the spark was fired about a degree before the physical start of the first injection, which reflects the need for the flow to stretch the spark plasma out from the plug electrodes. Solid color contours show the equivalence ratio ($0 < \phi < 2$). Liquid-phase fuel, both free spray and on the piston surface, is shown by bright red droplet parcels, and the flame is represented by a purple 1500 K temperature iso-surface. The liquid fuel and the 1500 K iso-surface are shown in 3D while the equivalence-ratio contours are shown on a cutting plane through the cylinder axis. The spark plug is offset behind this cutting plane so that only two small (white) portions are visible as they protrude through the cutting plane. Note that the crank angles of the last three images in each sequence are different for single and double injection.

For both single and double injection, a small (purple) flame kernel is visible near the center of the field of view around CA = 699° and 701°, although for double injection it is partially obscured at 699° by the trailing portion of the spray from the first pulse. With single injection, as described above, the flame kernel must chase the tail of the fuel plume downstream into the piston bowl. With double injection, the first spray (with just less than half the total fuel here) carries less momentum and generates less turbulence (Figure 32), thereby providing a more benign environment for flame-kernel formation. After the second injection (707°), the flame develops significantly more rapidly for double injection, as shown by the purple 1500 K iso-surfaces at 717°. Overall, both the simulation and the experimental results show a nearly twofold increase in the heat-release rate (Figure 32) and reduced fuel consumption with double injection, while the experiments also exhibit improved combustion stability and reduced hydrocarbon and soot emissions.

Correspondingly, the simulations show that, relative to single injection, double injection:

- reduces spray penetration and thereby greatly reduces piston wetting by virtue of the reduced spray penetration (5% of the total fuel on the piston with single injection vs. 0.05% for double injection), a clear benefit in terms of engine-out soot emission;[22]
- contains the fuel vapor more effectively within the piston bowl (e.g., the equivalence-ratio contours at CA = 711° show less fuel moving out of the bowl toward the cylinder head with double injection), which affects both flame propagation and unburned HC emissions;
- increases the overall burning rate and improves combustion stability by
    - delivering rich mixture to the flame kernel formed from the first injection;
    - reducing sensitivity to fluctuations in the propagation direction of the early flame kernel by imposing a strongly directed, relatively well organized flow that drives combustion down into the bowl where most of the fuel ultimately resides;
    - reducing turbulence intensity during initial flame-kernel formation but increasing turbulence intensity and thereby increasing the overall burning rate after the second injection (Figure 32) when the flame kernel is more robust.

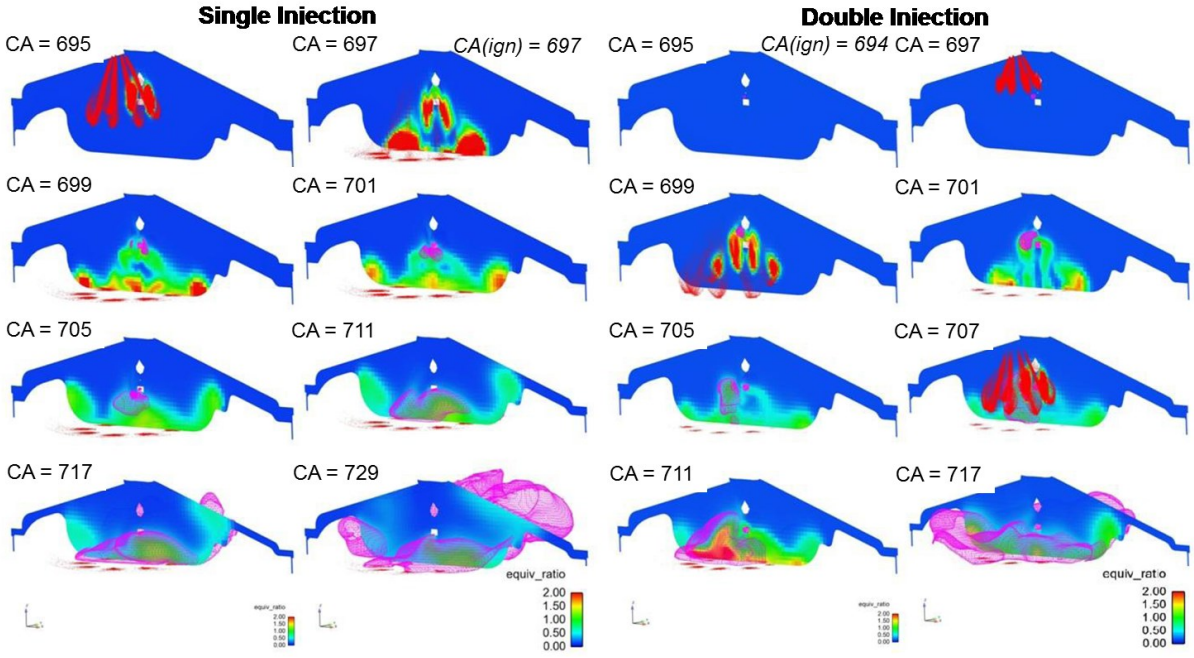

Figure 31. Numerical simulation of mixture formation, ignition and early-stage SGSC combustion with single- and double-pulse injection with a multi-hole injector. Adapted from [61].

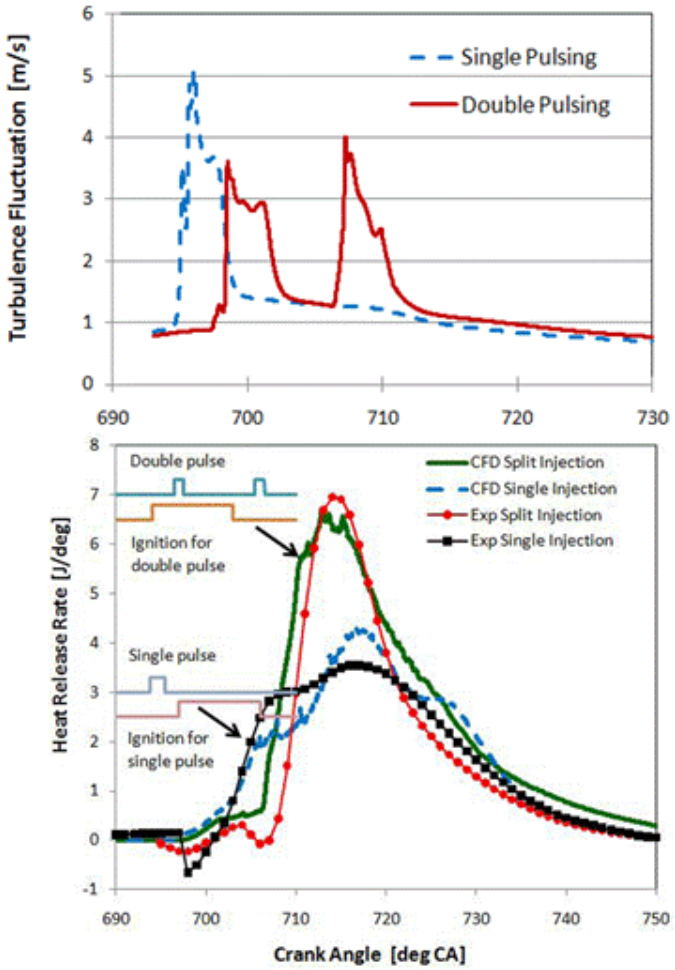

Figure 32. (a) Turbulence intensity at the spark gap ***(upper)*** and comparison of measured and simulated heat-release rates for single and double injection ***(lower)***. Adapted from [61].

Multi-hole-injection SGSC combustion with ethanol-gasoline blends

The use of ethanol, an oxygenated biofuel, in spray-guided engines has been the focus of studies at the SNL Combustion Research Facility[55-58]. Earlier research had shown NOx reduction with SGSC operation on ethanol-gasoline blends,[84, 85] especially for E85 in combination with retarded injection timing.[86] The SNL work achieved exceptionally low engine-out emissions of both soot and NOx (within the legislated limits) at a specific light load (1000 rpm, 260 kPa IMEP) using exceptionally late injection (near-TDC); however, achievement over a broader range at higher loads was inhibited by combustion instability. Continuing studies have therefore focused on the sources of combustion instability. Although the SNL objective was to assess the impact of ethanol fueling on SG engine operation, the study relied on comparisons between the use of gasoline and gasoline-ethanol blends (E0-E100), thereby providing insights that are useful for

understanding the combustion of both fuels. The review here will follow the logic of the previous sections, summarizing first the impact of the ethanol on stable combustion (relative to gasoline) and then turning to sources of combustion instability.

Stable SGSC combustion with ethanol-gasoline blends

As also described previously, stable combustion of the gasoline and ethanol blends was explored in the all-metal version of the SNL optical engine by systematically varying the injection and spark timing, thereby allowing the engine geometry and in-cylinder flow to determine the best timing for mixing, ignition, and combustion. As with the other multi-hole-injection engines in this paper, the lowest-emission, stable SGSC operation with gasoline used "tail ignition", i.e., the end of injection (EOI) and with spark timing (ST) such that the spark was fired as the end of the liquid spray passed the spark plug. In contrast, stable operation on E85 fuel with extremely low NO and soot emissions was achieved with "head ignition" in which the start of injection (SOI) was near TDC (5°BTDC) and spark timing was before the fuel left the injector. Successful head ignition of ethanol is consistent with head ignition of gasoline in the Gen 2 optical engine,[45] as summarized in connection with Figure 20, but the gasoline SOI was much earlier (physical SOI ≈ 48°BTDC). What is most remarkable in this work was the ability of the ethanol-dominated fuel to mix well and burn well from very early to near-TDC SOI timings, which resulted in very low soot and NOx.

This remarkably different combustion behavior led to comparison of properties between ethanol and gasoline that significantly affect the spray vaporization and mixing. Ethanol has oxygen in the fuel, lower heat of reaction, and higher latent heat of vaporization. Ethanol's lower heat of reaction requires more fuel at a fixed load and therefore requires either higher injection pressure or longer injection duration, either of which was hypothesized to increase turbulence and mixing.[55] The high latent heat of ethanol means that more in-cylinder air must be entrained to provide the enthalpy to evaporate the liquid. Therefore, once the ethanol has evaporated, the fuel-air-residual mixture will not be as rich as with gasoline, all other factors being equal. Modeling comparisons[55] of ethanol and isooctane (as a gasoline surrogate) demonstrated that the ethanol will have an equivalence ratio of 5 when sufficient air has been entrained to evaporate the liquid, compared to $\phi = 15$ for isooctane. Thus, once the ethanol has evaporated it will be locally leaner and, of course, create a locally cooler charge. In addition, the late injection of the

ethanol at higher gas density and temperature means greater entrainment of air and diluent, shorter liquid length, and lower penetration needed to achieve an equivalence ratio that can sustain combustion.[55] Furthermore, the momentum imparted by the spray into the bowl will be higher during the combustion near TDC and soon thereafter.

Regardless of the fuel, the magnitude and turbulence of the flow is expected to significantly affect the overall burning rate of SG combustion through fuel-air mixing and local burning rates of partially premixed regions. The spray momentum from the late injection is expected be a major contributor to the flow momentum near TDC due to the high velocity and high density of the liquid spray and the short time available for the momentum to dissipate. The larger injected mass and late injection and spark timings achievable with the ethanol make it a useful tool to evaluate the effect of spray-momentum on mixing and dissipation.

A glimpse into the relative contributions of the in-cylinder gas momentum (created by the intake and compression strokes) and the spray-induced momentum to burning rates was revealed by the heat-release analysis of Sjöberg, Zeng & Reuss.[57] There the in-cylinder gas momentum was varied by changing engine speed. Figure 33 compares the average apparent heat release rate (AHHR) for well mixed (early injection, EOI = 300°BTDC) and SGSC combustion. These tests were performed with fixed combustion phasing (constant crank angle of 50% mass burned (CA50)), one valve deactivated for enhanced swirl and tumble, and E70 fuel. Figure 33a shows the initially surprising result that the AHRR for stratified combustion appears to decrease with engine speed when plotted on a crank-angle basis (J/°CA). In contrast, Figure 33b demonstrates that the AHHR for *well mixed* combustion is self-similar when plotted on a crank-angle basis (i.e., AHRR scales with engine speed), as expected for burning rates that are controlled by the in-cylinder turbulence intensity, which is expected to scale with engine speed. This is, of course, the standard situation for premixed stoichiometric engine combustion. In contrast, Figure 33c shows that the AHRR for stratified SG combustion is self-similar in *time* (AHRR is approximately constant when expressed in J/ms or kW), not in crank angle, although the peak AHHR increases slightly with engine speed. Sjöberg and colleagues interpret this as evidence that the late-injection E70 SGSC combustion may be dominated by mixing, which is dominated by the time-based spray momentum for the very late injection timing and larger fuel quantity required for a given load with the high-ethanol blends.[57] Of course, this observation may be unique to the ethanol operation in the SG multi-hole injection system used in the SNL study, but it does

motivate further study with an eye toward time-based overall-heat-release rates to determine how often this observation is or is not applicable. Although the change of in-cylinder flow (implied by increased engine speed) did not produce a strong change in average heat release rate, the in-cylinder flow did affect the combustion stability as discussed next.

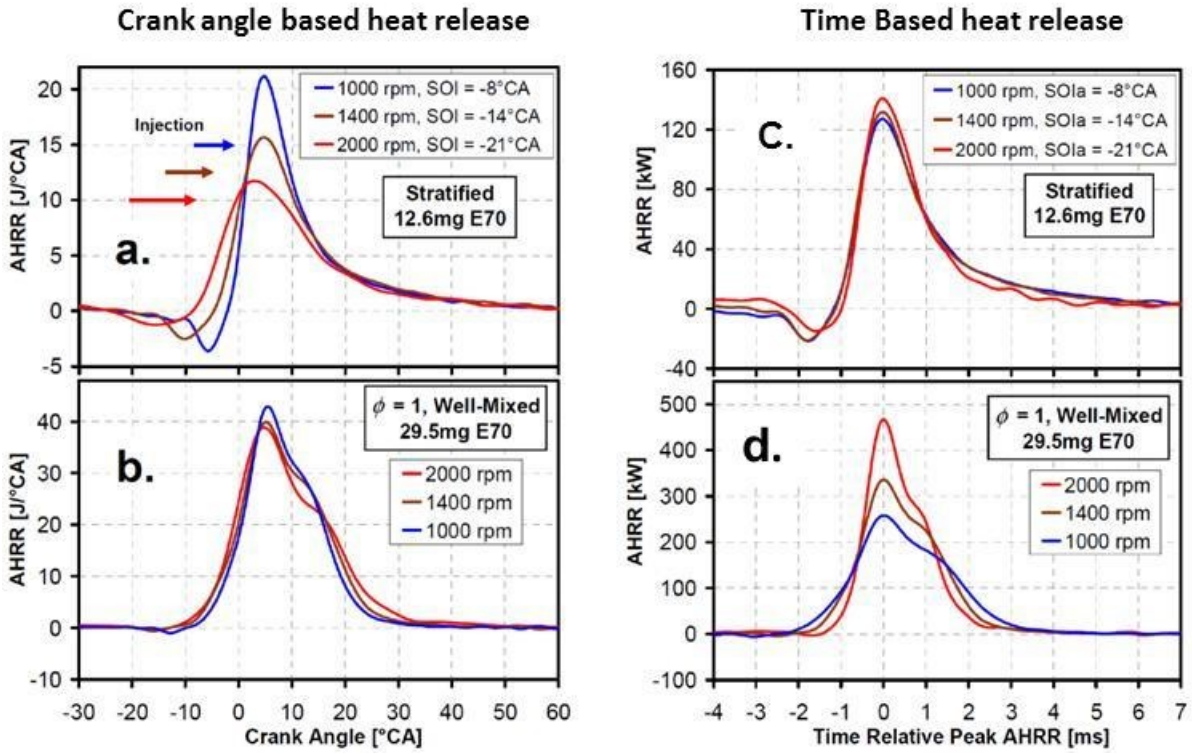

Figure 33. Data comparing stratified late-injection operation (a,c) with stoichiometric well mixed operation with EOI = 300°BTDC (b,d) on a crank-angle basis (a,b) and on a time basis (c,d) for E70 fuel. The ensemble-average apparent heat-release rate (AHRR) for well mixed operation is self-similar on a crank-angle basis, i.e., AHRR scales with engine speed, connoting "turbulence controlled" burning rates controlled by the turbulence generated by the intake and compression processes of the homogeneous (well mixed) combustion. "Mixing controlled" stratified combustion shows AHRR similarity on a time basis rather than on a crank angle basis.[57]

SGSC combustion instability with ethanol-gasoline blends

SGSC combustion instability limits were explored in the work of Sjöberg and colleagues[55, 57] by varying injection timing, spark timing, and oxygen concentration (nitrogen dilution) away from values where the engine operated with stable combustion. Figure 34a illustrates a dilution-induced "partial-burn limit", i.e. a stability limit due to an increased range of IMEP variability (phasing and/or partial burning), eventually leading to misfires. This is analogous to the dilution limits of well-mixed combustion. In contrast, Figure 34b,c exhibits random misfire limits for SGSC combustion, with most of the cycles burning very well and very

repeatably. This is the same rare and random misfire limit described in the GM and UM studies. In the SNL studies, this rare-misfire limit inhibited E85 operation with low NOx and low soot over a broader range. The SNL studies have explored too few operating conditions to predict a priori whether the partial burn limit or the misfire limit will be encountered first when varying parameters away from a stable ethanol-blend operating condition. However, the prevalence of the misfire limit motivates the quest to identify the causes and a solution to the rare misfires.

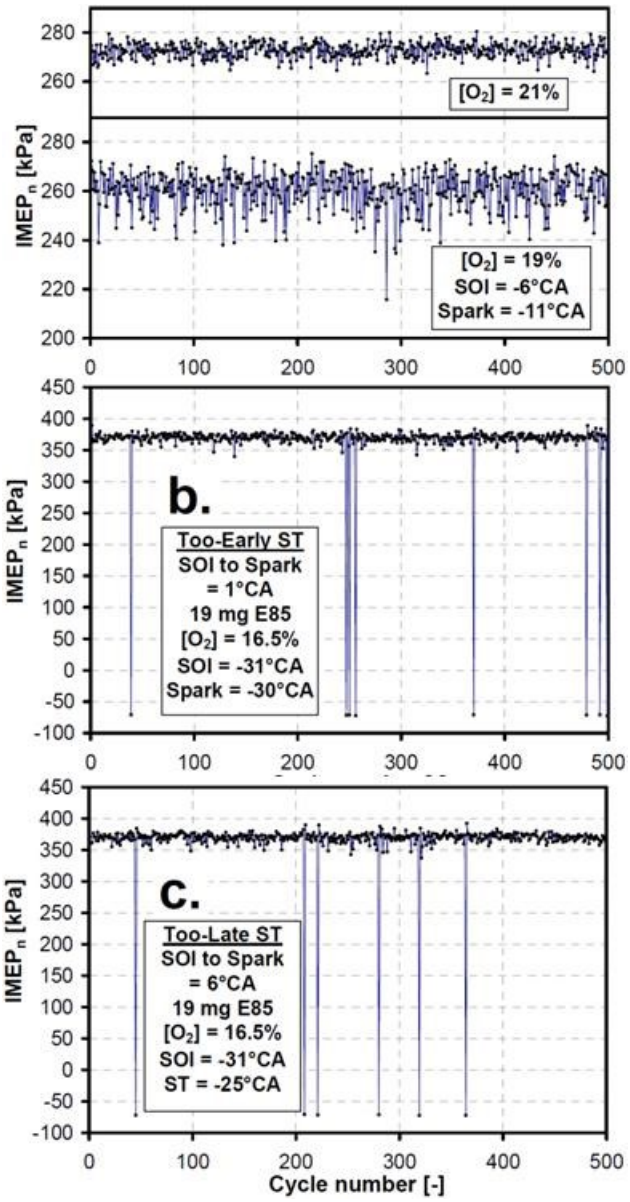

Figure 34. Unstable SGSC combustion with E85 fuel. **(a)** Unstable combustion induced by dilution; **(b)** appearance of misfire cycles for *advanced* spark timing; **(c)** appearance of misfire cycles for *retarded* spark timing.[55]

The results of Figure 33 implied that the average AHHR for stratified combustion depends more strongly on the spray-induced transport, turbulence and mixing than on the in-cylinder flow. However, the small but systematic increase in the average peak AHHR (Figure 33c) with increased engine speed is the first hint that the in-cylinder flow does contribute. The more prominent effect of the intake/compression-generated in-cylinder flow is the increased cyclic variability of the SGSC combustion with increased engine speed, as shown in Figure 35. Close inspection reveals that increased engine speed increases the occurrence of cycles that start to burn significantly earlier or later than the average. Apparently, in spite of the slow early burns, the late burning "catches up" so that the fuel burns to completion and is phased sufficiently well to extract the work (good IMEP). The prominence of misfires with otherwise well burning cycles implies that the misfire limit is caused by poor ignition or early flame-kernel growth, as noted in the previous multi-hole-injection SG studies reviewed here. The gasoline-ethanol blend studies reported thus far[55-58, 87], in agreement with Peterson's results using iso-octane[50], have found that ignition of the flame kernel always occurs, but that the combustion variability comes from inadequate growth of the early kernel. Since the cyclic variability of the flow is indeed the subject of this study, these results motivated a closer look into the comparative roles of the spray-induced and in-cylinder flow.

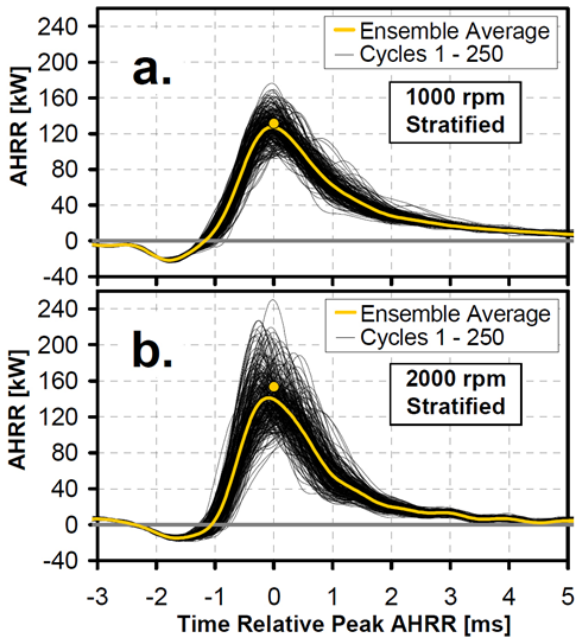

Figure 35. Cycle-to-cycle variations of apparent heat-release rate AHRR (expressed in kW and plotted against time in ms) for stratified E70 operation at engine speeds of **(a)** 1000 rpm and **(b)** 2000 rpm. Yellow circles represents average peak AHHR.[57]

To quantify and compare the momentum of the intake/compression-generated in-cylinder flow and the spray-induced flow, high-speed PIV measurements were made in the optically-configured version[58] of the SNL SG engine used to generate the data in Figure 33–Figure 35[57]. The measurements were made in a plane parallel to the cylinder axis, normal to the pent roof axis, bisecting the injector and spark plug electrode. To characterize the momentum of the flow and its variability, the measurements were used to compute the ensemble average and cyclic variability (COV) of the spatially averaged absolute value of the velocity over the field of view of the measurements. Comparisons were made between -70° and +30° ATDC, at 1000 and 2000 rpm, with and without injection. Figure 36a,b show the cycle-to-cycle variability (COV) of the spatially averaged momentum (absolute value of the velocity) with and with without injection, measured at 1000 and 2000 rpm, respectively. At both engine speeds, the noticeable decrease in COV during injection is due to the repeatability of the spray; nevertheless, the magnitude of the COV is significantly greater at 2000 rpm. The lower halves of Figure 36a,b show the spatially averaged flow speed from individual cycles. At 1000 rpm (Figure 36a), injection produces a clear step increase in the spatially averaged flow speed. At 2000 rpm (Figure 36b), not only have the magnitudes of the in-cylinder flow speed before injection increased, they are now comparable to the velocities induced by the spray. This is shown in more detail by the averages in Figure 36c, which points out that the spatially averaged flow speed after injection for 2000 rpm is 1.24 times higher than at 1000 rpm. This increase is comparable to the factor of 1.16 increase in the average peak AHHR observed in Figure 33.[58]

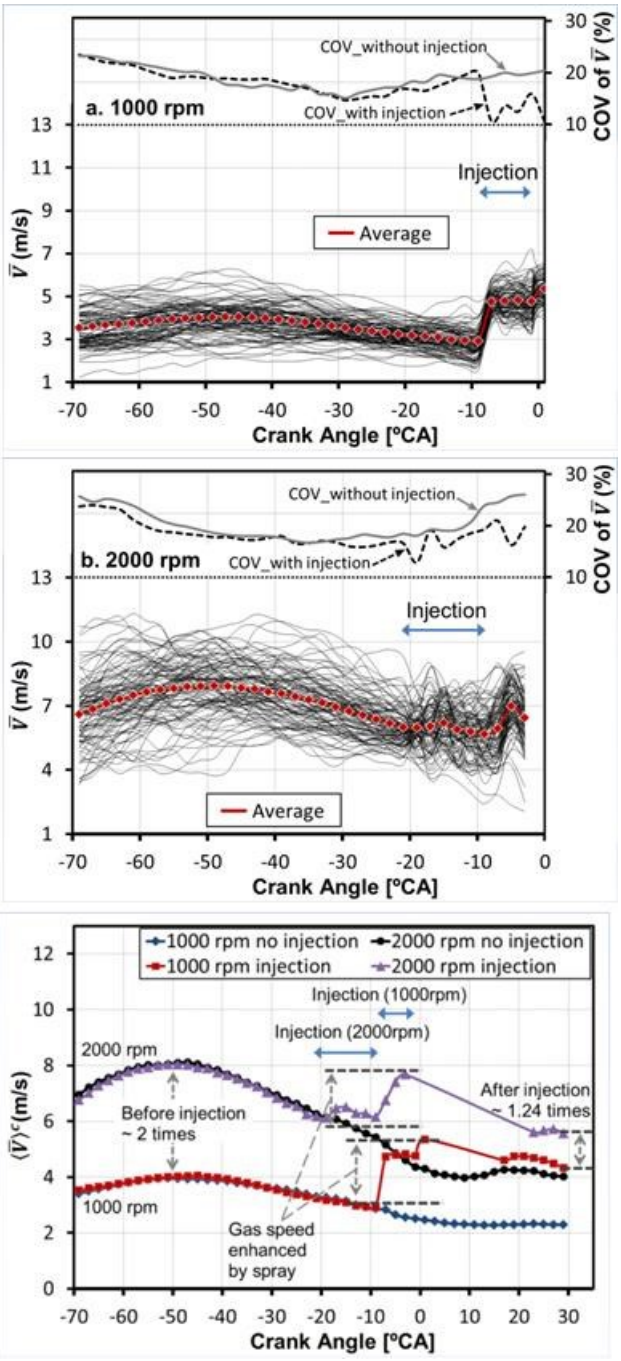

Figure 36. Cyclic variability of spatially averaged flow speed at **(a)** 1000 rpm and **(b)** 2000 rpm with E70 injection. **(c)** Ensemble average of spatially averaged flow speed for non-fired operation at 1000 rpm and 2000 rpm, with and without fuel injection.

High-speed spray imaging provided further revelations about the impact of the intake/compression-generated in-cylinder flow on the spray and mixing.[58] Volume illumination was used to show the cyclic variability of the liquid spray plumes at 2000 rpm and 333 rpm. The extremely low engine speed was used to approach the limit where the in-cylinder flow was

unimportant (simple scaling with engine speed (333/2000) suggests an overall reduction by ~80%). Results for individual cycles in Figure 37 reveal that at 2000 rpm, the spray plumes are considerably shorter and, show both more coalescence of liquid between the plumes, and more variable coalescence, and show more variability in the azimuthal direction of the plume centerline trajectories. Animations (not shown here) showed that the spray jets appeared to rotate in unison from cycle to cycle at 2000 rpm.

Taken together, the PIV and spray imaging[58] demonstrated that the in-cylinder flow momentum generated by intake and compression (1) is of the same order as the spray-induced gas-phase momentum, and (2) can markedly affect the liquid distribution and spray penetration. The implication is that the magnitude of cycle-to-cycle variability of the in-cylinder flow momentum is indeed sufficient to affect the cyclic variability of the fuel transport, mixing, and combustion development, thereby increasing combustion instability at 2000 rpm. The flow momentum at this operating condition was enhanced by the valve deactivation to create higher swirl and tumble. Further results addressing the interaction of the fuel spray with the in-cylinder swirl are published in a separate paper in this special journal issue[87]. In summary, the large range of stable combustion with ethanol blends has provided an opportunity to assess the causes of SGSC combustion instability, and has made clear the importance of spray-induced momentum at low engine speeds and the increasing contribution of fluctuations in the intake/compression-generated flow field with increasing engine speed.

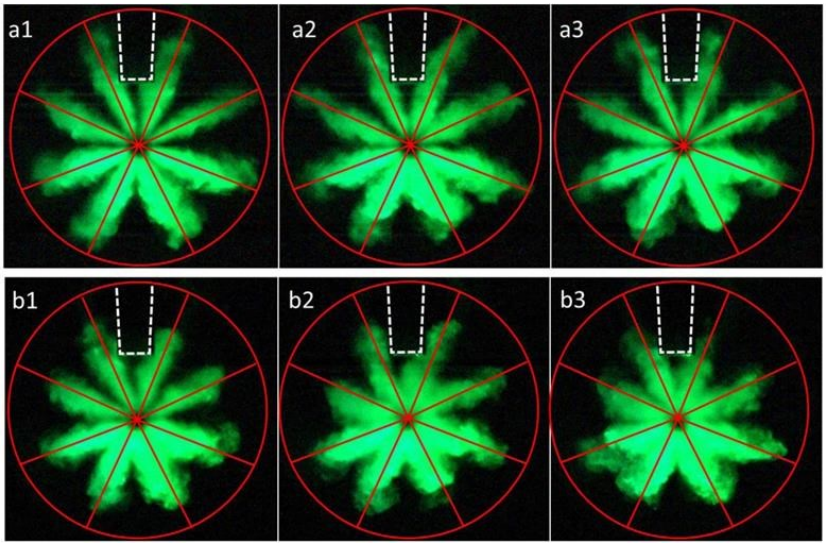

Figure 37. Volume-illuminated images of the E70 spray, 20% into the injection, showing cyclic variability of the liquid spray patterns from three cycles each at **(a)** 333 rpm and **(b)** 2000 rpm.[58]

Spray-guided combustion with piezo-electric injectors

All the spray-guided stratified-charge engines that have gone into production have used multiple-pulse injection with large-angle hollow-cone sprays generated by piezo-electrically actuated injectors,[23-27, 88] which were described briefly earlier and contrasted with solenoid-actuated multi-hole injectors in connection with Figure 4. In this section, as in our discussion of multi-hole-injection SGSC engines, we review the distinctive aspects of stable piezo-SGSC combustion; in the next section, we consider sources of combustion instability. Most of the papers in the open literature on piezo-injector SGSC engines are illustrative rather than systematic, especially in terms of linking fluctuations in spray characteristics or mixture distribution to combustion instability. These portions of our review must therefore less definitive than the corresponding material above on SGSC combustion with multi-hole-injectors.

Direct comparisons of multi-hole- and piezo-injection SGSC operation are scarce. A relatively early optical-engine study[36] used Mie scattering and exciplex LIF to image liquid and vapor fuel distributions and to estimate the best ignition locations for operation with pressure-swirl, multi-hole and piezo-electric injectors. High-speed flame-luminosity imaging and cylinder-pressure measurements were used to determine misfire rates and stable-operation ranges. The results favored the piezo-injector. However, the generality of this conclusion is limited by the use of a flat piston in the optical engine and range of conditions examined.

Smith, et al.[37] carried out a systematic comparison of SGSC engine performance with multi-hole and piezo injectors over a broad range of steady-state engine operating conditions from idle to full load. This work used a common cylinder head, but the piston-bowl geometry, charge motion, and the locations of the injector and spark-plug were optimized individually for each injector type. Closely spaced double- and triple-pulse injection was used with the piezo-injector, and single and double injection (widely and closely spaced) with the multi-hole injector. The principal conclusion was that, when optimized in this way, there was little difference in SGSC performance between the outwardly opening piezo injector and the multi-hole injector. Unfortunately, although commendably comprehensive in terms of the operating conditions examined, the paper did not present details of combustion stability as a function of spark and injection timing.

Piezo-spray structure and mixture distribution

Figure 4 illustrated how sprays from outwardly opening injectors differ strongly from multi-hole injector sprays, not only in the striated hollow-cone structure of the piezo spray but also in its recirculation vortex.[23, 24, 35, 39-41] In fact, simulations[40] (Figure 38), planar imaging[43] and PIV measurements[89, 90] show that recirculation vortices form at both the inner and outer edges of the hollow cone.

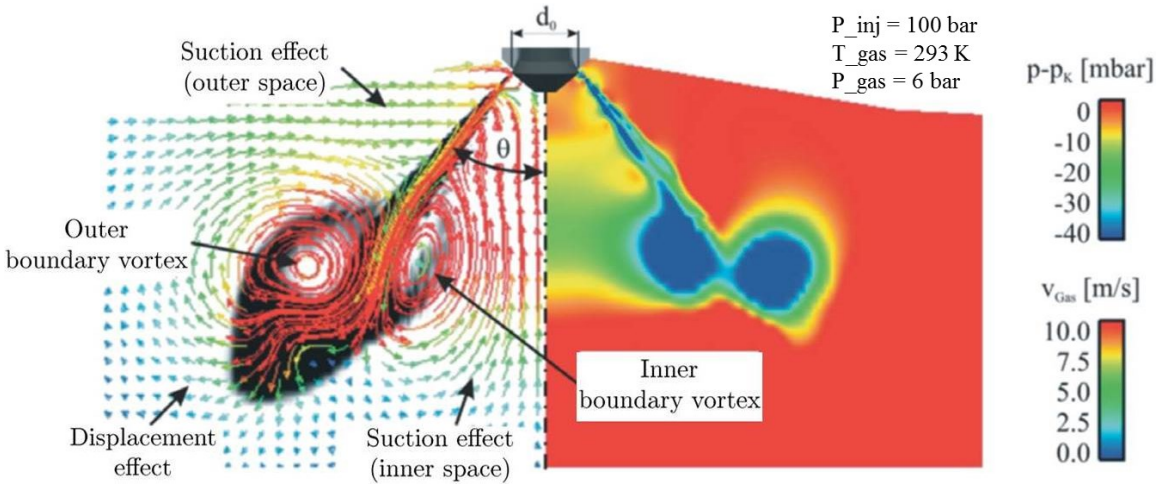

Figure 38. Fine-mesh simulation of a cross section through the hollow-cone spray of an outwardly opening injector into high-density quiescent gas. ***Left:*** Gas-phase velocity vector field and liquid mass fraction. ***Right***: Static pressure difference relative to the ambient gas pressure. Adapted from [40].

Fuel vapor and smaller droplets follow the recirculating flow and concentrate in the reduced pressure regions (Figure 38, right) within these vortices.[40, 43] With its relatively modest penetration and local velocities, the outer recirculation vortex therefore provides a favorable zone for ignition.[91] Since the spray penetration and hence the position of the recirculation vortex depend on the ambient gas density, injection timing is used to place the outer vortex at or near the spark gap as consistently as possible for stratified-charge operation.[81, 92, 93] Figure 39 shows ensemble-averaged images of the spray during a double-injection sequence in a Mercedes-Benz SGSC engine.[23] Note the positioning of the recirculation vortex by the spark gap during both injections as well as the essentially complete evaporation of the liquid fuel from the first injection by the start of the second injection.

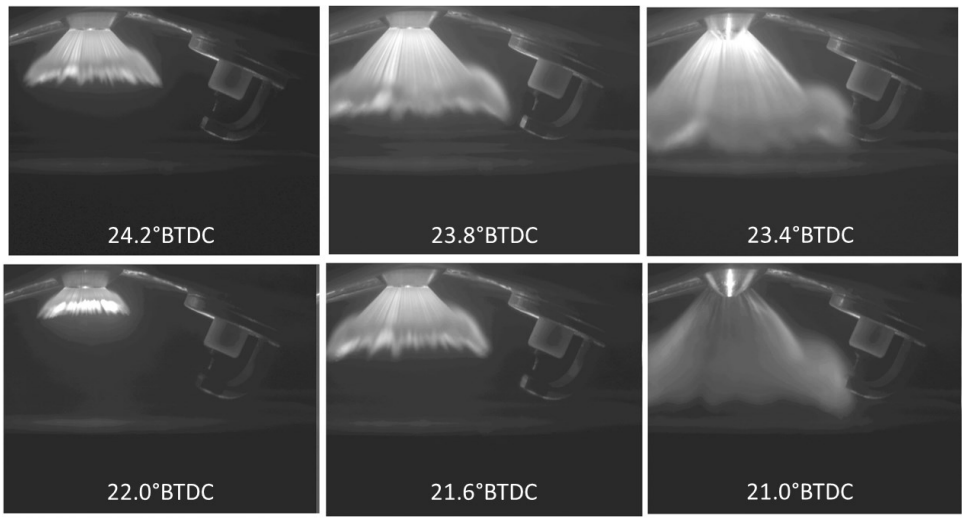

Figure 39. Fifty-injection ensemble-average images of liquid fuel during double injection in a Mercedes-Benz SGSC engine. Essentially all the liquid from the first injection has evaporated before the second injection. Adapted from[23].

Corresponding numerical simulations of the fuel spray and resulting vapor-phase distribution and of the mixture conditions within a small control volume centered on the spark gap are shown in Figure 40 and Figure 41, respectively, for part-load (3 bar IMEP) operation of the Mercedes-Benz piezo-SGSC engine at 2000 RPM engine speed.[23] Experimental measurements of the equivalence ratio at the spark gap (to be discussed later in more detail) for similar double-injection timings show peak equivalence ratios of about 10 and 9 during the first and second injection, respectively. In Figure 41, the black curve (open circles) shows the volume fraction of liquid within the control volume, while the gray curve (triangles), denotes the volume fraction of fuel vapor with excess air ratio in the range $0.8 < \lambda < 1.4$ (equivalence ratio approximately $0.7 < \phi < 1.25$), which is taken to indicate combustible mixture. The bar across the middle of the graph in Figure 41 indicates periods of low (dark gray) and high combustibility (dotted) as gauged by a combustible-mixture volume fraction > 50% within the control volume. The outer rectangles centered on crank angles –25° and –20° indicate times when liquid fuel in the control volume might inhibit ignition and flame-kernel formation. The maximum volume fraction of combustible mixture within the control volume occurs after the second injection at 16 °BTDC, which is the crank angle of the right-hand fuel-distribution image in Figure 40.

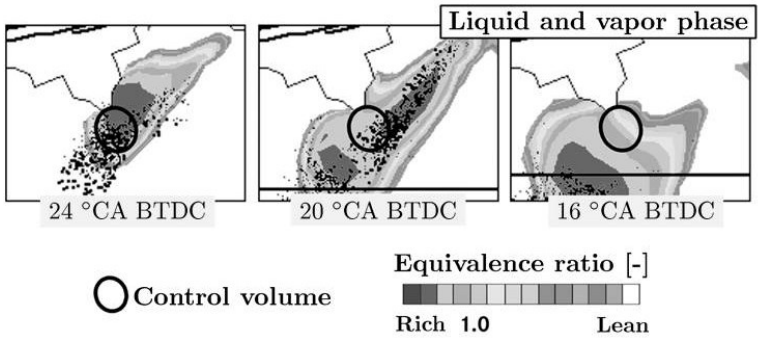

Figure 40. Simulation of fuel spray and mixture formation near the spark plug for three times during a double-injection spray image sequence similar to Figure 39. Droplet parcels indicate liquid fuel; gray contours show equivalence ratio. Operating conditions: 2000 RPM engine speed, 3 bar IMEP, 10.5 mg fuel injected (total), 50 mbar throttling. Translated from [23].

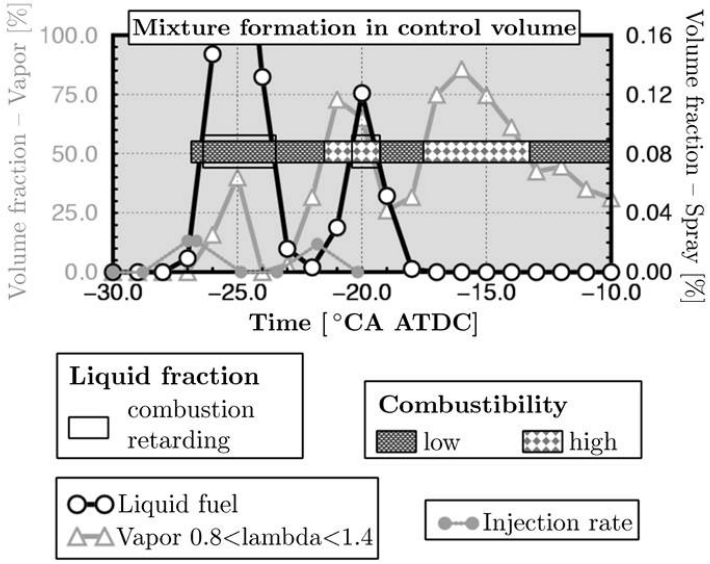

Figure 41. Mixture conditions within the control volume surrounding the spark gap marked on Figure 40 for the same operating conditions. Translated from[23].

Ignition and flame-kernel growth

Although the simulation results[23] in Figure 41 suggest that spark timing shortly after the second of two injections is favorable, optimum ignition timing depends strongly on engine geometry, load, the injection timing(s), and the need to balance reduced fuel consumption with acceptable emissions. Firing the spark between the first and second injections[24] or even before the first injection[23] have both proven advantageous under differing circumstances. Overall, our impression is that ignition some time before the final injection is more typical.

For example, Figure 42 shows an ensemble-averaged planar LIF image of the vapor and liquid fuel distributions resulting from double injection in a BMW SGSC engine.[24] As in the

preceding example (Figure 39), liquid fuel from the first injection has nearly all evaporated by the start of the second injection. The LIF image in Figure 42 nicely shows the fuel vapor that has been entrained into the recirculation vortex from the first injection. Note the more complex spark plug with multiple ground electrodes.

Extracts from high-speed imaging of the spray, spark and flame-kernel formation during a single engine cycle under similar (perhaps not identical) conditions are shown in Figure 43.[24] In this example, the spark is fired during the second injection (23.5° BTDC) while liquid fuel is clearly present. In the next two frames (20.1° and 18.8° BTDC), the spark plasma stretches out from the gap and ignites a flame kernel which is quite apparent at 18.8° BTDC (about 0.5 ms after firing the spark), although a kernel of size ~3 mm can also be seen in the preceding image at 20.1° BTDC by enlarging the region marked by the dashed rectangle and enhancing the image brightness and contrast. Robust combustion is apparent in the final image of the set at 13.2° BTDC. Note that the flame kernels here, like those illustrated in Figure 11 and Figure 12 for the multi-hole injector, are distinctly non-spherical at the earliest times shown.

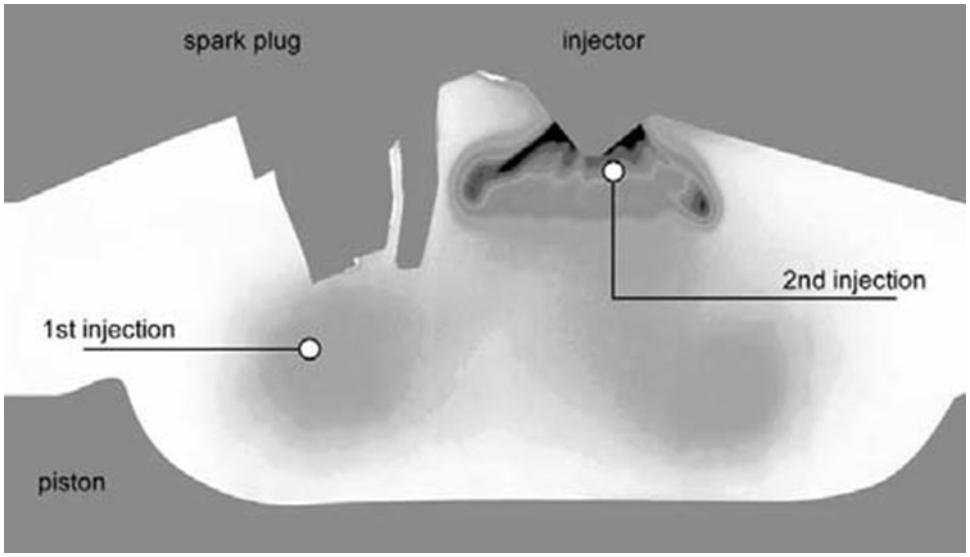

Figure 42. LIF image of fuel spray from second injection and vapor distribution (primarily from first injection) for stratified operating conditions.[24]

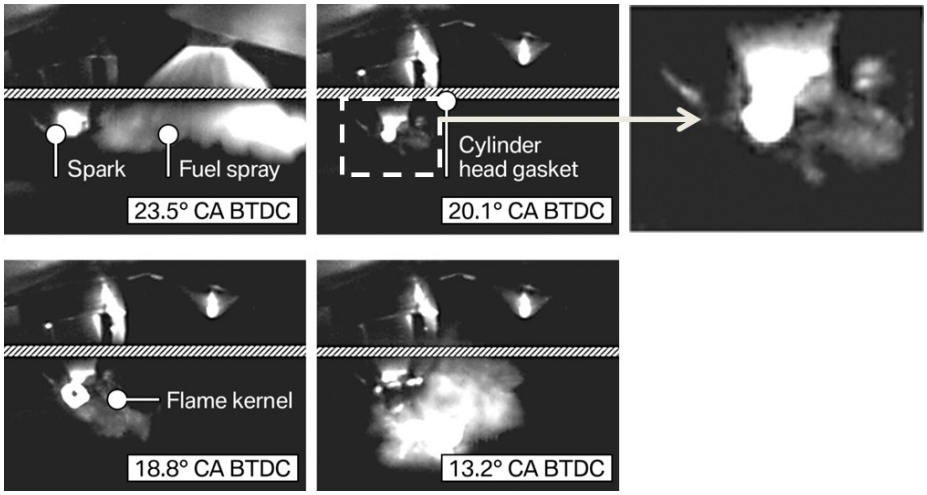

Figure 43. High-speed imaging of spark, ignition and early flame-kernel development in a BMW SGSC engine. The region in the dashed rectangle is enlarged and enhanced in the image at the far right to show a small (~ 3 mm) flame kernel. Adapted from [24].

Spray-guided combustion instability with piezo-injectors

As mentioned earlier, we have not found studies of combustion instability in piezo-injector SGSC engines that are as systematic as those summarized in this paper for SGSC combustion with multi-hole injectors. Papers on piezo-SGSC often omit details such as the level of EGR dilution or the injection or ignition timing. In this section, we summarize the information that we have found. Several striking contrasts to SGSC operation with multi-hole injectors will emerge.

Spray and flow-field fluctuations

Spray studies in quiescent chambers (e.g., [41, 43, 94]) have reported that the structure of piezo-injector sprays, in particular the spray angle, is very stable. The spray variability increases appreciably in an operating engine, however.[89, 90]

Planar LIF spray imaging in an early single-injection piezo-injected SGSC optical engine observed substantial variation in the angle of the spray as it emerged from the injector.[81] Misfire-free stratified operation could be obtained only over a narrow range of injection-to-ignition timings. Optimizing the injector reduced the spray-angle fluctuations and substantially increased the range of misfire-free operation. Although this paper did not describe how the injector was improved, similar fluctuations have been associated with air trapped within the injector[35] and have also been seen in an extensive study of spray-angle fluctuations in an optical engine for

three prototype piezo-injector designs with differing nozzle-exit geometries[42]. The latter paper also showed that varying the needle lift (in order to control injection rate and spray penetration) led to instability in the spray angle.

The direct correlation of spray-angle fluctuations with combustion instability by Hübner, et al.[81] described above motivated an extensive study with multi-hole injection in the Gen 1 optical engine.[48] As summarized earlier in this review, however, spray-angle fluctuations and non-uniformities in the liquid distribution did not correlate with combustion instability in the multi-hole case.

Further studies of piezo-spray fluctuations have focused on the interaction of the spray with the gas-phase flow field. For double injection, systematic Mie-scattering imaging showed a reduced spray angle and increased instability for the second injection, which was attributed to perturbation of the pre-existing (and evolving) in-cylinder flow field by the first injection.[42] Recent high-speed PIV measurements in firing SGSC engines have characterized the interaction of the piezo-spray with the in-cylinder flow in considerable detail for double[95] and triple injection, including effects on the second spray shape.[89, 90] Unfortunately, these studies do not relate the flow-field and spray measurements directly to combustion, nor do they actually show the final spray or its flow field. Nevertheless, the results are interesting in view of the earlier observations connecting spray fluctuations to combustion instability.[81]

Figure 44 shows endoscopic high-speed PIV measurements[95] of the mean flow field (averaged over 100 cycles) in a firing piezo-SGSC engine at three times (one before and two after the first injection), together with one example of the RMS velocity-fluctuation distribution and five individual-cycle flow fields at the same crank angle. The streamlines make the flow structure very clear, especially the recirculation vortices, but the individual velocity vectors are difficult to discern. The curving red arrow on the mean flow field at 35.5° BTDC highlights the upward so-called "funnel" flow beneath the injector induced by the large vortices on either side. This central flow structure, which was previously identified by Mie-scattering[41] and PIV measurements,[94] is accompanied by increased RMS velocity fluctuations. Interestingly, the RMS velocity fluctuations near the spark gap are appreciably smaller in magnitude than in this central region. The right column of Figure 44 shows individual-cycle examples of the flow within the region marked by the red dashed rectangle. Substantial large-scale cycle-to-cycle variations in the flow field are evident.

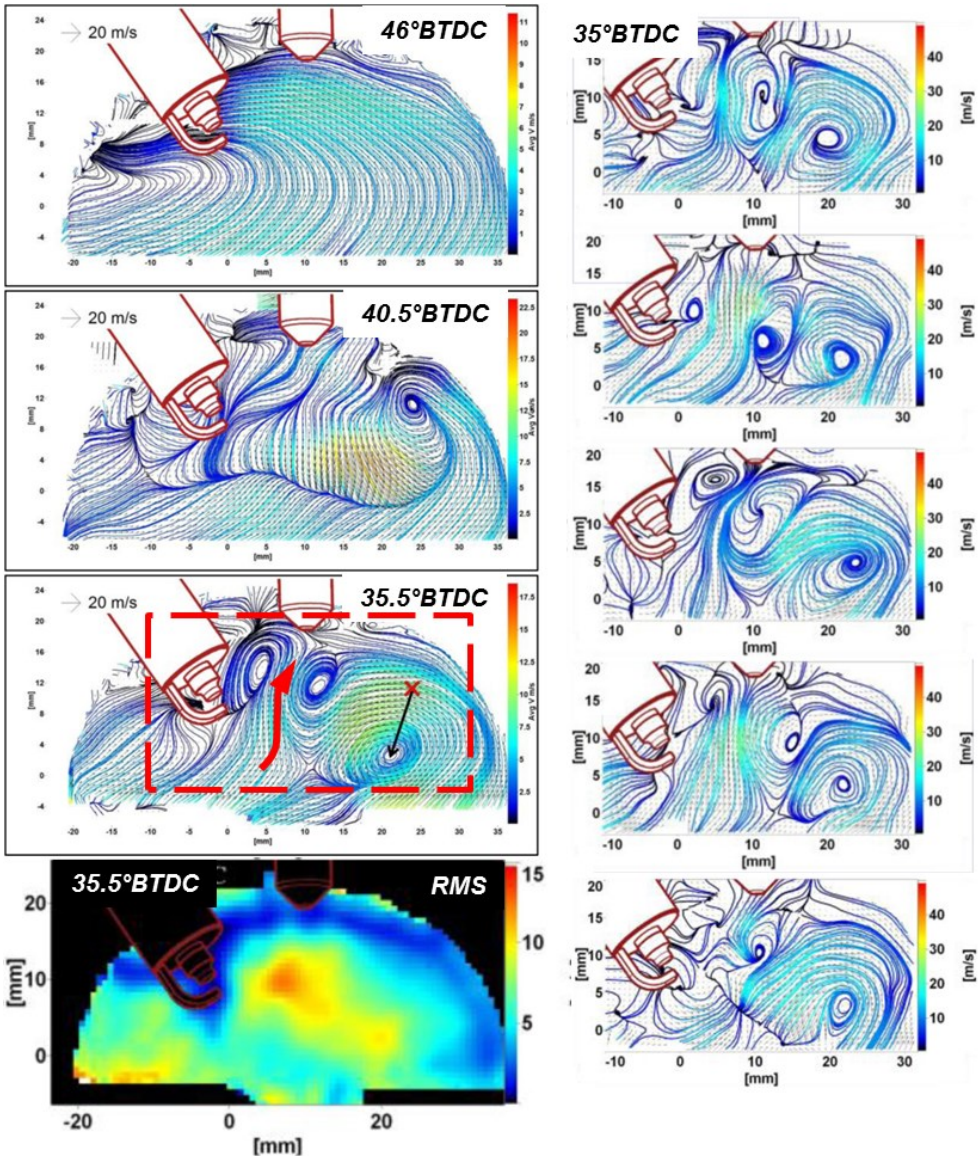

Figure 44. ***Left:*** Endoscopic high-speed PIV measurements of mean velocity fields (with streamlines) at crank angles before (46°BTDC) and after (40.5 and 35.5°BTDC) the first of two injections in in a firing piezo-injected SGSC engine. The bottom image is the RMS velocity field at 35.5°BTDC. ***Right***: Cycle-to-cycle variation of the flow field in the central region (red dashed rectangle) illustrated by five individual-cycle flow fields at 35°BTDC. Adapted from [95]

High-speed PIV measurements with higher spatial resolution in an optical engine of similar design have investigated the link between flow-field fluctuations and spray fluctuations.[89, 90] Although the engine was fired with triple injection, the published results relate variations in the second spray to the flow field from the first injection and – remarkably – to the flow field *before* the first injection. The metric chosen to characterize variations in the second

spray, which the authors refer to as spray height (SH), is the distance from the cylinder head to the upper edge of the spray (as identified by planar Mie scattering) at specified locations on either side of the injector. As illustrated in Figure 45, variations in the spray height of order 3 mm correspond to substantial variations in the spray shape, angle and location of liquid fuel relative to the spark plug.

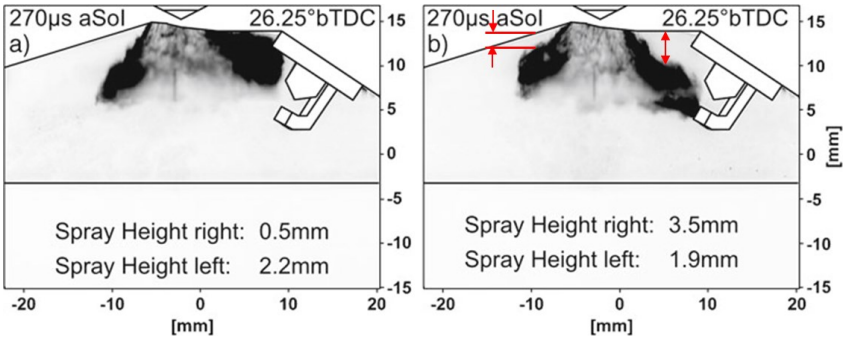

Figure 45. Planar Mie-scattering images of the second spray in a triple-injection sequence in a firing SGSC engine.[89] The individual-cycle images were recorded 0.25 degrees before firing the spark. Spray height is defined as the distance from the cylinder head to the upper edge of the spray, as shown by the red arrows on the right-hand image. Adapted from[89].

The upward "funnel" flow beneath the injector is also clear in these measurements, as seen in the upper part of Figure 46; indeed, the mean velocity fields at comparable crank angles in Refs. [89, 90] and [95] agree well. The fact that this upward flow is accompanied by locally increased flow variability (Figure 44, bottom left image and right column) suggests that it may be responsible for the increased variability observed in the second spray.[42] The lower part of Figure 46 shows that the spray height near the spark plug is in fact correlated with the vertical component of the upward flow beneath the injector (correlation coefficient $R^2 \approx -0.7$).[89]

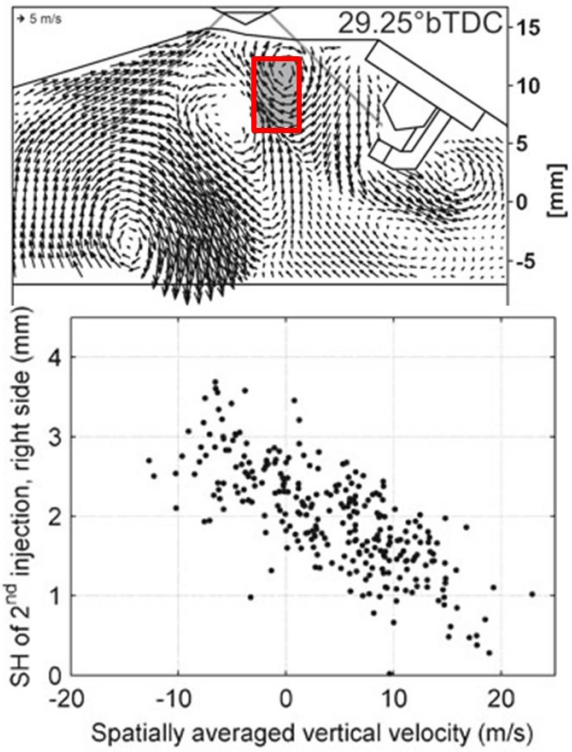

Figure 46.***Upper***: Conditionally averaged velocity field for cycles with the lowest spray height for the second injection. ***Lower***: Spray height (SH) near the spark plug for the second injection plotted against the spatial average of the vertical velocity component in the red rectangle above. Adapted from [89].

That the flow field after the first injection affects the stability of the spray from the second injection is not too surprising. What is quite remarkable, however, is that the stability of the second injection correlates almost as strongly with the in-cylinder tumble flow field before the first injection, as illustrated in Figure 47. Stiehl, et al. argue that, by creating the fluctuating upward flow beneath the injector, the first spray amplifies the effect of fluctuations in the pre-injection flow field generated by intake and compression.[90]

Two important implications of these results are:

(1) The spray variations in Figure 45–Figure 47 are *not* intrinsic to the injector itself despite some similarity in appearance to spray fluctuations that have been related to the injector's internal and nozzle-exit flows.[42]

(2) Contrary to what has sometimes been assumed, the gas-phase flow field within the cylinder, whether pre-injection or between injections, is not simply overwhelmed by the spray and can have a significant influence on the spray itself as well as on the vapor-phase fuel distribution.

Indeed, these results, together with the SNL results for multi-hole SGSC[55-58] summarized earlier in this review, make clear that the interaction between the spray and the flow field goes both

ways, with the spray and flow field each influencing the other to varying degrees depending on such factors as engine speed, injected quantity, and injection timing.

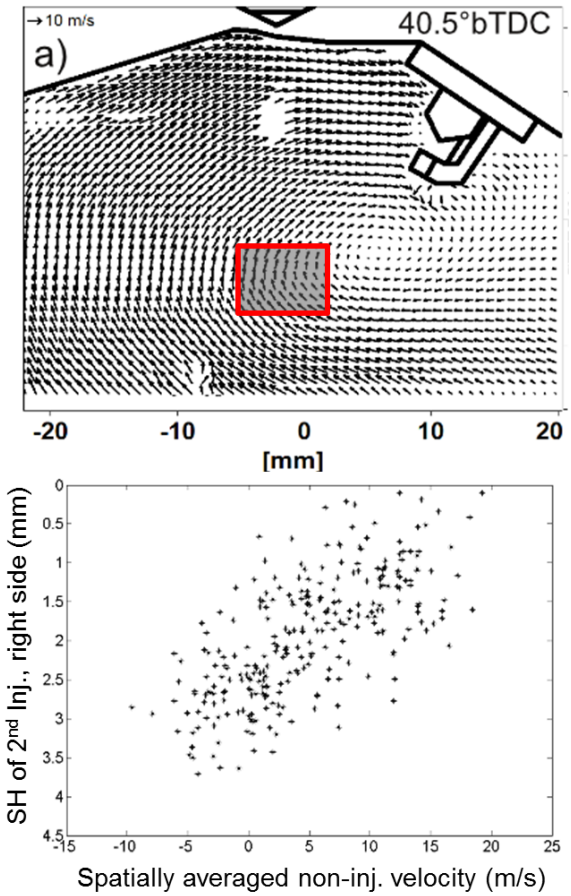

Figure 47. ***Upper***: Ensemble-average in-cylinder flow field preceding the first injection under nearly the same injection-timing conditions as in Figure 46. ***Lower***: Spray height (SH) near the spark plug for the second injection plotted against the spatially averaged velocity within the red rectangle of the pre-injection flow field in the upper image.[90]

Unfortunately, without experimental data or LES simulations for fluctuations in the fuel vapor distribution or combustion imaging that correspond to Figure 44–Figure 47, we can only offer the reasonable expectation that the spray fluctuations discussed here will sometimes cause locally unfavorable conditions for ignition and flame-kernel growth. The studies cited here do not discuss the mechanism by which the final injection (after ignition) of a double- or triple-injection sequence leads to greater ignition stability and more robust combustion, but one aspect is to reduce overall spray penetration and help keep the recirculation vortex near the spark gap.

The benefits outlined earlier for multi-hole double injection appear likely to accrue with multiple injection piezo-SGSC as well: delivering rich mixture to the flame kernel formed from

the previous injection(s); imposing a relatively well organized and well directed flow that drives the burning mixture into the piston bowl and toward the remaining fuel; and reducing turbulence intensity during initial flame-kernel formation but increasing turbulence intensity and thereby increasing the overall burning rate after the final injection when the flame kernel is more robust.

Interestingly, Oh, et al.[96] found poorer combustion stability with triple injection (one-third of the total fuel in each pulse) than with double injection (half the fuel in each pulse) at the particular light-load condition investigated (1200 rpm; about 3 bar IMEP). They attributed this result to overly rich mixture at the spark plug due to low penetration of the third injection. The discussion here suggests that another explanation might be that the fluctuations in the pre-existing flow field would affect a smaller-quantity third injection more strongly than they would affect a larger-quantity second injection in a double-injection sequence.

To close this discussion of piezo-spray fluctuations, we mention the interesting observation from these investigations that fuel-rail pressure fluctuations did not significantly affect the variability of the second spray.[89]

Equivalence-ratio fluctuations

Several studies have described, with varying levels of detail, the use of optical information on the fuel distribution or CFD simulation of the mean equivalence-ratio distribution (e.g., Figure 40–Figure 41) together with measurements in all-metal piezo-SGSC engines to expand the range of injection and spark timings over which stable combustion could be achieved while maintaining acceptable engine-out emissions.[23-27, 39, 81, 88, 92, 93, 96, 97] However, almost nothing quantitative appears to have been published to connect variability in the fuel distribution to combustion instability.

The lone exception that we have found is Figure 48,[23] which shows the ensemble-mean equivalence ratio at the spark gap and its RMS variation [i.e,, one standard deviation $\sigma(\phi)$] from cycle to cycle as measured by spark-emission spectroscopy[29] for double injection in a Mercedes-Benz SGSC engine. Comparing the piezo-SGSC data in Figure 48 to the similar measurements for the multi-hole-injector Gen 1 engine in Figure 7 shows that the peak equivalence ratios for both the first and second injections are substantially higher with the piezo injector. For both the piezo-injector and the multi-hole injector, the RMS cyclic variations in equivalence ratio are comparable to the mean values and are thus fractionally very large.

The white line in Figure 48 shows the corresponding misfire rate (right axis), which exhibits interesting contrasts to the multi-hole-injector SGSC results summarized earlier. Most apparent is that misfire-free combustion could not be initiated until after the second injection when the equivalence ratio had fallen to less than about 1.8, whereas substantially richer equivalence ratios were typically favored in all three multi-hole SGSC engines (Gen 1, Gen 2 and UM). One factor that may contribute to this difference is charge dilution, which was unspecified for Figure 48 but was substantial for most of the UM and GM experiments. Recall that the SparkCIMM simulations showed that with high levels of dilution, Lewis-number and flame-curvature effects dramatically enhance the laminar flame speed under rich conditions but reduce the laminar flame speed for lean conditions, as illustrated in Figure 14.

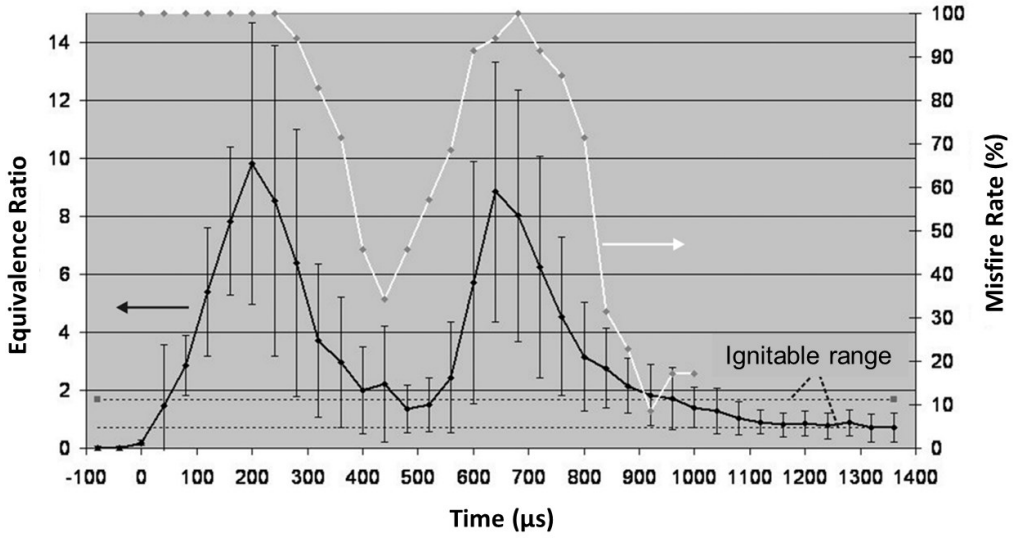

Figure 48. Equivalence ratio vs. time (black) at the spark gap measured by spark emission spectroscopy during stratified combustion with double injection using a spark duration of 50 µs. The corresponding misfire rate is shown in white (right axis). The dotted horizontal lines show the presumed range of ignitable equivalence ratios.[23]

Time-resolved measurements of spatially integrated OH* chemiluminescence together with spark current and voltage in the Mercedes-Benz piezo-SGSC engine led to the conclusion (based on several thousand fired cycles) that misfires were *never* due to extinction of a flame kernel once it had been formed. Misfires occurred *only* due to failure to ignite a flame kernel.[23]

In stark contrast, the GM and UM experiments found that for reasonable timings (as opposed to, e.g., grossly overadvanced spark timing relative to injection[45]), the spark *always* ignited a flame kernel and misfires were *always* due to flame-kernel extinction. The extent to

which misfires in other piezo-injected SGSC engines are caused by the failure to ignite a flame kernel is unclear due to lack of systematic information in the literature. In contrast to the Mercedes-Benz results, however, LIF, Mie-scattering and high-speed imaging in a flat-piston optical piezo-SGSC engine operating with triple injection (ignition between the second and third injections) revealed extinction when the flame kernel had to propagate downstream into a fuel distribution that was too lean. This effect was likely exaggerated by the flat-piston design;[97] as discussed in the Introduction, viable SGSC engines all employ a piston bowl to help confine the fuel and reduce over-leaning.

Spark characteristics with piezo-sprays

The spark duration and attendant spark stretching may be another important factor in the different equivalence ratios for robust ignition between the piezo-SGSC engine of Ref.[23] and the multi-hole-injection SGSC engines discussed earlier. For the piezo-SGSC measurements in Figure 48, the spark duration was reduced to just 50 μs in order to relate the misfire rate definitively to the instantaneous fuel concentration at the spark gap. The spark plasma was therefore confined to the gap and could not reach nearby mixture that might possibly have been more readily ignited. For the multi-hole cases, the equivalence-ratio measurements using spark-emission spectroscopy in Figure 7 were based on the first 150 μs of the total spark duration (~1–3 ms), allowing local ignition to occur later along the stretched spark, as discussed at length above.

Recent piezo-injected SGSC engines use multi-strike ignition that can rapidly fire many short duration sparks over the ~1–3 ms period of a typical transistorized-coil ignition system.[25, 27, 66, 98] Spark duration and spark stretching are also important for multi-strike ignition systems.

Hese, et al.[98] investigated two different multi-strike ignition strategies for stratified operation, which are illustrated in Figure 49. Ignition Strategy 1 (in the upper row) generated 10 sparks, each of which broke down anew across the spark gap and whose duration was so short that they did not stretch significantly out of the spark gap. Ignition Strategy 2 (whose behavior appears similar to that of another multi-strike ignition system[66]) caused ~20 discharges into the "left-over" plasma channel from the initial breakdown, which allowed the individual spark discharges to stretch out substantially from the spark gap.

Figure 50 compares combustion stability with these two multi-strike ignition strategies in a piezo-injected SGSC engine. The engine normally operated with triple injection, but these tests were performed with single injection, perhaps to provide a more challenging environment for ignition. In contrast to the multi-hole-injector SGSC results discussed earlier, Figure 50 shows a clear benefit for the series of short-duration spark breakdowns without spark stretching created by Ignition Strategy 1. Hese, et al.[98] suggest two reasons for this preference. First, the initial breakdown phase, which typically lasts some nanoseconds, transfers the spark energy to the gas with substantially greater efficiency than the ensuing arc and glow discharge phases.[99] Second, the initial breakdown creates more free radicals than the later phases.

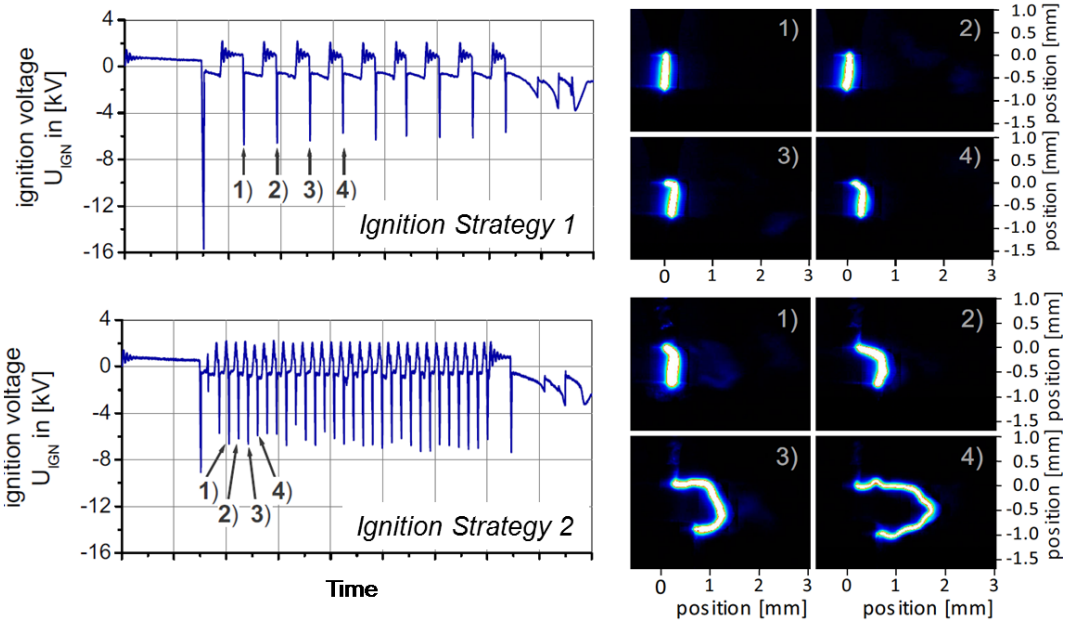

Figure 49. Ignition system secondary voltage (left) and resulting spark plasma images at four times after initial breakdown for a multi-spark ignition system. ***Upper row***: For Ignition Strategy 1, the system creates a series of short-duration sparks each of which breaks down anew across the spark gap. ***Lower row***: For Ignition Strategy 2, the system generates a single initial breakdown across the gap followed by repeated discharges into the plasma channel remaining from the previous spark. Adapted from [98].

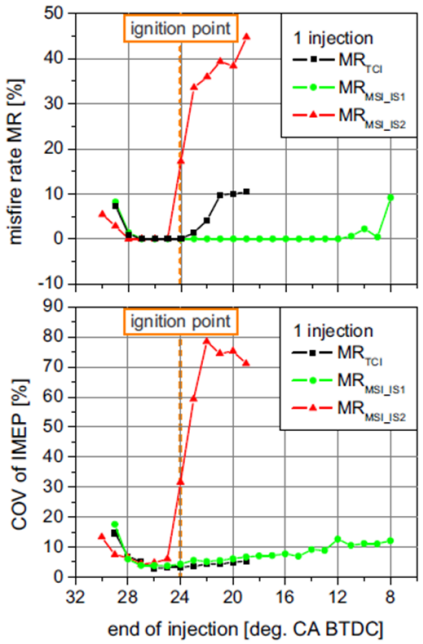

Figure 50. Misfire rate (MR) and COV(IMEP) for standard transistorized coil ignition (TCI) and the multi-spark ignition (MSI) system's two ignition strategies (IS1, IS2). Operating conditions: engine speed 2000 RPM, IMEP = 3 bar, stratified charge, single injection.[98]

Without the detailed and systematic information from our studies of multi-hole-injected SGSC ignition, it is difficult to say too much more about this result or about the contrast to cases where spark stretching proved beneficial. The concepts embodied in the SparkCIMM modeling above make clear that detailed differences in the local flow field, turbulence intensity and equivalence-ratio distributions are very important in all cases and that spark stretching is especially helpful for the multi-hole injector case where the flame kernel has to "chase the tail" of the fuel plume.

Certain spark-plug designs (e.g., multi-electrode) may also make spark stretching more advantageous. For example, Figure 43 above showed a piezo-SGSC example with spark stretching. Indeed, for that engine design, fine-mesh CFD was used to optimize the spark-plug electrode configuration and the air flow around the electrodes in order to stretch the spark plasma channel into the fuel vapor near the spark gap, as illustrated in Figure 51.[25] In addition to allowing the spark plasma to ignite mixture outside the spark gap, the optimized arrangement should also reduce the flame kernel's contact with the electrodes and thereby reduce heat losses from the kernel, which can be more severe with multi-electrode designs (e.g., Figure 26 and Figure 51).

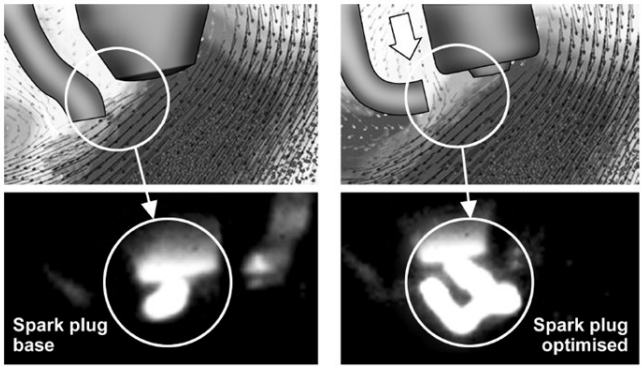

Figure 51. Simulated air flow near the spark gap and corresponding experimental images of the stretched spark plasma for a base and an optimized spark-plug design.[25]

SGSC development directions

In this paper, we have only discussed light-to-moderate-load, naturally aspirated SGSC engine operation and have largely ignored emissions-related issues. For completeness, we mention a few development directions.

Ongoing research and development on SGSC engines includes higher injection pressures[100-102] and boosted operation (turbo- and/or super-charged) to extend the upper load limit of stratified operation without excessive engine-out soot production.[88, 102-105] Multi-pulse injection (up to eight pulses per cycle) is being pursued aggressively both for mixture preparation (combustion stability; NOx, soot, and hydrocarbon emissions) and to avoid fuel impingement on surfaces (spark plug[106], piston bowl or cylinder wall)[27, 88, 105, 107]. Multi-strike ignition systems[25, 27, 66, 98, 105, 107] are also being used in combination with these strategies. Lean-NOx aftertreatment, the need for which is a major factor in the development and introduction of SGSC engines into the marketplace, continues to be an area of significant activity.[108]

Historical note

With the perspective of a century since Ricardo's early divided-chamber stratified-charge engine[1], it is interesting to consider the progress that has been made in both fundamental understanding and practical development – a century of trying to get it "just right."

An early (circa 1950)[7] – and persistent[19] – concept underlying what we now call spray-guided stratified-charge engines was that ignition of the first fuel to reach the spark plug would establish a stationary flame front into which the remaining fuel would be fed and would burn as

quickly as it arrived. Roughly a generation later, high-speed films in rapid-compression-machine experiments at MIT[109] to simulate the TCCS engine and at GM[15] to simulate the DISC engine showed a very different situation, viz., what we have referred to in this review as the flame "chasing the tail" of the fuel cloud. Both the TCCS and DISC engines employed fuel injection into a strongly swirling flow. Using schlieren imaging, Solomon[15] observed that the fuel was rapidly distributed around the chamber by the combined effects of the bulk swirl and the spray while the flame kernel "sheltered" behind the spark electrodes in the wake of the spray. "The ignition process was observed to be governed by the delayed formation, growth and transport of a flame kernel which spreads to complete the major portion of the burn only after the injection process has been completed." Another result from that time period that hints at phenomena that we have reviewed in detail was Sinnamon's suggestion – based on high-speed schlieren imaging of fuel sprays in a see-through optical DISC engine – that cyclic variation in the in-cylinder flow field could lead to ignition instability.[110]

As reviewed here, the development and application of advanced optical diagnostics has led to a wealth of detailed and quantitative information on SGSC flows, sprays, mixture preparation, ignition and combustion. The insights have gone a long way toward understanding the sources of combustion instability that can still be problematic. The experimental results and insights have also aided the development of advanced numerical simulation tools with a strong physical basis and a significant degree of predictive capability.

Summary and conclusions

Direct injection and spark ignition of fuel under stratified charge (SC) conditions offers thermodynamic benefits that make this approach an attractive strategy towards improved internal combustion engines. The issue of combustion stability – in particular, rare (often << 1:1000 cycles), apparently random misfires and partial burns that are not due to gross injection- or ignition-system failure – has plagued SC engines from the earliest attempts and continues to limit the maximum dilution and the range of injection and ignition timings that can be achieved in practice.

This review presented research done to understand combustion instabilities in spray-guided (SG) stratified-charge engines operated at part load with highly stratified fuel-air-residual mixtures. The primary emphasis has been on experimental work to identify and understand the

physical and chemical reasons for combustion instabilities. Modeling and simulation work has been integrated as well in order to illustrate the development of advanced models based on a wide range of experimental observations and the emergence of a comprehensive conceptual framework from the interplay of experiment and simulation.

In addition to traditional cylinder-pressure-based measurements and analysis, the principal experimental tools were advanced high-speed imaging diagnostics based on Mie scattering, particle image velocimetry, laser induced fluorescence, spark emission spectroscopy, and flame luminosity. Systematic applications of these techniques to a range of optical engine designs have provided multi-dimensional, crank-angle resolved measurements for hundreds of consecutive cycles, thereby enabling the capture of rare and random misfires and partial burns. In particular, fuel concentration, spark characteristics, velocity distributions, and flame imaging have been compared between well burning and misfired or partially burned cycles. This capability has enabled characterization and quantification of the sensitivity of ignition and flame propagation to strong, cyclically varying temporal and spatial gradients in the flow field and the fuel-air-residual mixture distribution. The experimental results and insights have been supplemented by and interpreted within the understanding of spray-guided ignition and combustion that emerges from recent numerical simulations with a new model (SparkCIMM) that highlights the importance of local conditions along and in the vicinity of the extended spark channel (equivalence ratio, dilution, temperature, convective velocity, and turbulent velocity and equivalence-ratio fluctuations) for successful ignition and early flame-kernel development.

During ignition and flame-kernel growth, the close injection-ignition coupling in SGSC engines produces high velocities and intense turbulence (up to an order of magnitude higher than in homogeneous-charge SI engines). The spark plasma (which can be dramatically stretched), the ignition kernel(s), and the growing flame all are subjected to steep and cyclically varying gradients in the liquid and vapor fuel concentrations and the velocity fields. These factors, which can produce unfavorable conditions for robust ignition and flame growth, are a central focus of this review.

Results from the four multi-hole-injection SGSC engines discussed here in detail indicate that combustion instability is dominated by factors that delay or inhibit the flame kernel from propagating into the main stratified fuel cloud while allowing the fuel cloud to lean out due to transport and mixing. We conclude that poor cycles are indeed characterized by combustion

instability and not ignition instability since an initial flame kernel has been observed in all cases. Specific factors for combustion instabilities identified here are (1) convective flow fluctuations that impede motion of the flame kernel toward the bulk of the fuel, (2) low flame speeds due to locally lean mixtures adjacent to the kernel, and (3) retarded ignition kernel development that allows further lean mixing. Detailed numerical simulation of ignition and early flame propagation under highly diluted spray-guided conditions using the SparkCIMM model revealed the favorability of surprisingly rich conditions (equivalence ratios as high as 4) and the suppression of laminar flame speed for lean conditions due to Lewis-number and curvature effects. These results suggest that locally lean mixtures may affect early flame kernels even more strongly than one might expect from intuition based on classical planar premixed flames. Overall dilution (with EGR in "real" engines and simulated in the optical engines with nitrogen) reduces flame speed and exacerbates the effect of the factors identified here.

Although most published work has been performed with gasoline or gasoline-surrogate fuels, results obtained with gasoline-ethanol blends contributed further insights to a common framework to explain the causes of rare combustion instabilities. Experiments using extraordinarily late injection and ignition timings for SGSC operation with ethanol-dominated fuels (e.g., E85) have demonstrated very low NOx and soot emissions. Heat-release analysis and high-speed imaging and PIV have revealed the importance of the spray-induced momentum and turbulent mixing at low engine speeds as well as the increasing contribution of fluctuations in the intake/compression-generated flow field to combustion instability with increasing engine speed. These experiments, in which the spray-induced mixing is clearly of great importance, also raise the interesting question of the comparative roles of partially premixed flame propagation and mixing-controlled combustion.[34, 55-58, 79]

For multiple injections per cycle, simulation studies showed that, relative to single injection, double injection reduces spray penetration and thereby reduces piston wetting and engine-out soot emission; contains the fuel vapor more effectively within the piston bowl, which favorably affects both flame propagation and unburned HC emissions; increases the overall burning rate; and improves combustion stability. Specific factors by which multiple injection improves combustion stability include delivering rich mixture to the flame kernel formed from the previous injection(s); imposing a relatively well organized and well directed flow that drives the burning mixture into the piston bowl and toward the remaining fuel; and reducing turbulence

intensity during initial flame-kernel formation but increasing turbulence intensity and thereby increasing the overall burning rate after the final injection when the flame kernel is more robust. This is all a result of improved flexibility in tailoring the mixture cloud and its surrounding conditions. With their extremely fast response, piezo-electric injectors are particularly advantageous for multiple-injection strategies.

Although all SGSC engines that have so far gone into commercial production have used piezo-injectors with outwardly opening nozzles, less information is available in the open literature than for multi-hole SGSC engines. The major differences between these injector types in spray structure and in the interaction of the spray with the flow field and spark plug lead to significant fundamental differences in mixture formation, ignition and early flame-kernel development. With multi-hole injection, the nascent flame kernel must "chase the tail" of the fuel cloud as it moves rapidly downstream of the spark gap. This effect is much less pronounced with ignition in the characteristic recirculation vortex of piezo sprays, particularly when multi-pulse injection is used.

Flow-field fluctuations have emerged as a common element of combustion instability with both injection systems. Although the piezo spray structure is very stable when examined in quiescent spray test chambers, it appears that the interaction of the spray with the pre-injection flow field can affect the spray and have a strong impact on combustion stability. Indeed, this result, together with the results for multi-hole SGSC with ethanol-dominated fuel, makes clear that the interaction between the spray and the flow field goes both ways, with the spray and flow field influencing each other to varying degrees depending on such factors as engine speed, injected quantity, and injection timing. However, the limited quantitative information that has been published about SGSC operation with piezo-injectors does not allow us to draw firmer or more extensive conclusions.

In substantial contrast to the many multi-hole SGSC studies in which we have participated directly, one piezo-spray study showed that misfires were never due to extinction of a flame kernel once it had been formed. Misfires occurred only due to failure to ignite a flame kernel. The extent to which misfires in other piezo-injected SGSC engines are caused by the failure to ignite a flame kernel is unclear due to lack of systematic information in the literature.

The efforts reviewed here focused on the instabilities during the ignition-delay period associated with ignition and early flame-kernel growth. Less fundamental information is

available on the fully developed flame portion of the combustion event, where the mixing of the heterogeneous fuel-air mixture within the bowl becomes important. There is yet much to be learned about the effects of the in-cylinder flow cyclic variability, which is generated by the intake and compression strokes, by the late injection (near TDC) of the liquid spray, and by their interaction with the piston bowl. Flow-field variability has been shown to create ignition and flame-kernel variability. This is expected, in turn, to affect the main combustion period (say, >10% mass burned) by changing the state of mixing of the heterogeneous fuel-air distribution, as well as by changing the turbulence intensity encountered by a partially-premixed flame. This lack of information identifies a direction for future research.

In the end, the suspicions of Ricardo a century ago turn out to be true: stratified charge engines need to be designed and operated "just right" to work. A careful and delicate balance between a multitude of factors is required. As reviewed here, a key element in achieving that balance is conceptual and quantitative understanding of the complex and interacting phenomena that govern ignition and flame-kernel growth under the severe conditions that can occur in spray-guided stratified-charge engines.

Acknowledgements

It is a pleasure to acknowledge the contributions of several colleagues: Dr. Michael C. Drake who collaborated closely in all the GM experiments, some of which go back well over a decade; Dr. Brian J. Peterson who carried out much of the UM experimental work and analysis; and Dr. Magnus Sjöberg and Dr. Wei Zeng of Sandia National Laboratories. At GM, Marty Rosalik, Jason Rakowski and especially Jerry Silvas provided technical support. We also acknowledge the valuable interactions with the many students and colleagues who were co-authors with us on papers cited here. The UM research described here was carried out with financial support from General Motors Company through the GM-UM Collaborative Research Laboratory in Engine Systems Research.

References

1. Ricardo HR. Recent Research Work on the Internal Combustion Engine. *SAE Trans*. 1922; 14: 30-2.
2. Quader AA. The Axially-Stratified-Charge Engine. SAE Paper 820131, 1982.
3. Kiyota Y, Akishino K and Ando H. Concept of Lean Combustion by Barrel-Stratification. SAE Paper 920678, 1992.
4. Hardalupas Y, Taylor AMKP, Whitelaw JH, Ishii K, Miyano H and Urata Y. Influence of Injection Timing on In-Cylinder Fuel Distribution in a Honda VTEC-E Engine. SAE Paper 950507, 1995.
5. Wood CD. Unthrottled Open-Chamber Stratified Charge Engines. SAE Paper 780341, 1978.
6. Zhao F, Lai M-C and Harrington DL. Automotive spark-ignited direct-injection gasoline engines. *Prog Energy Combust Sci*. 1999; 25: 437-562.
7. Barber EM, Reynolds B and Tierney WT. Elimination of Combustion Knock - Texaco Combustion Process. *SAE Quarterly Transactions*. 1951; 5.
8. Mitchell E, Cobb JM and Frost RA. Design and Evaluation of a Stratified Charge Multifuel Military Engine. SAE Paper 680042, 1968.
9. Alperstein M, Schafer GH and Villforth FJ. Texaco's Stratified Charge Engine - Multifuel Efficient, Clean, and Practical. SAE Paper 740563, 1974.
10. Bishop IN and Simko A. A New Concept of Stratified Charge Combustion — The Ford Combustion Process (FCP). SAE Paper 680041, 1968.
11. Simko A, Choma MA and Repko LL. Exhaust Emission Control by the Ford Programmed Combustion Process - PROCO. SAE Paper 720052, 1972.
12. Scussel AJ, Simko AO and Wade WR. The Ford PROCO Engine Update. SAE Paper 780699, 1978.
13. Lancaster D. Diagnostic Investigation of Hydrocarbon Emissions from a Direct-Injection Stratified-Charge Engine with Early Injection. *I Mech E Paper C397-80*. 1980.
14. Diwakar R. Multidimensional Modeling Applied to the Direct-Injection Stratified-Charge Engine—Calculation versus Experiment. SAE 810225, 1981.
15. Solomon ASP. A Photographic Study of Fuel Spray Ignition in a Rapid Compression Machine. SAE Paper 860065, 1986.
16. Fansler TD and French DT. Swirl, Squish and Turbulence in Stratified-Charge Engines: Laser-Velocimetry Measurements and Implications for Combustion. SAE Paper 870371, 1987.
17. Siewert RM and Groff EG. Unassisted Cold Starts to −29°C and Steady-State Tests of a Direct-Injection Stratified-Charge (DISC) Engine Operated on Neat Alcohols. SAE Paper 872066, 1987.
18. Fansler TD and Drake MC. Flow, mixture preparation and combustion in direct-injection two-stroke gasoline engines. In: Arcoumanis C and Kamimoto T, (eds.). *Flow and Combustion in Reciprocating Engines*. Heidelberg: Springer-Verlag, 2009, p. 67-136.
19. Lewis JM. UPS Multifuel Stratified Charge Engine Development Program-Field Test. SAE Paper 860067, 1986.
20. Shawcross D, Pumphrey C and Arnall D. A Five-Million Kilometre, 100-Vehicle Fleet Trial, of an Air-Assist Direct Fuel Injected, Automotive 2-Stroke Engine. SAE Paper 2000-01-0898, 2000.
21. Drake MC and Haworth DC. Advanced gasoline engine development using optical diagnostics and numerical modeling. *Proc Combust Inst*. 2007; 31: 99-124.
22. Drake MC, Fansler TD, Solomon AS and Szekely GA. Piston Fuel Films as a Source of Smoke and Hydrocarbon Emissions from a Wall-Controlled Spark-Ignited Direct-Injection Engine. SAE Paper 2003-01-0547, 2003.
23. Altenschmidt F, Bertsch D, Bezner M, et al. The analysis of the ignition process on SI-engines with direct injection in stratified mode. *7th Intl Symp on Internal Combustion Diagnostics*. Baden-Baden, Germany 2006, p. 395-411.

24. Fischer J, Kern W, Unterweger G, et al. Methods for the Development of the Spray Guided BMW DI Combustion System. *7th Intl Symp on Internal Combustion Diagnostics*. Baden-Baden, Germany 2006, p. 413-23.
25. Langen P, Melcher T, Missy S, Schwarz C and Schünemann E. New BMW Six- and Four-Cylinder Petrol Engines with High Precision Injection and Stratified Combustion. *28th International Vienna Motor Symposium*. 2007.
26. Waltner A, Lückert P, Doll G, Herwig H, Kemmler R and Weckenmann H. The new V6 petrol engine with direct injection from Mercedes-Benz. *31st International Vienna Motor Symposium*. 2010.
27. Lückert P, Breitbach H, Waltner A, Merdes N and Weller R. Potential of spray-guided combustion systems in conjunction with downsizing concepts. *32nd International Vienna Motor Symposium*. 2011.
28. Peterson B, Reuss DL and Sick V. High-speed imaging analysis of misfires in a spray-guided direct injection engine. *Proc Combust Inst*. 2011; 33: 3089-96.
29. Fansler T, Drake M, Stojkovic B and Rosalik M. Local fuel concentration, ignition and combustion in a stratified charge spark combustion in a stratified charge spark ignited direct injection engine: Spectroscopic, imaging and pressure-based measurements. *Int J Engine Res*. 2003; 4: 61-86.
30. Fujikawa T, Nomura Y, Hattori Y, Kobayashi T and Kanda M. Analysis of cycle-by-cycle variation in a direct injection gasoline engine using a laser-induced fluorescence technique. *Int J Engine Res*. 2003; 4: 143-53.
31. Ghandhi JB and Bracco FV. Mixture Preparation Effects on Ignition and Combustion in a Direct-Injection Spark-Ignition Engine. SAE Paper 962013, 1996.
32. Zeng W, Idicheria CA, Fansler TD and Drake MC. Conditional Analysis of Enhanced Combustion Luminosity Imaging in a Spray-Guided Gasoline Engine with High Residual Fraction. SAE Paper 2011-01-1281, 2011.
33. Husted HL, Piock W and Ramsay G. Fuel Efficiency Improvements from Lean, Stratified Combustion with a Solenoid Injector. *SAE Int J Engines*. 2009; 2: 1359-66.
34. Drake MC, Fansler TD and Lippert AM. Stratified-charge combustion: modeling and imaging of a spray-guided direct-injection spark-ignition engine. *Proc Combust Inst*. 2005; 30: 2683-91.
35. Ando H and Arcoumanis C. Flow, mixture preparation and combustion in four-stroke direct-injection gasoline engines. In: Arcoumanis C and Kamimoto T, (eds.). *Flow and Combustion in Reciprocating Engines*. Heidelberg: Springer-Verlag, 2009, p. 137-71.
36. Raimann J, Arndt S, Grzeszik R, Ruthenberg I and Wörner P. Optical Investigations in Stratified Gasoline Combustion Systems with Central Injector Position Leading to Optimized Spark Locations for Different Injector Designs. SAE Paper 2003-01-3152, 2003.
37. Smith J, Szekely Jr G, Solomon A and Parrish S. A Comparison of Spray-Guided Stratified-Charge Combustion Performance with Outwardly-Opening Piezo and Multi-Hole Solenoid Injectors. *SAE Int J Engines*. 2011; 4: 1481-97.
38. Blokkeel G, Samson E and Soulères T. Coupled approach using CFD and optical diagnostics tools for next generation GDI engine design. *7th Inl Symposium on Internal Combustion Diagnostics*. Baden-Baden, Germany 2006, p. 319-30.
39. Achleitner E, Bäcker H and Funaioli A. Direct Injection Systems for Otto Engines. SAE Paper 2007-01-1416, 2007.
40. Hermann A, Krüger C, Schaupp U, et al. Numerical and Diagnostic Analysis of Spray Propagation and Vortex Formation of Piezo-A-Injectors and their Sensitivity to the Internal Nozzle Flow. *8th Intl Symp on Internal Combustion Diagnostics*. Baden-Baden, Germany 2008, p. 471-86.
41. Skogsberg M, Dahlander P and Denbratt I. Spray Shape and Atomization Quality of an Outward-Opening Piezo Gasoline DI Injector. SAE Paper 2007-01-1409, 2007.
42. Marchi A, Nouri J, Yan Y and Arcoumanis C. Spray stability of outwards opening pintle injectors for stratified direct injection spark ignition engine operation. *Int J Engine Res*. 2010; 11: 413-37.
43. Zigan L, Schmitz I, Flugel A, Wensing M and Leipertz A. Structure of evaporating single- and multicomponent fuel sprays for 2nd generation gasoline direct injection. *Fuel*. 2011; 90: 348-63.

44. Drake MC, Fansler TD and Dahms R. Visualization and Simulation of Ignition and Early Flame Kernel Growth in SG-SIDI Engines. *10th Intl Symp on Internal Combustion Diagnostics*. Baden-Baden, Germany 2012.
45. Drake MC, Fansler TD and Peterson KH. Stratified Ignition Processes in Spray-Guided SIDI Engines. *9th Intl Sympon Internal Combustion Diagnostics*. Baden-Baden, Germany 2010.
46. Fansler TD and Drake MC. "Designer diagnostics" for developing direct-injection gasoline engines. *J Phys: Conf Ser*. 2006; 45: 1-17.
47. Fansler TD, Drake MC and Böhm B. High-Speed Mie-Scattering Diagnostics for Spray-Guided Gasoline Engine Development. *8th Intl Symp on Internal Combustion Diagnostics*. Baden-Baden, Germany 2008.
48. Fansler TD, Drake MC, Düwel I and Zimmermann FP. Fuel-Spray and Spark-Plug Interactions in a Spray-Guided Direct-Injection Gasoline Engine. *7th Intl Symp on Internal Combustion Diagnostics*. Baden-Baden, Germany 2006.
49. Lippert AM, Fansler TD, Drake MC and Solomon AS. High-speed imaging and CFD modeling of sprays and combustion in a spray-guided spark ignition direct injection engine. *6th Intl Symp on Internal Combustion Diagnostics*. Baden-Baden, Germany 2004.
50. Peterson B, Reuss DL and Sick V. On the ignition and flame development in a spray-guided direct-injection spark-ignition engine. *Combust Flame*. 2014; 161: 240-55.
51. Peterson B and Sick V. High-speed flow and fuel imaging study of available spark energy in a spray-guided direct-injection engine and implications on misfires. *Int J Engine Res*. 2010; 11: 313-29.
52. Fajardo CM and Sick V. Flow field assessment in a fired spray-guided spark-ignition direct-injection engine based on UV particle image velocimetry with sub crank angle resolution. *Proceedings of the Combustion Institute*. 2007; 31: 3023-31.
53. Smith JD and Sick V. Crank-Angle Resolved Imaging of Fuel Distribution, Ignition and Combustion in a Direct-Injection Spark-Ignition Engine. *SAE Transactions Journal of Engines*. 2005; 114: 1575-85.
54. Smith JD and Sick V. High-speed fuel tracer fluorescence and OH radical chemiluminescence imaging in a spark-ignition direct-injection engine. *Applied Optics*. 2005; 44: 6682-91.
55. Sjöberg M and Reuss D. NOx-Reduction by Injection-Timing Retard in a Stratified-Charge DISI Engine using Gasoline and E85. *SAE Int J Fuels Lubr*. 2012; 5: 1096-113.
56. Sjöberg M and Reuss DL. High-speed imaging of spray-guided DISI engine combustion with near-TDC injection of E85 for ultra-low NO and soot. *Proc Combust Inst*. 2013; 34: 2933-40.
57. Sjöberg M, Zeng W and Reuss D. Role of Engine Speed and In-Cylinder Flow Field for Stratified and Well-Mixed DISI Engine Combustion Using E70. *SAE Int J Engines*. 2014; 7.
58. Zeng W, Sjöberg M and Reuss D. Using PIV Measurements to Determine the Role of the In-Cylinder Flow Field for Stratified DISI Engine Combustion. *SAE Int J Engines*. 2014; 7.
59. Szekely GA and Alkidas AC. Combustion Characteristics of a Spray-Guided Direct-Injection Stratified-Charge Engine with a High-Squish Piston. SAE Paper 2005-01-1937, 2005.
60. Dahms RN, Drake MC, Grover RO, Solomon AS and Fansler TD. Detailed Simulations of Stratified Ignition and Combustion Processes in a Spray-Guided Gasoline Engine using the SparkCIMM/G-Equation Modeling Framework. *SAE Int J Engines*. 2012; 5: 141-61.
61. Yang X, Solomon A and Kuo T-W. Ignition and Combustion Simulations of Spray-Guided SIDI Engine using Arrhenius Combustion with Spark-Energy Deposition Model. SAE Paper 2012-01-0147, 2012.
62. Fansler TD, Stojkovic B, Drake MC and Rosalik ME. Local fuel concentration measurements in internal combustion engines using spark-emission spectroscopy. *Applied Physics B-Lasers and Optics*. 2002; 75: 577-90.
63. Khalighi B, El Tahry SH, Haworth DC and Huebler MS. Computation and Measurement of Flow and Combustion in a Four-Valve Engine with Intake Variations. SAE International, 1995.
64. Ewald J, Freikamp F, Paczko G, Weber J, Haworth DC and Peters N. GMTEC: GMTEC developer's manual. *Technical Report*. Aachen, Germany: Advanced Combustion GmbH, 2003.

65. Dahms RN, Drake MC, Fansler TD, Kuo TW and Peters N. Understanding ignition processes in spray-guided gasoline engines using high-speed imaging and the extended spark-ignition model SparkCIMM. Part A: Spark channel processes and the turbulent flame front propagation. *Combust Flame*. 2011; 158: 2229-44.
66. Piock WF, Weyand P, Wolf E and Heise V. Ignition Systems for Spray-Guided Stratified Combustion. *SAE Int J Engines*. 2010; 3: 389-401.
67. Smith JD and Sick V. Factors Influencing Spark Behavior in a Spray-Guided Direct-Injected Engine. SAE Paper 2006-01-3376, 2006.
68. Dahms R, Fansler TD, Drake MC, Kuo TW, Lippert AM and Peters N. Modeling ignition phenomena in spray-guided spark-ignited engines. *Proc Combust Inst*. 2009; 32: 2743-50.
69. Mosburger M, Sick V and Drake MC. Quantitative high-speed imaging of burned gas temperature and equivalence ratio in internal combustion engines using alkali metal fluorescence. *Int J Engine Res*. 2013; 15: 282-97.
70. Dahms RN, Drake MC, Fansler TD, Kuo TW and Peters N. Understanding ignition processes in spray-guided gasoline engines using high-speed imaging and the extended spark-ignition model SparkCIMM: Part B: Importance of molecular fuel properties in early flame front propagation. *Combust Flame*. 2011; 158: 2245-60.
71. Dahms R, Felsch C, Röhl O and Peters N. Detailed chemistry flamelet modeling of mixed-mode combustion in spark-assisted HCCI engines. *Proc Combust Inst*. 2011; 33: 3023-30.
72. Felsch C, Hoffmann K, Vanegas A, et al. Combustion model reduction for diesel engine control design. *Int J Engine Res*. 2009; 10: 359-87.
73. Duclos J-M and Colin O. Arc and kernel tracking ignition model for 3D spark-ignition engine calculations. *Fifth Intl Symp Diagnostics & Modeling of Combustion in IC Engines (COMODIA)*. 2001.
74. Tan Z and Reitz RD. An ignition and combustion model based on the level-set method for spark ignition engine multidimensional modeling. *Combust Flame*. 2006; 145: 1-15.
75. Richard S, Dulbecco A, Angelberger C and Truffin K. Development of a 1D CFD modeling approach to predict cycle-to-cycle variability in spark-ignition engines based on physical understanding acquired from LES. *Int J Engine Res*. 2014; submitted to special issue on cyclic dispersion in engine combustion.
76. Ewald J and Peters N. On unsteady premixed turbulent burning velocity prediction in internal combustion engines. *Proc Combust Inst*. 2007; 31: 3051-8.
77. Frank RM and Heywood JB. Combustion Characterization in a Direct-Injection Stratified-Charge Engine and Implications on Hydrocarbon Emissions. SAE Paper 892058, 1989.
78. Stojkovic BD, Fansler TD, Drake MC and Sick V. High-speed imaging of OH* and soot temperature and concentration in a stratified-charge direct-injection gasoline engine. *Proc Combust Inst*. 2005; 30: 2657-65.
79. Oh H and Bae C. Effects of the injection timing on spray and combustion characteristics in a spray-guided DISI engine under lean-stratified operation. *Fuel*. 2013; 107: 225-35.
80. Zigan L, Shi J-M, Krotow I, Schmitz I, Wensing M and Leipertz A. Fuel property and fuel temperature effects on internal nozzle flow, atomization and cyclic spray fluctuations of a direct injection spark ignition–injector. *Int J Engine Res*. 2013.
81. Hübner W, Witt A, Hoss B, Albrecht T, Durst B and Abdelfattah A. Methodeneinsatz bei der Entwicklung eines weiterführenden DI-Brennverfahrens. *Direkteinspritzung im Ottomotor IV*. Essen: Expert-Verlag, 2003, p. 199-218.
82. Sick V, Drake MC and Fansler TD. High-speed imaging for direct-injection gasoline engine research and development. *Exp Fluids*. 2010; 49: 937-47.
83. Peterson B and Sick V. High-speed flow and fuel imaging study of available spark energy in a spray-guided direct injection engine and implications on misfires. *9th Intl Symposium on Internal Combustion Diagnostics*. Baden-Baden, Germany 2010, p. 8-19.

84. Price P, Twiney B, Stone R, Kar K and Walmsley H. Particulate and Hydrocarbon Emissions from a Spray Guided Direct Injection Spark Ignition Engine with Oxygenate Fuel Blends. SAE Paper 2007-01-0472, 2007.
85. de Francqueville L. Effects of Ethanol Addition in RON 95 Gasoline on GDI Stratified Combustion. SAE Paper 2011-24-0055, 2011.
86. Oh H, Bae C and Min K. Spray and Combustion Characteristics of Ethanol Blended Gasoline in a Spray Guided DISI Engine under Lean Stratified Operation. *SAE Int J Engines*. 2010; 3: 213-22.
87. Zeng W, Sjöberg M and Reuss D. *Int J Engine Res*. 2014; submitted to special issue on cyclic dispersion in engine combustion.
88. Vent G, Enderle C, Merdes N, Kreitmann F and Weller R. The new 2.0 l turbo engine from the Mercedes-Benz 4-cylinder engine family. *2nd Aachen Colloquium China*. 2012.
89. Stiehl R, Schorr J, Krüger C, Dreizler A and Böhm B. In-Cylinder Flow and Fuel Spray Interactions in a Stratified Spray-Guided Gasoline Engine Investigated by High-Speed Laser Imaging Techniques. *Flow Turbulence Combust*. 2013; 91: 431-50.
90. Stiehl R, Schorr J, Krüger C, Dreizler A and Böhm B. Investigation of the interaction of in-cylinder flow and fuel injection in an optically accessible direct injection gasoline engine. *ILASS – Europe 2013, 25th European Conference on Liquid Atomization and Spray Systems, Chania, Greece, 1-4 September 2013*. 2013.
91. Martin D, Pischke P and Kneer R. Investigation of the influence of multiple gasoline direct injections on macroscopic spray quantities at different boundary conditions by means of visualization techniques. *Int J Engine Res*. 2010; 11: 439-54.
92. Iyer CO, Han Z and Yi J. CFD Modeling of a Vortex Induced Stratification Combustion (VISC) System. SAE Paper 2004-01-0550, 2004.
93. VanDerWege BA, Han Z, Iyer CO, Muñoz RH and Yi J. Development and Analysis of a Spray-Guided DISI Combustion System Concept. SAE Paper 2003-01-3105, 2003.
94. Sauter W, Pfeil J, Velji A, et al. Application of Particle Image Velocimetry for Investigation of Spray Characteristics of an Outward Opening Nozzle for Gasoline Direct Injection. SAE Paper 2006-01-3377, 2006.
95. Disch C, Kubach H, Spicher U, Pfeil J, Altenschmidt F and Schaupp U. Investigations of Spray-Induced Vortex Structures during Multiple Injections of a DISI Engine in Stratified Operation Using High-Speed-PIV. SAE 2013-01-0563, 2013.
96. Oh H, Bae C, Park J and Jeon J. Effect of the Multiple Injection on Stratified Combustion Characteristics in a Spray-Guided DISI Engine. SAE 2011-24-0059, 2011.
97. Skogsberg M, Dahlander P and Denbratt I. An experimental study of mixture preparation and combustion in an optical engine using a piezo-actuated injector. *Direkteinspritzung im Ottomotor VI*. Essen, Germany Expert-Verlag, 2007, p. 143-59.
98. Hese M, Tschöke H, Breuninger T, Altenschmidt F and Winter H. Influence of a Multispark Ignition System on the inflammation in a Spray-guided Combustion Process. *SAE Int J Fuels Lubr*. 2009; 2: 376-86.
99. Maly RR and Herweg R. Spark ignition and combustion in four-stroke gasoline engines. In: Arcoumanis C and Kamimoto T, (eds.). *Flow and Combustion in Reciprocating Engines*. Heidelberg: Springer-Verlag, 2009, p. 1-66.
100. Buri S, Busch S, Kubach H and Spicher U. High Injection Pressures at the Upper Load Limit of Stratified Operation in a DISI Engine. *SAE Int J Engines*. 2009; 2: 40-7.
101. Buri S, Kubach H and Spicher U. Effects of increased injection pressures of up to 1000 bar – opportunities in stratified operation in a direct-injection spark-ignition engine. *Int J Engine Res*. 2010; 11: 473-84.
102. Schumann F, Sarikoc F, Buri S, Kubach H and Spicher U. Potential of spray-guided gasoline direct injection for reduction of fuel consumption and simultaneous compliance with stricter emissions regulations. *Int J Engine Res*. 2013; 14: 80-91.

103. Lang O, Habermann K, Krebber-Hortmann K, et al. Potential of the Spray-guided Combustion System in Combination with Turbocharging. SAE Paper 2008-01-0139, 2008.
104. Kneifel A, Buri S, Velji A, Spicher U, Pape J and Sens M. Investigations on Supercharging Stratified Part Load in a Spray-Guided DI SI Engine. *SAE Int J Engines*. 2008; 1: 171-6.
105. King J, Schmidt L, Stokes J, Seabrook J, Nor F and Sahadan S. Multiple injection and boosting benefits for improved fuel consumption on a Spray Guided Direct Injection gasoline engine. *FISITA 2012 World Automotive Congress*. Springer, 2013, p. 229-41.
106. Hemdal S, Andersson M, Dahlander P, Ochoterena R and Denbratt I. In-cylinder soot imaging and emissions of stratified combustion in a spark-ignited spray-guided direct-injection gasoline engine. *Int J Engine Res*. 2011; 12: 549-63.
107. Schmidt L, Seabrook J, Stokes J, et al. Multiple Injection Strategies for Improved Combustion Stability under Stratified Part Load Conditions in a Spray Guided Gasoline Direct Injection (SGDI) Engine. SAE Paper 2011-01-1228, 2011.
108. Philipp S, Hoyer R, Adam F, et al. Exhaust Gas Aftertreatment for Lean Gasoline Direct Injection Engines - Potential for Future Applications. SAE Paper 2013-01-1299, 2013.
109. Wong VW, Rife JM and Martin MK. Experiments in Stratified Combustion with a Rapid Compression Machine. SAE Paper 780638, 1978.
110. Sinnamon JF, Lancaster DR and Steiner JC. An Experimental and Analytical Study of Engine Fuel Spray Trajectories. SAE Paper 800135, 1980.